Ground displacements due to tectonics and gravity in Corace River Catchment. Gimigliano case study in Calabria Region (Italy).

Overview

This thesis aims to present some methodologies developed and new correlation among some parameters to analyse a basin river catchment with a view to constrain recent tectonic activity and ground deformation.

This work provides a detail detection of landslide-induced displacements at basin scale in Corace catchment and at local scale in Gimigliano site, Calabria Region. Also, this work presents the results of applying the matrix method in a Geographic Information System (GIS) to the drawing of maps of susceptibility to slope movements in different sectors of the Corace River Basin. This paper presents results obtained to assess the influence of active tectonics as one of the different determinant factor to be accounted for GIS landslide susceptibility mapping. This is made by an approach based on using different active tectonics geomorphic indexes related to the river drainage network, river basins and mountain front. These indexes are assessed in a GIS application and supported by field observations. Several landslide occurrences and the relationships of some controlling parameters with various events have been evaluated using GIS techniques and correlated with measured geomorphic indexes.

Regarding the active tectonic factor, the GIS analysis provides a significant correlation landslides occurrences . In general the observed instable zones are related to steep slopes in under excavated rivers resulting from deforestation, soil erosion and active tectonics. A higher frequency of landslides is related to areas with higher indexes of active tectonic in the eastern slopes of Corace Basin and also in, with high to very high of the active tectonic indexes values correspondence of Gimigliano Village. These correlations between density of landslides and active tectonics intensity, expressed by geomorphic indexes, suggest the usefulness of the integration of the active tectonics among the main determinant factors in landslide susceptibility assessment of the Gimigliano area which may be applied to similar areas around the world. The approach of this paper is to provide a quantitative method to focus on areas for more detailed work to establish rates of active tectonics. On this purpose, some geomorphic indexes were calculated in the whole area of Corace Basin catchment and seven third order river sub-basins. Some geomorphic indexes of active tectonics known to be useful in active tectonic studies were selected including:

• Stream length-gradient index (*SL*);

• Drainage basin Asymmetry (*Af*);

• Hypsometric integral (*Hi*);
• Ratio Valley-floor weight to valley height (*Vf*);
• Index of drainage basin shape (*Bs*);
• Index of mountain front sinuosity (*Smf*).

A method to evaluate an index over an area that represents relative tectonic activity (*Ifat*) it is present. The various indices is divided into three classes, with class one being high activity and class three being low activity. In order to develop an aerial index. *Ifat* is obtained by the average of the different classes of geomorphic indices and divided into four classes, where class 4 is very high tectonic activity class 3 is high tectonic activity class 2 is moderately active tectonics class 1 is low active tectonics.

The proposed GIS methodology allows a map showing relative tectonic activity of the landscape to be produced. This method has been linked to landslide susceptibility mapping **.** Finally the landslide susceptibility map for each landslide type are presented. Maps were validated, checking out degree of adjustment between landslide inventories and resulting susceptibility classes. The validation showed high correlations between new landslides and the available landslide susceptibility classes and degree of adjustment above 72% for high to very high susceptibility classes and below 10% for low to very low susceptibility classes, showing the usefulness of these landslide susceptibility maps to forecast future landslide areas.

By mean this research in the Gimigliano area it is possible to highlight that PS data are enable to detail and study spatial and temporal evolution of ground movements underling the capability for detecting, mapping and monitoring ground deformations.

Rock weathering of the outcropping sedimentary and metamorphic litotypes across time could be caused an increasing in ground displacement phenomenon.

Landslide events are complex geological and geomorphological processes due to a different factors and therefore it is very difficult to classify the existing one and predict the future occurrences. Aim of third section is the utilising of remote-sensing data to detect and map landslides, to assess their activity and velocity. Also, to determine the spatial-temporal variation of landslides and related consequences. InSAR techniques may improve towards to high robustness for landslides movement monitoring and it may be used as new methods for landslide mapping and inventory.

In order to assess any spatial and temporal patterns of deformation and to provide a detailed detection of landslide-induced displacements at local scale on Gimigliano site Sentinel 1 data acquired in October 2014 – October 2016 were compared with geological and geomorphological evidences resulting from auxiliary data such as landslide databases and orthophotos referred to different dates, finally validated with recent field checks. The applied approach demonstrated to

have a successful operative usefulness to support landslide susceptibility evaluation, since PSI technique has the potential to work in synergy with conventional geo-morphological tools and to improve the quality and the temporal reference of existing landslide inventories.

Remote sensing data by SAR interferometry (InSAR) have become a powerful tool for spatio-temporal monitoring ground movements such as subsidence, surface displacements due to landslides or tectonic activity, volcanism and anthropic processes in urbanized areas In the last decade, the methods for the detection of ground displacements by space borne synthetic aperture radar interferometry have greatly progressed. In the last few years differential interferometry of RADAR images has become one of the most accurate remote sensing techniques in assessing during natural or anthropically induced landslide activity related to natural hazard or natural resources studies. In particular Differential SAR Interferometry has become a very useful remote sensing tool for accurately measuring the spatial and temporal evolution of surface displacements over broad area. The analysis is focused on DInSAR results exploration of ground deformation.

In the study of assessment of ground deformation it is useful to incorporate the study of active tectonic processes and estimation of the amount landslides.

First section
Geological and Geomorphological setting

Landscapes in tectonically active areas result from a complex integration of the effects of vertical and horizontal motions of crustal blocks and erosion or deposition by surface processes (Burbank and Anderson, 2001). As a consequence, geomorphic investigation in regions of active tectonics is a powerful tool for studies of tectonic geomorphology (Azor et al., 2002).

The aim of this study is to establish rates of active tectonics by using quantitative method to focus on areas for more detailed work. In recent studies related to geomorphologic and morphometric analyses of landforms and topographic analyses are utilized to obtain active tectonics (Della Seta et al., 2008).

It was used geomorphic indices of active tectonics, known to be useful in active tectonic studies (Bull and McFadden, 1977; Azor et al., 2002; Keller and Pinter, 2002; Silva et al., 2003; Molin et al., 2004).

Geomorphic indices applicable to fluvial systems in different regions and of varying size correlate with independently derived uplift rates (Kirby and Whipple, 2001) and are applicable to a variety of tectonic settings where topography is being changed (Bull and McFadden, 1977; Azor et al., 2002).

All the measurements have been carried out by using drainages and contours extracted from DEM in GIS environment.

The study area is located in the Calabrian Arc (southern Italy), along the northeaster flanks of the Catanzaro Basin (Fig 1). The area is about 200 km^2, located in the southeaster sector of Sila Piccola Massif (Fig. 1).

The Gimigliano area lies on Liguride and Calabride Complexes, including an important “tectonic window” made up of Mesozoic ophiolite rocks. The main lithotypes that cropout in the area are referred to metamorphic units (Ophiolite Unit) such as metabasites, serpentinites, and phyllites belonging to the Liguride Complex (Amodio Morelli et al., 1976; Liberi and Piluso, 2009), tectonically overthrusted by metamorphic and crystalline rocks (Calabrian Complex) such as orto- and para-gneisses (Messina et al., 1994; Tansi et al., 2007).

The geomorphologic setting is characterized by widespread slope movements. Diffuse landsliding with occasional deep-seated gravitational slope deformations have been recognized in the whole area (Sorriso Valvo & Tansi, 1996; Gullà et al., 2005) . The overlap of recent and past cartographic maps evidences that the area results already affected by hydrogeological hazard.

Chapter One

Geological and structural setting

1. Geological and structural regional setting of the study area

The study area is in the southern Italy along the northeaster flanks of the Catanzaro Basin. The area is about 282 large, located in the southern sector of Sila Piccola Massif (Fig. 1).

A number of tectonic units belonging to the Calabrian Arc constituted, from bottom to top, by:

· Ophiolite Unit ("Gimigliano Unit" of Amodio-Morelli et al., 1976). A HP-LT metamorphic serpentinite-metabasite polychrome schist-Calpionella limestone sequence (Tithonian-Neocomian).

· Slate and metapelite Unit. Dominantly foliated slates, black metapelites and metasilts, interbedded with quartzite strata defining isoclinal folds, and red mudrocks and thin levels of laminate marble (Paleozoic-Mesozoic). According to Ogniben (1973) and Amodio-Morelli et al. (1976), these terranes should be ascribed to two distinct units: the Mesozoic Frido Unit, and the Paleozoic Bagni Unit, belonging to two distinct complexes. The first (of oceanic origin) was, in fact, ascribed to the Liguride Complex, while the second (of continental origin) to the Calabride Complex.

Above these units, the following are to be found:

· Orthogneiss Unit (Castagna Unit of Amodio-Morelli et al., 1976). Made of mylonitic augen-gneiss, micaschist, and subordinately marbles (Paleozoic).

· Paragneiss Unit (Monte Gariglione Unit of Amodio-Morelli et al., 1976; Sila Unit of Messina et al., 1994). Made of high-grade metamorphic rocks (biotite-sillimanite-garnet gneiss), intruded by plutonic bodies (Paleozoic).

From a geological viewpoint, the Catanzaro Basin is a graben-like structure bordered by normal faults (with a typical 120° northward orientation (Tansi et al., 2007; Tripodi et al., 2013). Late Miocene evaporite and clastic sequences (Critelli, et al., 2013) and Lower Pliocene to Middle Pleistocene sediments fill the Catanzaro Basin to form a ca900 m thick succession. The Pliocene-Pleistocene sedimentary succession of this basin consists in deep-water mudstones passing upward to sub-littoral siltstones; the upper transgressive interval is represented by silici/bioclastic mixed arenites, grading upwards into open-marine siltstones and clay (Critelli et al., 2013; Longhitano et al., 2012; Longhitano et al., 2014). Finally, the entire succession is overlain by Middle to Upper Pleistocene deposits (Brutto et al., 2016), from marine to continental , that have been removed in some areas by intense erosional processes.

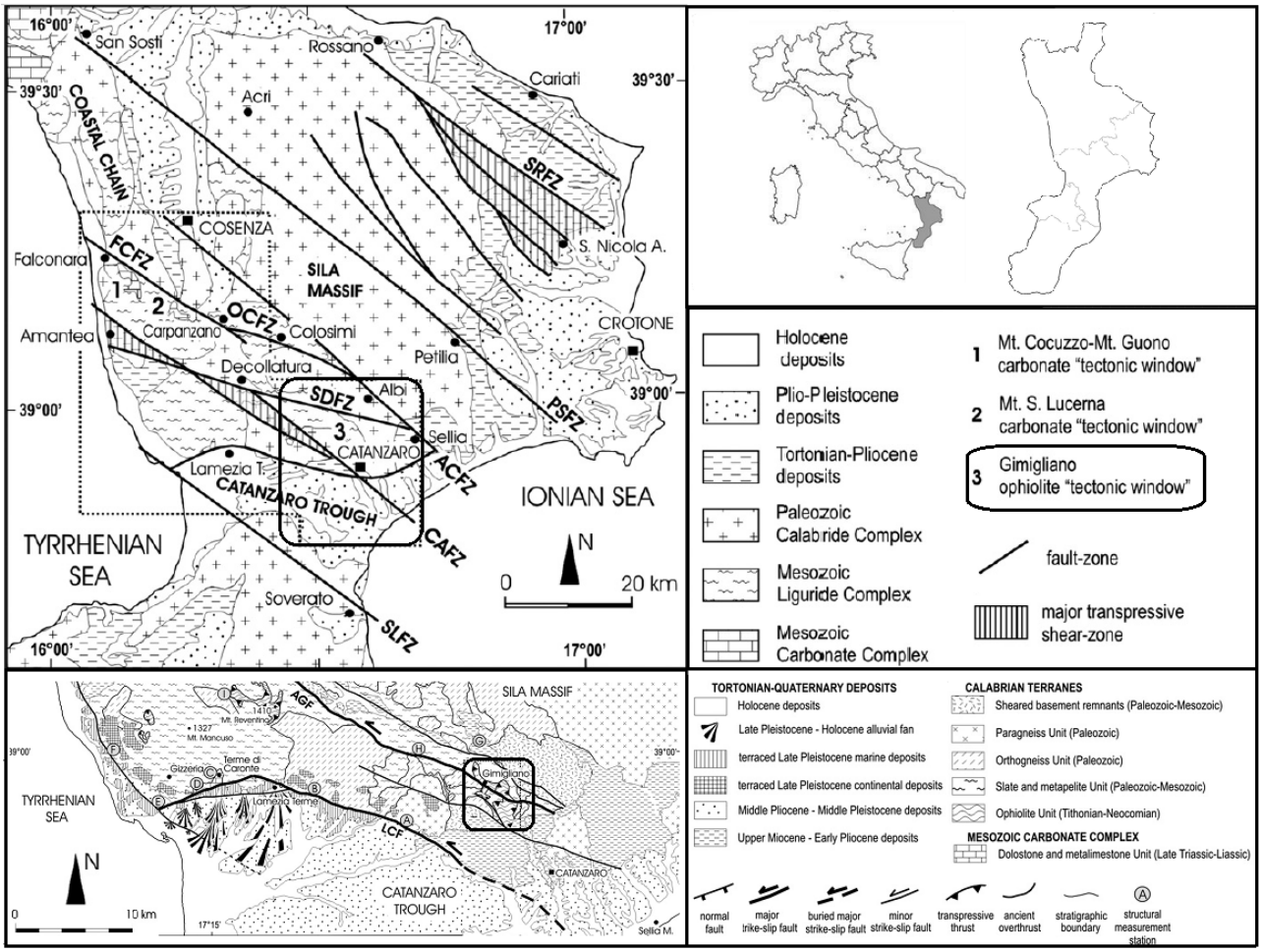

Figure 1 Schematic tectonic map showing the main Middle Miocene-Middle Pleistocene left-lateral strike-slip lineaments of central-northern Calabria (after Van Dijk et al., 2000, modified). Key: (SLFZ) Soverato-Lamezia Fault Zone; (CAFZ) Catanzaro-Amantea Fault Zone; (ACFZ) Albi-Cosenza Fault Zone; (SDFZ) Sellia-Decollatura Fault Zone; (OCFZ) Ospedale-Colosimi Fault Zone; (FCFZ) Falconara-Carpanzano Fault Zone; (PSFZ) Petilia-S. Sosti Fault Zone; (SRFZ) S. Nicola-Rossano Fault Zone. Dotted polygon indicates the study area.

A Middle Miocene-Middle Pleistocene regional NW-SE left-lateral strike-slip fault system profoundly conditioned the evolution of central Calabria, during the late tectonic phases (Van Dijk et al., 2000; Tansi et al., 2007). This system dissected an Oligocene-Early Miocene orogenic belt, made up of Alpine nappes overthrusted on the Apennine Chain (Amodio Morelli et al., 1976; Critelli et al., 2013) .

In the sectors of overlapping of the faults, the transpressional regime induced tectonic extrusions of the deep-seated units of the Chain, producing push-ups within the overlying crystalline-metamorphic complexes. In the sector of fault overstepping, the primary geometric relationships among the units of the orogenic belt were locally altered (Van Dijk et al., 2000, Tansi et al., 2007).

In particular, push-ups structures, induced by strike-slip crustal faults, made up of the ophiolite unit are the main tectonic setting of the Gimigliano area.

These fault systems characterized and conditioned the Pliocene-Lower Plestocene evolution of whole area and also influence the tectono-stratigraphic architecture of the Catanzaro Basin. The

Middle-Upper reactivation of the major faults with normal kinematics is result still active as resulted by historical and strumental earthquakes (Monaco and Tortorici, 2000; Tansi et al., 2007).

The outcropping rocks show a stone behaviour, even if schistosity and jointing lead to the formation of deep granular layers that turn out to be geotechnically soft and highly erodible.

The area of study interest is located in Gimigliano municipality (Catanzaro province, CZ) in Calabria Region (Italy).

From a tectonic point of view, the metamorphic nappes show tectonic contacts marked by pre-Neogene sub-horizontal thrusts, striking NE-SW, displayed by the Neogene-Quaternary regional NW-SE transpressive fault zones. In particular, the Gimigliano ophiolite outcrops are placed in the transpressional sector, developed between the regional Amantea-Gimigliano Fault and a couple of minor Neogene-Quaternary left- lateral strike-slip NW-SE oriented faults, extending from Gimigliano Inferiore village to Cavorà. Gimigliano village is located on a "flower structure" belonging to a push-up system according Tansi et al., 2007.

The transpressional mechanism also dragged up deep-seated units towards SE the Gimigliano site, where ancient thrusts separate the "Ophiolite", the "Slate and Metapelite" and the "Orthogneiss" Units (Van Dijk et al., 2000; Tansi et al. 2007). The well-structured fault zones generate many wide cataclastic zones characterized by weathered and intensively fractured rocks. The outcropping rocks show a stone behavior, even if schistosity and jointing lead to the formation of deep granular layers that turn out to be geotechnically soft and highly erodible.

The Gimigliano ophiolite outcrops (Colonna and Piccarreta, 1975, 1977; Rossetti et al., 2001) consist of metabasite and serpentinite belonging to the basal portion of the Calabrian Terranes. They are located in the tranpressional sector induced by the interaction between the Amantea-Gimigliano Fault and a couple of minor left-lateral strike-slip faults belonging to the NW-SE regional fault system (Van Dijk et al., 2000).

The Catanzaro Basin is a graben-like structure bordered by normal faults (Tansi et al., 2007; Tripodi et al., 2013; Brutto et al., 2016). A Middle Miocene-Middle Pleistocene regional NW-SE left-lateral strike-slip fault system profoundly conditioned the evolution of central Calabria, during the late tectonic phases.

From the Neogene to Quaternary combined with the progressive migration of Calabrian Arc overthrusting occurred along a NW-SE to WNW-ESE-trending regional strike-slip fault system characterized by left- and right-lateral movements in the northern and in the southern sector of the Calabrian Arc, respectively (Ghisetti and Vezzani, 1981; Rehault et al., 1987; Turco et al., 1990; Knott and Turco, 1991; Monaco and Tansi, 1992; Catalano et al., 1993). The fault system

constitutes a regional shear zone, dissecting the pre-existing thrust sheets, and played an important role in the Neogene-Quaternary geodynamic evolution of the Central Mediterranean area.

These systems were characterized and lead Plio-Quaternary evolution of whole area and also were influence the tectonostratigraphic architecture of Catanzaro Basin configuring it as grabens or half-grabens. Tectonic context is dominated by strike-slip tectonics, lasting from Late Miocene to Quaternary (and, presumably, still active) in which late emplacement mechanisms of the deep-seated Mesozoic carbonate rocks, and their geometric relationships with the overlying units of the Calabrian Arc are led by the development of the area. Since Middle Pleistocene, the reverse kinematics of faults were reactived by extensional tectonics. As a consequence, several cases either of deep-seated gravitational or tectono-gravitational accommodation of pre-existing reverse faults have been recently documented in Calabria (Iovine et al., 1996; Iovine and Tansi, 1998; Sorriso-Valvo et al., 1998; Tansi et al., 2005a,b): such a reactivation mechanism could also explain some of the normal kinematic evidence.

The Lamezia-Catanzaro fault is placed in the context of NW-SE left-lateral strike-slip fault system; this master fault belongs to a wider and broader system, Amantea-Gimigliano, characterized by vertical displacement accumulated in Neogene-Quaternary higher than 1000m.

The Amantea-Gimigliano Fault extends from the Tyrrhenian Sea (where it bounds the south edge of the Coastal Chain) towards SE, cutting through the southern margin of the Sila Massif. At its westernmost end, it separates Late Miocene deposits from the *Slate and metapelite Unit* (Fig 1). Along its middle portion, the fault delimits, to the south, an elongated outcrop of *Sheared basement remnants* from the *Slate and metapelite Unit*. This fault segment roughly corresponds to the Catanzaro-Amantea Fault Zone recognized by Van Dijk et al. (2000).

The topographic elevation of the study area has an average value of 260 m a.s.l. and a maximum value of 1427 m a.s.l. The slope gradients computed from the DEM range from 0 to ~83 degrees, while the average is approximately ~18 degrees (Fig.2).

.

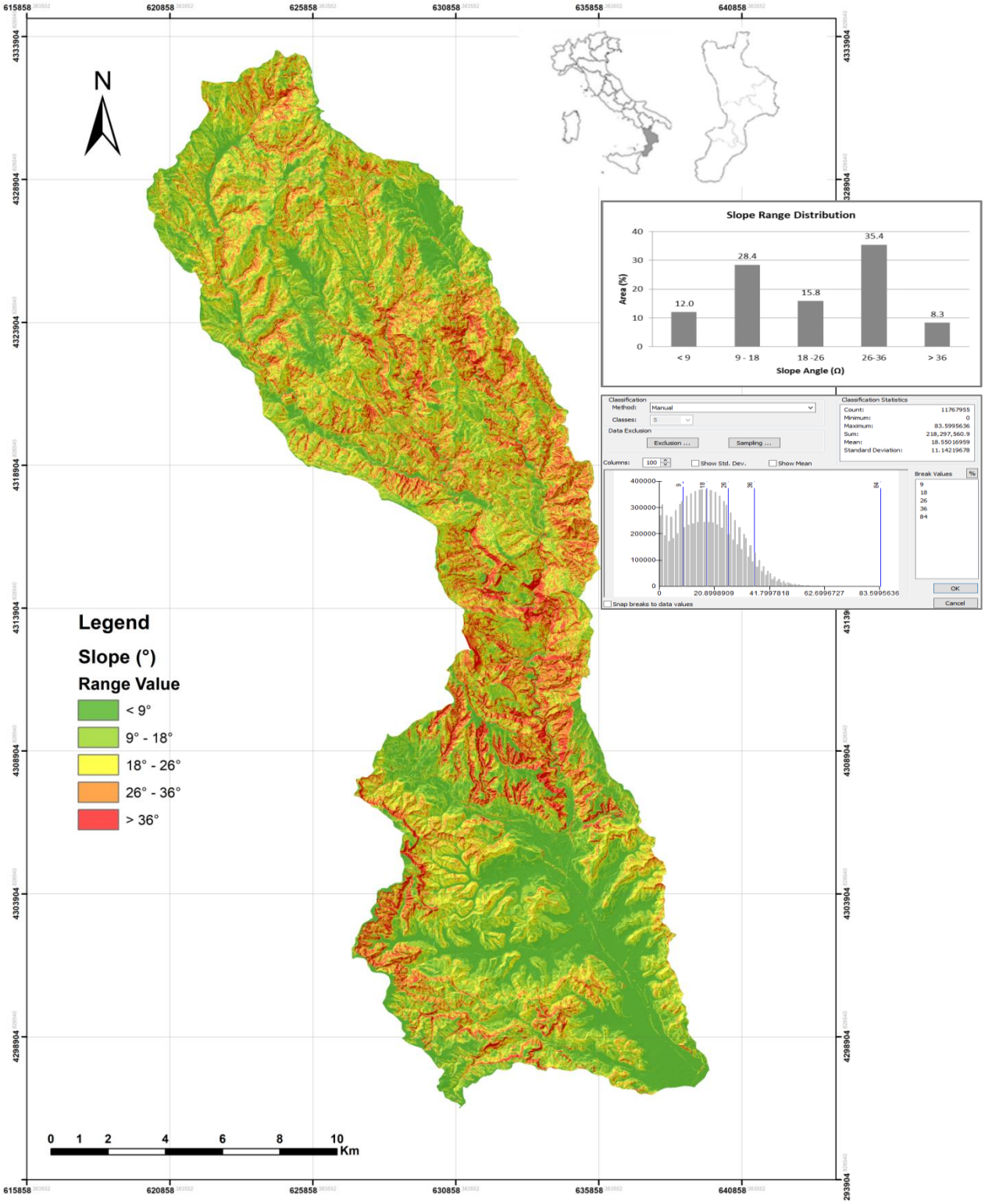

Figure 2 Morphometric parameteres: topographic elevation of the study area has an average value of 260 m a.s.l. The slope gradients computed from the DEM range from 0 to ~83 degrees.

Corresponding on Gimigliano area a push-up structure was recognized. Here, deep-seated serpentinite and overlying metabasite are overthrust by the Orthogneiss Unit and the Slate and Metapelite Unit bounded by a NNE-striking W-verging thrust. In southeast side metabasite overthrusted the Slate and metapelite Unit bounded by a NNE-striking E-verging thrust.

In particular, push-ups are either made of ophiolite. In these sectors, the primary geometric relationships among the units of the orogenic belt were locally altered (Van Dijk et al., 2000, Tansi et al., 2007). deep-seated units of the Chain of Gimigliano were dragged up and ancient thrusts separating the Ophiolite, Slate and metapelite and Orthogneiss units crop out.

The push-up developed between the Amantea Gimigliano Fault and a minor left-lateral strike-slip fault extending from Gimigliano Inferiore to C.da Cavorà.

The transpressional mechanism also dragged up deep-seated units towards SE Gimigliano site, where ancient thrusts separate the “Ophiolite”, the “Slate and Metapelite” and the “Orthogneiss” Units (Van Dijk et al., 2000; Tansi et al. 2007).

This region of Calabria is known as one of the most landslide-prone areas in Italy due to its geological and climatic characteristics (Antronico, Sorriso-Valvo, Tansi, & Gulla`, 2001; Antronico et al., 2013; Gulla` et al., 2008)

Figure 3 NE-SW fault evidenced in metabasite (San Giorgio site).

Figure 4 Grey phillites quarzite and meta-limestone alterncance due to sub-vertical isoclinal folds.

Figure 5 On the left, phyllites meta-limestones; on the right, detail of metacalcarenti in which the original texture is recognizable.

Figure 6 Overview of the left side of the Corace river cachment; ophiolite units affected by folding, the core area is occupied by serpentinite and metabasite is visible while the carbonate-silicoclastica. Metacalcari coverage and phyllites are verticalized right and tend to tip over. The structure is truncated in the upper part of the slope by the ovethrust of the Bagni Unit

Chapter Second
Geomorphological setting

1. Geomorphological setting

Geomorphological survey aims to characterize geomorphological setting of a wide area in Calabria Region, in southern Italy.

An accurate identification of unstable slopes and an exhaustive landslides inventory map, based on aerial photog interpretation and conventional field geology survey, was carried out.

Geological structure deeply controls geomorphological context: structural discontinuities and variation in erodibility of different lithotype influence the hydrography and the whole landscape.

The geomorphologic setting of the study area is characterized by widespread slope movements. Diffuse landsliding with occasional deep-seated gravitational slope deformations have been recognized (Fig.)The overlap of recent and past cartographic maps evidences that the Gimigliano area was always affected by hydrogeological hazard. Geological structure strongly influences geomorphological context. Hydrographic network and landscape are conditioned by structural discontinuities and erodibility changes of outcropping lithology. Geomorphological field observations of the north western area of Catanzaro Basin were carried out using a 1:10.000 scale topographical map (Fig. 7). The Corace River catchments suggests typical subsequent relation among erosional processes and structural discontinuities. Corace Stream is a 7th order basin (Fig. 8) and has two 6 order tributaries, 5 fifth tributaries and 32 fourth order tributaries (Tab.1). It is flanked by the Sila Piccola Massif in the North, in south, Catanzaro straight in the west, Serre Massif in the east and Ionian Sea in south. This river basin is elongated in north-west direction and the river follows a straight line course there by manifesting tectonic control on the stream development. The drainage pattern is subdendritic to sub parallel, in general, and the higher order streams, in particular, show more or less trellis drainage pattern. Most of the higher and medium order streams follow general structural trend which indicates structural control.

The tributaries are oriented in the WNW-ESE, N-E directions in the upper portion and NNE-SSW directions in downer portion and most of the tributaries are short in length and align perpendicular to the main stream.

The basin is confined and has a restricted north-south development. In general right bank of the basin is more elevated and receives more tributaries than the left bank . Elevation of study area varies between 0 m and 1435 above sea level. (Fig. 2). Lithostructural conditioning is evident in the section immediately above the town of Gimigliano, where the NE-SW trend of Corace River suggests the presence of an anticlinal.

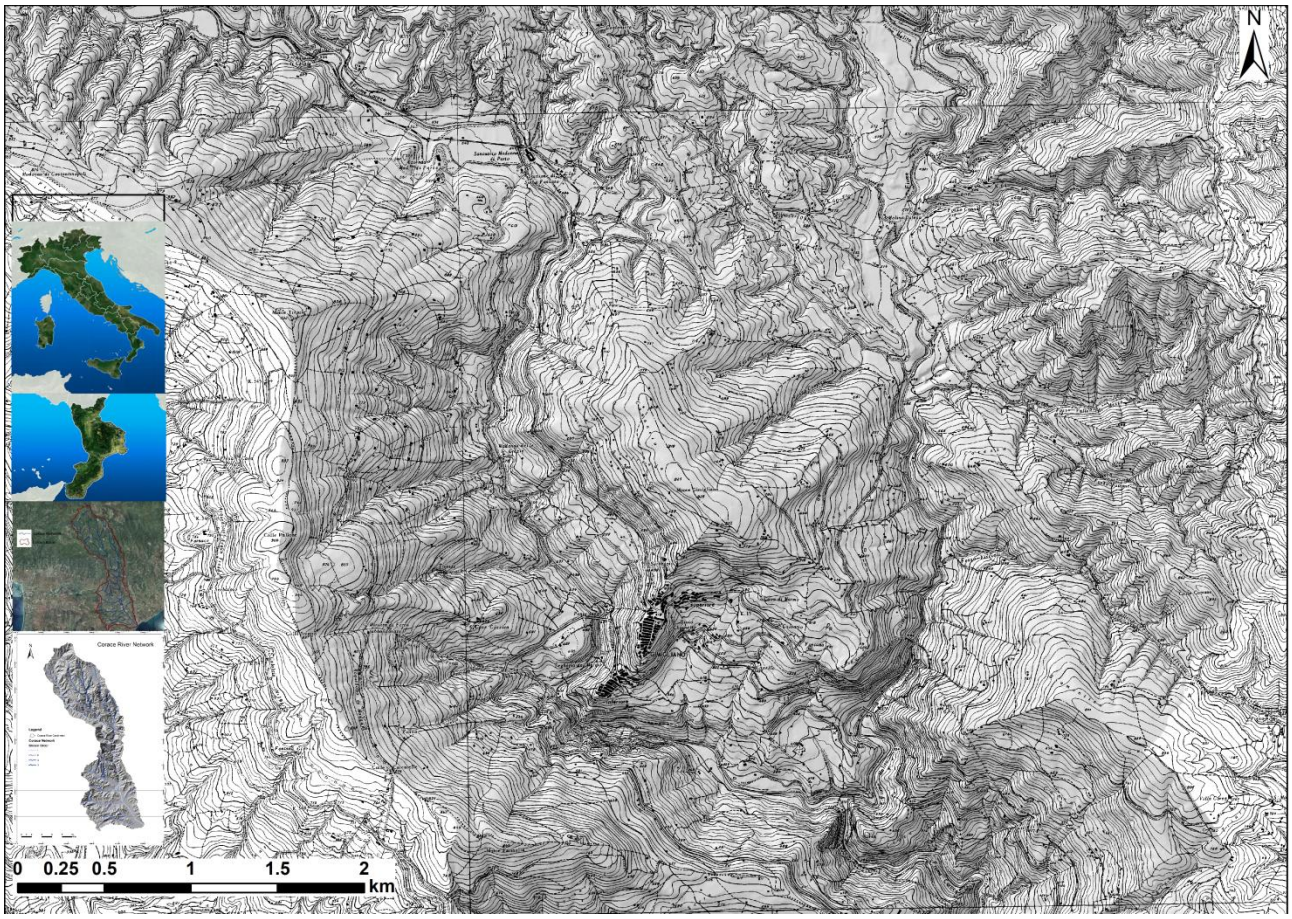

Figure 7 Geomorphological field observations of the north western area of Catanzaro Basin were carried using 1:10.000 scale topographical map. In particular Gimigliano Municipality.

Basin	Square kmq	Perimeter Km	Higth m	Maximum H m	Mean H m
Corace	**295**	**113**	**1**	**1385**	**565**
Fiume Corace from the confluence with the Borgia Fiumarella up to its closing point.	3.5	9	1	99	32
Fiumarella di Borgia	19	27	13	375	229
Fiume Corace from the confluence with Torrente Usito and Fiumarella di Borgia	16	17	12	369	80
Torrente Usito	22	24	39	350	162
Fiume Corace from the confluence with Fiume Fallaco and T. Usito	10	15	37	225	103
Fiume Corace from the confluence with F. Melito and F. Fallaco	31	31	51	800	349
Fiume Fallaco	36	29	53	620	200
Fiume Corace from the confluence with F. Pomo with Fiume Melito.	13	17	350	930	655
Fiume Melito	41	43	360	1322	858
Fiume Pomo	44	33	567	1381	970
Fiume Corace from start poin and confluence with Fiume Pomo	59	48	575	1385	881

Table 1 Corace River Catchment Idrographic Characteristics.

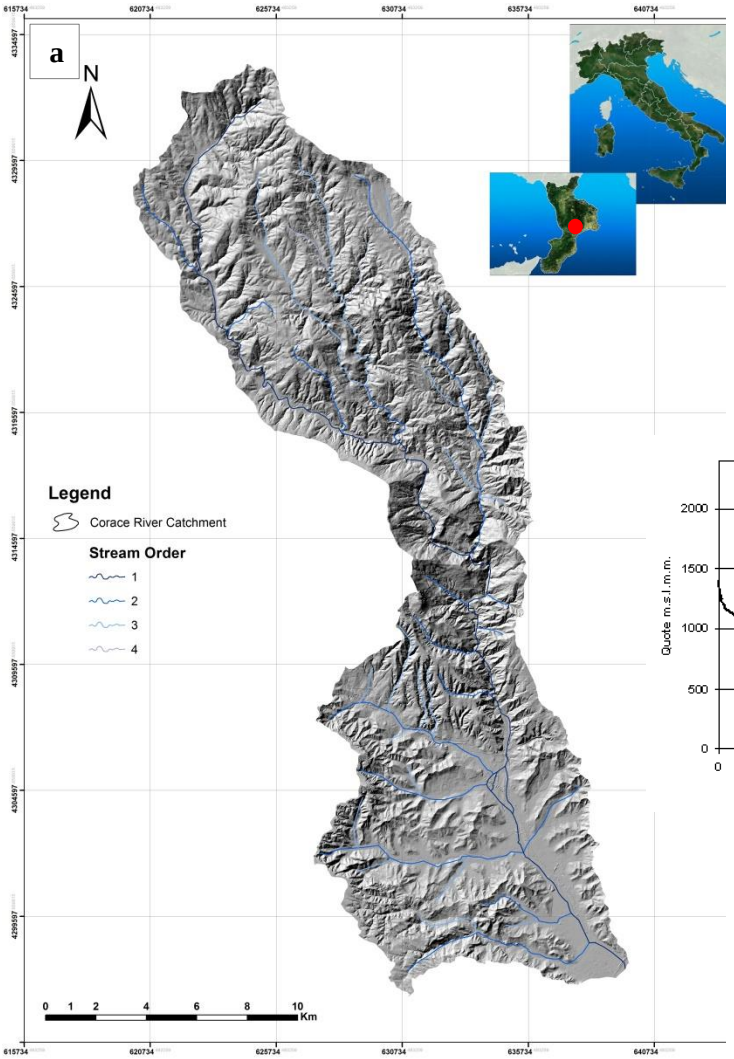

Order	Numbers	Length km
1	3110	689
2	724	277
3	158	146
4	32	59
5	6	67
6	2	22
7	1	10

b

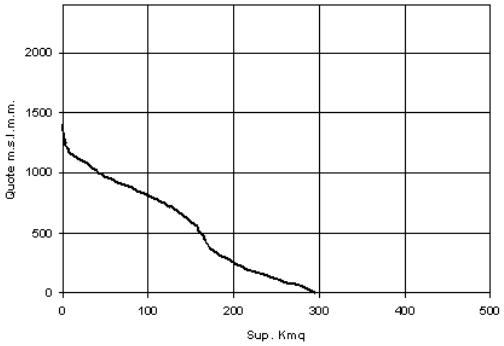

Figure 8 a-b Corace Stream is a 7th order basin and has two 6 order tributaries, 5 fifth tributaries and 32 fourth order tributaries (Tab.1). It is flanked by the Sila Piccola Massif in the North, in south, Catanzaro straight in the west, Serre Massif in the east and Ionian Sea in south. c Corace ipsometric Curve.

The morphology of the range reflects a dynamic equilibrium between present-day tectonics and surface processes.

On the southeaster portion of Gimigliano municipality a antiformal fold is recognized (Van Dijk et al., 2000; Rossetti et al., 2004). Tectonic control is also evident on south side of Gimigliano municipality in correspondence of the Melito River confluence. Some large landslides involved more erodible lithology (Fig.9).

Although also the Melito River is conditioned by the geological structure and in particular variations of erodibility in the stretch upstream of the confluence with the Corace River: this main tributary is oriented NE-SW, corresponding to a significant structural discontinuity.

Immediately downstream of the confluence with the Fosso Patrone, the Melito River cuts across the anticline structure of the area of up to the confluence with the Corace River, thereafter the main stream follows quite closely the axis of the anticline structure. Base levels on the flanks of the range

may be controlled by either the tectonics of the underlying thrust fault or by external conditions related to sediment deposition or erosion by the fluvial system.

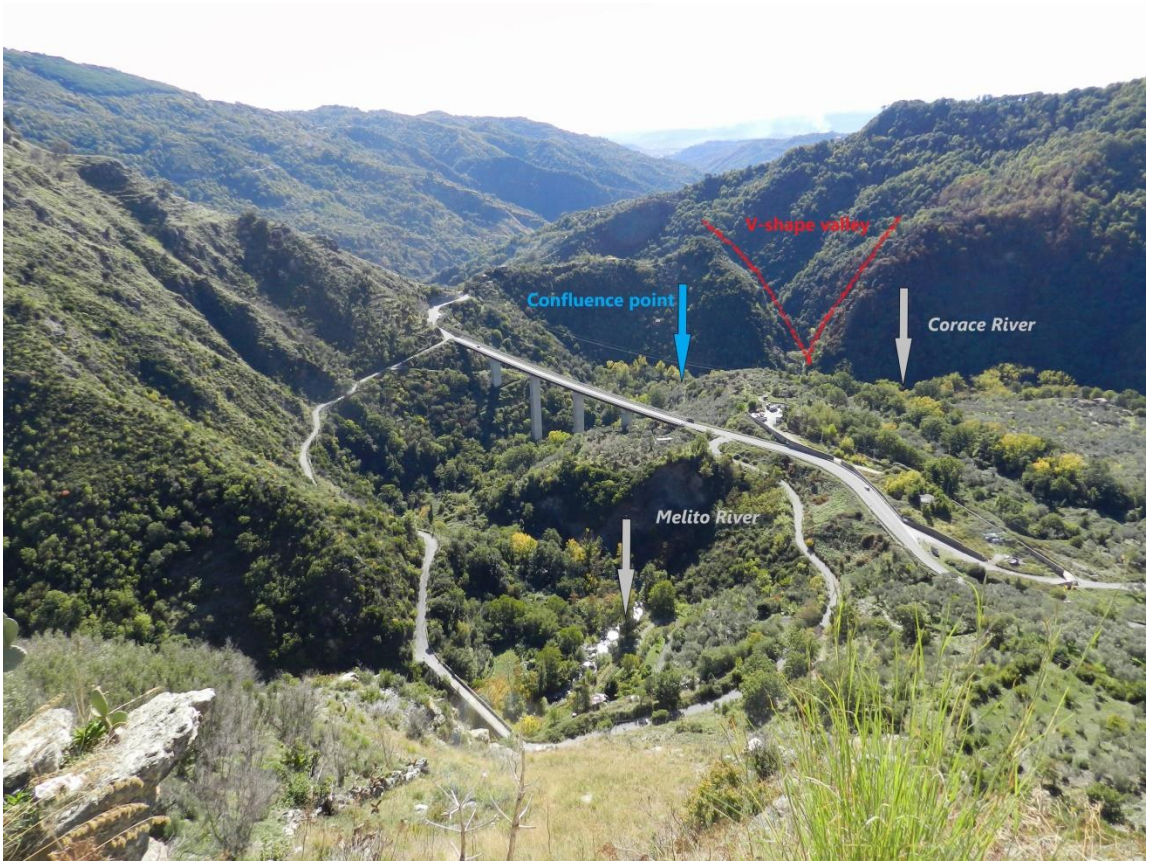

Figure 9 Tectonic control evidents on south side of Gimigliano municipality in correspondence of the Melito River confluence. Melito River is conditioned by the geological structure and in particular variations of erodibility in the stretch upstream of the confluence with the Corace River: this main tributary is oriented NE-SW, corresponding to a significant structural discontinuity.

The terraces provide good constraints on incision rates across the Monte Gimigliano frontal folds where rivers are forced to cut down into rising anticlines and have abandoned numerous terraces.

Sediment yield derived from the measurement of suspended load in the Corace River basin suggests that fluvial incision drives hillslope denudation of the landscape at the scale of the whole range.

These hydrographic and orographic phenomena unconformity is probably due to phenomena of river network superimposition. Path stream network has preserved during this first incision phase despite the possible lithostructural control.

Low gradient paleosurface that represents an old local base level was recognized at altitude reach from 600 to 650 m above sea level and the velocity and eroding power of the water was temporarily lost. This slope failures suggest a steady state of incision processes, responsible of erosion of the paleosurface.

The topographic area is 294 km^2 extended and presents an elongated shape. The upper reaches of the basin, with elevation ranging from 700 to 1000 m asl, are made up of conglomerate rocks. The gravels are constituted of metamorphic rock fragments and are highly permeable and resistant to

erosional processes. In the lower reaches the source rock lithology changes to silts clays interbedded with silty and sandy marine deposits. The Corace river-mouth is constituted of sediments varying the texture from granules to cobbles.

Carta geologica 25000 faglie idrotuttutooooo

2. Climate

The study area (Calabria region) is a peninsula in Italy (Figure 1) with a high climatic variability due to its geographic position and its mountainous nature (Buttafuoco et al., 2001a). In fact, in Calabria orography controls the rainfall amount and distribution over the region and the interaction between the orography and mesoscale circulations leads to a precipitation gradient between the Tyrrhenian and Ionian side of the Calabrian peninsula. In particular, the Ionian side, which is influenced by currents coming from Africa, has high temperatures with short and heavy precipitation, while the Tyrrhenian side is influenced by western air currents and presents milder temperatures and considerable orographic precipitation. In the inland zones there are colder winters (with snow) and fresher summers (with some precipitation) than those marking the costal zones (Buttafuoco et al., 2011b). Large-scale patterns play a role in the type of storms affecting this region; in fact, western Calabria is more exposed to storms originating in the lee of the Alps, while eastern Calabria is more exposed to African storms (originating in the lee of Atlas and propagating toward the central Mediterranean). The influence of the Azores anticyclone in summer favours a rather dry and temperate climate, while breeze circulations develop on the coast and inland. In the other seasons, Mediterranean cyclogenesis affects Calabria.

The precipitation data was prepared using the last 10 years (2006–2016) of historical rainfall data. In our methodology we used long-term precipitation for a 30 year period. An average annual rainfall contour map is mapped out from the daily rainfall data measurements. Also, the IDW method using Gis Software was used for spatial interpolation on the contour maps. IDW interpolation explicitly implements the assumption that things that are close to one another are more alike than those that are farther apart. To predict a value for any unmeasured location, IDW will use the measured values surrounding the prediction location. Those measured values closest to the prediction location will have more influence on the predicted value than those farther away. Thus, IDW assumes that each measured point has a local influence that diminishes with distance. It weights the points closer to the prediction location greater than those farther away, hence the name inverse distance weighted. The annual average rainfall depth is about 1500 mm. (Fig.10)

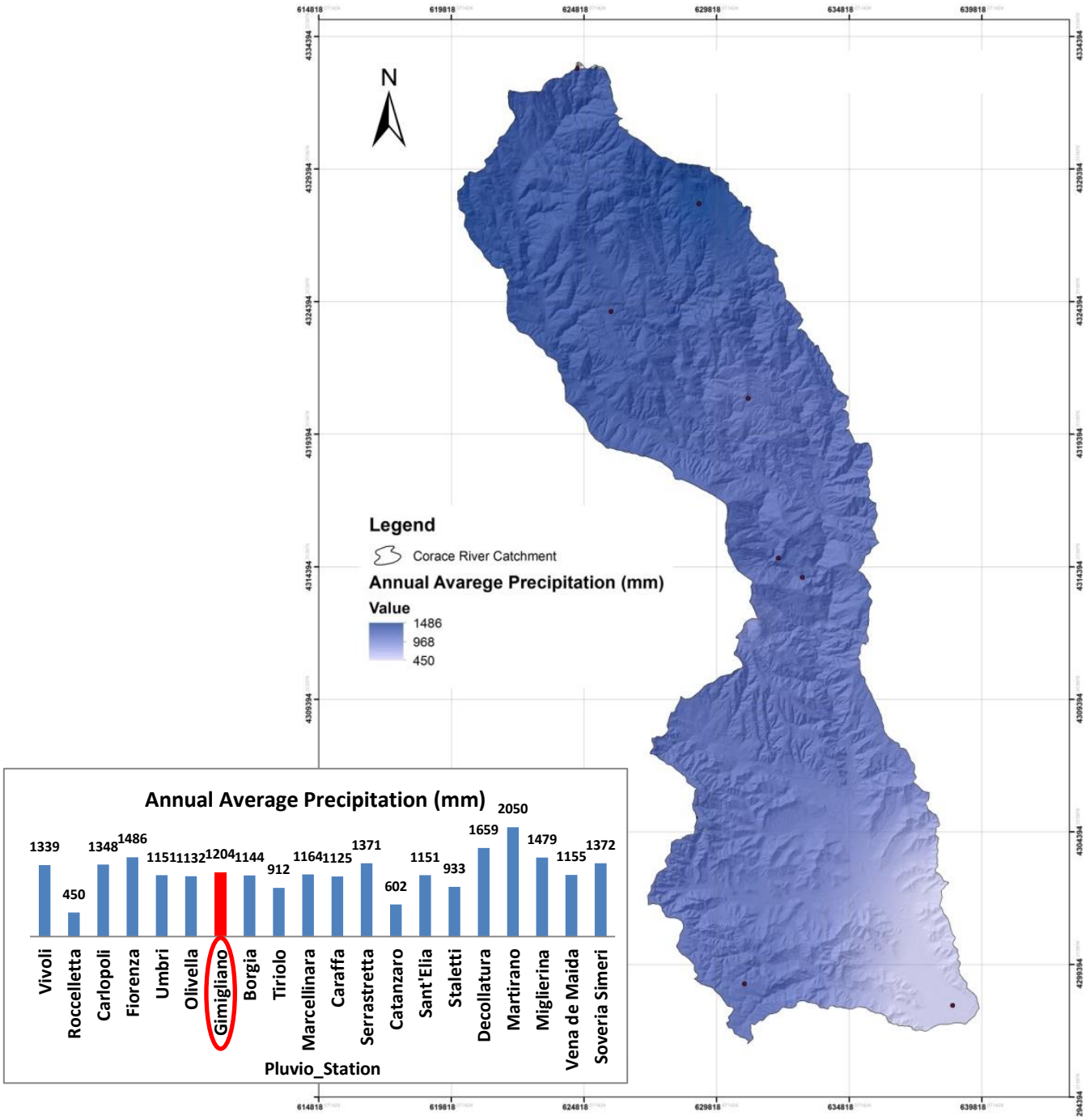

Figure 10 IDW Map of precipitation. It assumes that each measured point has a local influence that diminishes with distance. It weights the points closer to the prediction location greater than those farther away, hence the name inverse distance weighted. The annual average rainfall depth is about 1500 mm.

3. Slope Instability

Calabria Region is known as one of the most landslide-prone areas in Italy due to its geological and climatic characteristics (Antronico et al., 2001b; Antronico et al., 2013; Gullà et al., 2008; 2009).
Geomorphological survey aims to characterize geomorphological setting of a wide area in Calabria Region.
An accurate identification of unstable slopes and an exhaustive landslide inventory map based on aerial photointerpretation and conventional field geology surveying including the slope-rupture zone and the downward zone of mass accumulation was carried out.
In order to delineate geomorphological features such as scarps, landslide masses and related features an initial survey was made using 1:33.000 aerial photos from 1995 to 1998 provided by Military Geographic Institute-IGM. The field observations were plotted on a 1:10.000 topographical map and the mapped informations were digitalised and introduced into a GIS database.
A geomorphological analysis of the land morphology temporal evolution was performed through a set of aerial photographs, referred to the period from 1991 to 1994. Orthophotos analysis is exploited to identify geomorphologic evidences, soil erosion indications, anomalies or differences in vegetation coverage, allowing the possible identification and mapping of ground instabilities and land movements. Photointerpretation of optical aerial and satellite images is a traditional tool for geomorphological studies; its combination with topographic maps or DEM layers facilitates the recognition of counter slope variations as landslide indicators and the delimitation of the geometry of unstable areas.
The geomorphologic setting is characterized by widespread slope movements. Diffuse landslides with occasional deep-seated gravitational slope deformations have been recognized in the whole area. The overlap of recent and past cartographic maps evidences that area already affected by hydrogeological hazard (Fig.11 a-b).
Geological structure deeply controls geomorphological context: structural discontinuities and variation in erodibility of different lithotypes.

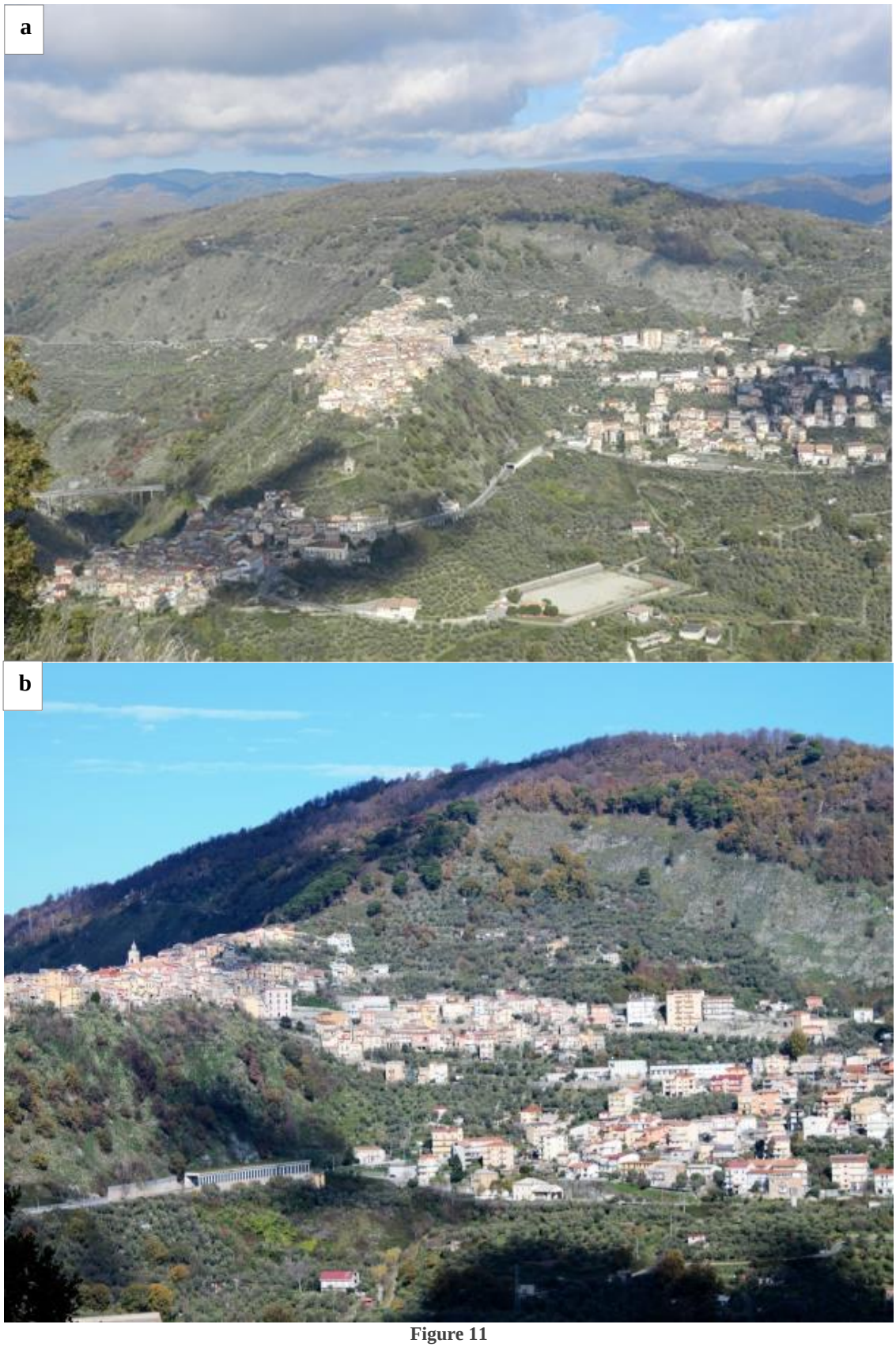

Figure 11
a. Overview of the Gimigliano landslides system.
b. The landslide on the right affects the entire town and has a translational kinematics with low rotational component. The landslide on the left shows a more pronounced rotational component.Widespread slope movements. Diffuse land sliding with occasional deep-seated gravitational slope deformations have been recognized in the whole area.

Second section

Impact Factor of Active Tectonics as determinant factor in GIS susceptibility landslide mapping

Using and developing of GIS provide a powerful tool for spatial data analysis and management in almost all the science disciplines, above all structural geology, tectonics, geomorphology, etc. GIS allows not only representing data, but also performing geostatistical analysis and building models. In geomorphology, the traditional use of GIS capabilities can be found in works that require multi-criterium analysis.

All of the analyses require the combination of different spatial data in addiction with statistical analysis. GIS is becoming a powerful tool to evaluate tectonic geomorphology and landscape evolution linked to the recent tectonics of the area. Activity of folds and faults can be assessed by the analysis of drainage network and the evaluation of geomorphic indexes. Through the application of new GIS-based methodologies for drainage network and landscape analysis it is possible to reach a better understanding of the tectonic activity and landscape evolution. The technologies that GIS provides to perform statistical analyses, as well as the great availability of high-precision DEM, have allowed the advance in the field of geomorphic indexes. It is possible to extract river networks with stream gradients and catchment areas from DEM. The analysis of drainage networks is a powerful tool to detect recent tectonic activity and uplift (e.g. Ouchi, 1985; Clark et al., 2004) as river channels are very sensitive to changes in the parameters that control their shape and gradient (e.g. Whipple and Tucker, 1999; Korup, 2006).

By means of geomorphic indices it is possible to detect landform responses to tectonics and therefore it have been broadly used to investigate tectonic geomorphology (El Hamndouni, 2008).

Active deformation that may affect the topography in this region can be quantified using geomorphic indices.

Geomorphic indices are capable of detecting landform responses to tectonics and therefore have been broadly used to investigate tectonic geomorphology (Keller and Printer, 2002; Chen et al., 2003; Kobor and Roering, 2004; El Hamdouni et al., 2008).

The present study is based on the calculation of five geomorphic indices: Hypsometric integral (Hi), Stream-length gradient index (SL), asymmetry factor (AF), drainage basin shape (Bs), valley floor width-to-height ratio (Vf) and Index of mountain front sinuosity (Smf) for seven sub-basins of the Corace river basin. All the measurements have been carried out by using drainages and contours extracted from DEM in GIS environment.

A high value of SL index near the Gimigliano municipality, expresses lithological changes in metabasites, serpentinites, and phyllites of the Liguride Complex tectonically overthrusted by metamorphic and crystalline rocks of the Calabrian Complex, such as orto- and para-gneisses. (Tansi et al., 2007) The outcropping rocks show a resistant behaviour, even if weathering throughout schistosity and jointing leads to the formation of granular layers that turn out to be meccanically soft and highly erodible. (Fig. 1).The Af index was computed for 7 selected sub-basins of third drainage network order. Higher values of Af index in the NE and NW basins of the Corace River basin correlate to tectonic activity and lithological control.The computed Hi values of the sub-basins range from 0.24 to 0.51. Specifically those sub-basins, in the southeasten part of the basin, show low Hi values. Nevertheless sub-basins with structural control show concave-convex hypsometric curves with anomalies and high integral values. The Vf index is a measure of incision and not uplift; but in an equilibrium state, incision and uplift are nearly matched. For each of the selected basin, the required valley width and height data were obtained along valley cross-sections perpendicular to the drainage basin axis to calculate the Vf. The obtained values were classified into three categories: <0.5; 0.5-1.5; 1.5-2.5;>2.5. Relatively young drainage basins in tectonically active areas tend to be elongated in shape normal to the mountain topographic slope. In the study area, northern sub-basins show moderate to high Bs values which indicate its elongated shape. On the contrary, sub-basins in the southwestern part show low Bs values. Values of Smf were readily calculated from topographic maps or aerial photography. However, the value obtained depends upon the scale.

A method to evaluate an index over an area that represents impact factor of active tectonics (IFAT) is present. The various indices are divided into three classes, with class one being high activity and class three being low activity. In order to develop an aerial index, IFAT is obtained by the average of the different classes of geomorphic indices and divided into four classes, where class 4 is very high tectonic activity class 3 is high tectonic activity, class 2 is moderately active tectonics and class 1 is low active tectonics. The proposed GIS methodology allows a map showing impact factor of active tectonics of the landscape is prodeuces . This method has been linked to landslide susceptibility mapping.

A higher frequency of landslides is related to areas with higher indexes of active tectonics in the northeaster slopes of Corace basin and most of all in the Gimigliano village. These correlations between density of landslides and active tectonics intensity, expressed by geomorphic indexes, suggest the usefulness of the integration of the active tectonics between the main determinant factors in landslide susceptibility assessment of mountain alpine areas which may be applied to similar areas around the world.

Chapter two

Analysis and evaluation of susceptibility landslide mapping

The concept of landslide “susceptibility” was originally design in the USGS to indicate “how prone to generate a landslide is a geological unit”; this can be measured from the correlation between determining factors together with the spatial distribution of the movements . The main steps for this kind of analysis were

- a collection of information about historical or antecedent events;
- compilation of a landslide inventory from field and aerial photography surveys;
- GIS (ArcGIS, ESRI) implementation using a DEM and detailed thematic maps and analysis of landslide determinant factors;
- Landslide inventory map

A landslide classification system based on Varnes (1978) was applied, whereby five basic movement types were distinguished: rockfalls; slides; debris flows; shallow and very slow creeping and solifluction. Movements were considered to be complex if they resulted from a combination of two or more of the main types. At the first the inventory map was compiled by interpretation of the 1:33.000-scale stereoscopic aerial photographs provided by IGM Military Geographic Institute, that cover a time period from 1954 to 1998.

Once the movements have been mapped, a field survey was carried out in order to verify the typology of each movement and state of activity.

Determining factors were analysed, some derived from the digital elevation model (DEM) such as altitude, slope, aspect, hillshade, curvature of the slope, and other one obtained from thematic maps, resulting from field research or from published maps such as lithology, land cover usage, average annual precipitation, proximity to flow channel and last but not least the relative active tectonic index.

Chapter three

Matrix method

The matrix method of susceptibility analysis (DeGraff and Romesburg, 1980, with GIS development by Irigaray, 1995) is a quantitative method for establishing an instability index for a given area. The modelling was performed using the matrix method (DeGraff and Romesburg, 1980) in a GIS environment (Irigaray, 1995; Irigaray et al., 1999; Fernandez, 2001; El Hamdouni, 2001), based on the determination of all the possible combinations between the types of factors considered. The resulting landslide susceptibility map of the Corace River Basin was expressed using five classes.

The ‘‘Landslide Matrix’’ was built from the inventory of rupture zones of the slope movements, calculating the surface area affected by the movements in each combination of factors. In the ‘‘Management Unit Matrix’’, the total surface area of each combination of factors was calculated. Finally, in the ‘‘Landslide-Susceptibility Matrix’’ the value of each cell was determined by dividing those corresponding to the landslide matrix by those of the management unit matrix. The landslide-susceptibility matrix values constitute the proportion of slope movements with respect to the total area and represent the relative susceptibility of each combination of factors. Finally, the values obtained are visualized showing 5 susceptibility levels (very low, low, moderate, high, very high (Irigaray, 1995) using the natural-breaks method.

The landslide susceptibility analysis was carrying out using matrix method. Furthermore, the analysis results were validated checking-out degree of adjustment between landslide inventories and resulting susceptibility classes.

The relative distribution of movements was calculated by ratio of the relationship Mi / ti in which Mi represents the area, in km2, of the observed movements lie in different levels of susceptibility and ti as well as the total area in km classified with a certain level of susceptibility (ti). The Σ mi / ti multiplied by 100 is that best defines the degree of adjustment (Baeza, 1994). When the majority of the movements are left very low or low susceptibility levels, will mean that the method does not capable of reproducing conditions of instability; On the contrary, if the majority are located at higher levels (moderate, high or very high) will indicate a better fit.

Chapter One

Impact Factor of Active Tectonics (IFAT) using geomorphic indices

Introduction

Using and developing of GIS provide a powerful tool for spatial data analysis and management in almost all the science disciplines, above all structural geology, tectonics, geomorphology, etc. GIS allow not only representing data, but also performing geostatistical analysis and building models. In geomorphology, the traditional use of GIS capabilities can be found in works that require multi-criterium analysis.

All of the analyses require the combination of different spatial data in addiction with statistical analysis. GIS is becoming a powerful tool to value tectonic geomorphology and landscape evolution, too to link recent tectonics. Activity of folds and faults can be assessed by the analysis of drainage network and the evaluation of geomorphic indexes. Through the application of new GIS-based methodologies for drainage network and landscape analysis it is possible to reach a better understanding of the tectonic activity and landscape evolution The technologies that GIS provide to perform statistical analyses, as well as the great availability of high-precision DEM, have allowed the advance in the field of geomorphic indexes. It is the possible DEM to extract river networks with stream gradients and catchment areas. The analysis of drainage networks is a powerful tool to detect recent tectonic activity and uplift as river channels are very sensitive to changes in the parameters that control their shape and gradient (Whipple and Tucker, 1999).

Landscapes in tectonically active areas result from a complex integration of the effects of vertical and horizontal motions of crustal rocks and erosion or deposition by surface processes. In a sense, many landscapes can be thought of as resulting from a competition among those processes acting to elevate the earth's surface and those that tend to lower it. The study of this competition and the interpretation of the geodynamic and geomorphic implications of such landscapes is the focus of tectonic geomorphology.

1. GIS as tool for tectonic geomorphology

Surface dynamics and tectonic geomorphology can indicate tectonic activity of a region

Gis allow performing geostatistical anlysis, building models and in this case representing and analysing drainage networks with a view to link recent tectonic activity.

GIS and DEM have greatly developed the value and efficiency of investigations into the processes of tectonics uplift.

Geomorphology studies that require multi-criterium analysis GIS capabilities can be used. All of these analysis require the combination of different spatial data and statistical analysis.

A DEM can be represented as a raster (a grid of squares, also known as a height map when representing elevation) or as a vector-based triangular irregular network (TIN). The TIN DEM dataset is also referred to as a primary (measured) DEM, whereas the Raster DEM is referred to as a secondary (computed) DEM. The DEM could be acquired through techniques such as photogrammetry, Lidar, InSAR, land surveying, etc. (Li et al. 2005). DEMs are commonly built using data collected using remote sensing techniques, but they may also be built from land surveying. DEMs are used often in geographic information systems, and are the most common basis for digitally produced relief maps. While a DSM may be useful for landscape modelling, city modelling and visualization applications, a DTM is often required for flood or drainage modelling, land-use studies, geological applications, and other applications. Digital Topographic Models (DTM) include elevation data at very different scales, bathymetry of marine basins and even data from other planets obtained in spatial mission (Luo, 2002).

GIS techniques are relatively recently in study of tectonic geomorphology and landscape evolution, The availability of DEM, has produces a great revolution in this field. Nowadays it is possible to extract river network with stream gradients, catchment areas and other value directly from DEM, allowing for better and faster analysis of topographic parameters.

2. Geomorphic indices

By means of geomorphic indices it is possible detecting landform responses to tectonics and therefore it have been broadly used to investigate tectonic geomorphology (El Hamndouni, 2008).
Active deformation that may affect the topography in this region can be quantified using geomorphic indices.
Geomorphic indices are capable of detecting landform responses to tectonics and therefore have been broadly used to investigate tectonic geomorphology (Keller and Printer, 2002; Chen et al., 2003; Kobor and Roering, 2004; El Hamdouni et al., 2008), and some indices are particularly useful for identifying relative tectonic activity.
Geomorphic indices applicable to fluvial systems in different regions and of varying size correlate with independently derived uplift rates (Kirby and Whipple, 2001) and are applicable to a variety of tectonic settings where topography is being changed (Bull and McFadden, 1977; Azor et al., 2002).
On this purpose, some geomorphic indexes were calculated in the area of Corace Basin catchment and seven sub-basins. Some geomorphic indexes of active tectonics known to be useful in active tectonic studies were selected. The present study is based on the calculation of five geomorphic indices:

- Hypsometric integral (Hi),
- Stream-length gradient index (SL),
- Asymmetry factor (AF),
- drainage basin shape (Bs),
- valley floor width-to-height ratio (Vf) and
- Index of mountain front sinuosity (S*mf*)

for seven, third sub-basins of the Corace River basin. All the measurements have been carried out in GIS environment, by using drainages and contours extracted from DEM, provided by Calabria Region.

2.1. Hypsometry and Hypsometric integral (Hi)

Hypsometry is one of the most useful parameters that describe and analyse the distribution of elevations in an area at different elevations (Strahler, 1952; Schumm, 1956) and can be estimated using the hypsometric curve or the hypsometric integral (HI).

The hypsometric curve represents the relative proportion of area below (or above) a given height (Figure 1a).

The hypsometric integral corresponds to the area below the hypsometric curve and therefore is correlated with the shape of this curve (Pike and Wilson, 1971; Keller and Pinter, 2002).

The hypsometric intergral can be approximated by means of the following equation:

$$H = \frac{mean\ elevation - minimum\ elevation}{maximum\ elevation - minimum\ elevation}$$

In this study we obtain HI values for regular squares of an analysis grid instead of values for basins and sub-basins. This way, we obtain a regular HI value distribution that is independent of basin geometry and drainage area.

HI values do not strictly represent a measure of dissection but instead represent how rapidly elevation changes within each square (van der Beek and Braun, 1998). We examine variations in the hypsometric integral for grid obtained for a drainage basin in the central Calabria, the Corace River. This river drains the sediments of the Catanzaro Strait, one of the largest half-graben of the Central Calabria. Its evolution is marked by strike-slip tectonics during the Pliocene-Lower Pleistocene time and extensional reactivation of faults starting from Middle Pleistocene.

2.1.1. Extraction of HI Values

In this study, the analysis using different digital elevation models (DEMs) of 40m and 5m of resolution was performed. Both DEMs were provided by Calabria regional government database. This model is georeferenced on a universal transverse Mercator projection using UTM WGS 84 33N. All the models were pit filled using geographic information system software generic tools in order to fill possible voids HI values was calculated for basins and sub-basins utilising DEM of 40m of resolution and also for 1 km regular squares in order to obtain a regularly spaced value distribution for the area. To obtain HI values for a grid of regular squares (analysis grid), zonal statistics over a DEM to extract maximum, minimum, and mean elevations was used. With the aid of geographic information system software, this procedure becomes almost direct. Where tectonics play an important role, HI values should follow a general trend, showing high HI value and a convex curve in lower part.

The HI values in the six cases follow a normal distribution with a mean average slightly under 0.5 The spatial distribution in each case offers a view of value distribution because of high local variations (Fig. 9; Tab.1). Nevertheless, there are similarities between HI distributions for the two different approachs.

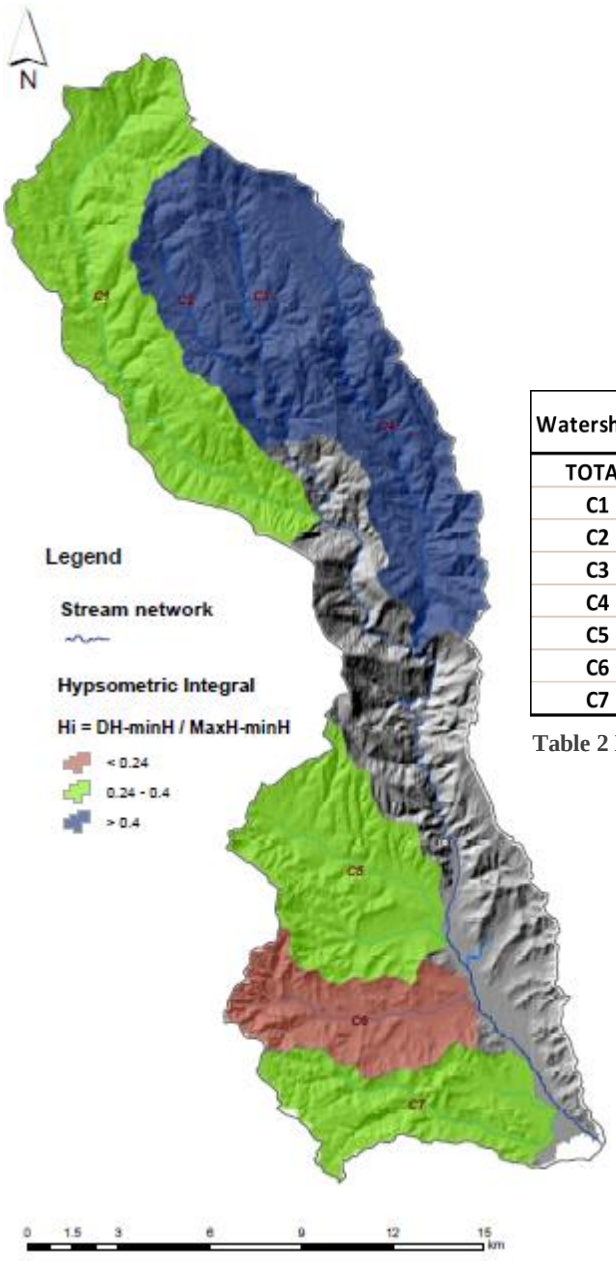

Watersheed	*H MAX*	*H min*	*H Mean*	*δ H*	*Hi*
TOTAL	1435	0	570.14	1435	**0.40**
C1	1413	551	890	862	**1.03**
C2	1333	658	979.5	675	**1.45**
C3	1435	657	1028.9	778	**1.32**
C4	1375	332	865.6	1043	**0.83**
C5	967	0	349.7	967	**0.36**
C6	660	46	614	614	**1.00**
C7	384	31	149.4	353	**0.42**

Table 2 HI value distribution in seven sub-basins.

Figure 12 HI distributions using elevation models of 5 m and for an analysis grid sizes and sub basin area.

Hypsometry is affected principally by tectonic, lithologic, and climatic factors. Masek et al. (1994) proposed a climatological effect on hypsometry by comparing two large-scale basins in central Andean plateau. Lifton and Chase (1992) pointed to the influences of lithology in the hypsometric integral at small scale (100 km2) and the influence of tectonics at larger scales (1.000 km2). They also showed, through a numerical model, that the hypsometric integral is positively correlated with

the uplift rate. Lithology are correlate with the HI values obtained for the 1 km analysis grid using the 5 m DEM. This lithologic analysis was carried out on the basis of 1:25,000 geologic maps, reclassifying and simplifying the different lithologies in 14 lithological classes in accordance with the geotechnical behaviour.

High HI values are present in the sub-basin, S and SW edges of the Corace basin and in the northern flank There are also high values in the NE corner of watershed Nevertheless, there are no high values at the mouth of the Corace River, where the capture by the Melito took place

In the NE corner of the Corace sedimentary basin, the distribution of HI values coincides with the distribution of the main active faults in this area. High HI values are concentrated in the footwall of the main active NW-SE normal faults where tectonic uplift is most active.

These normal faults have been active in the upper Pleistocene (Monaco and Tortorici, 2000; Tansi et al., 2007) and are associated with large historical earthquakes.

The high HI values in the SW corner of the Corace basin occur in the hanging wall of the separates Jurassic marls and limestones (Fig.12) from Plio-Quaternary sediments.

In the NE corner of the Catanzaro sedimentary basin, the distribution of HI values coincides with the distribution of the main active faults in this area (Fig.). Low HI values occur in regions of Holocene sedimentation in the hanging wall of the main active faults. The low HI values also coincide with the region where the shallowest earthquakes occur in the hanging wall of the main normal SW dipping faults . The convexity of the hypsometric curve is an indicator of the erosional stage of the basin (Strahler,1952). Younger less eroded basins yield convex shapes with higher hypsometric integrals. The area below the hypsometric curve portrays the amount of material left after erosion. Thus, when the curve gradient becomes higher in its upper part the amount of material left after erosion is smaller (Lou, 2000). This fact can be considered a sign of maturity of the basin, since it indicates that the lateral erosion must have been intensive in the river head (Keller and Printer, 2002).

All the curves of the eastern termination of the Catanzaro Strait were formed when the range started to develop, thus having roughly the same age. As climatic and lithologic factors are very similar in both slopes, the differences in the curves of the north and the south slopes can be attributed to tectonic factors. The southern mountain front is fault-controlled, while the norther one has no relevant faults. The faulting zone in the southern mountain front have been active during the Neogene and Quaternary, having uplift the footwall, where the catchments are located. This relative uplift is responsible for a continuous base level lowering in the rivers, thus maintain high vertical erosion rates. Therefore, the basins of the southwestern slope of Gimigliano have been suffered continuous rejuvenation processes and preserving convex profile overtime (Fig.13-14)

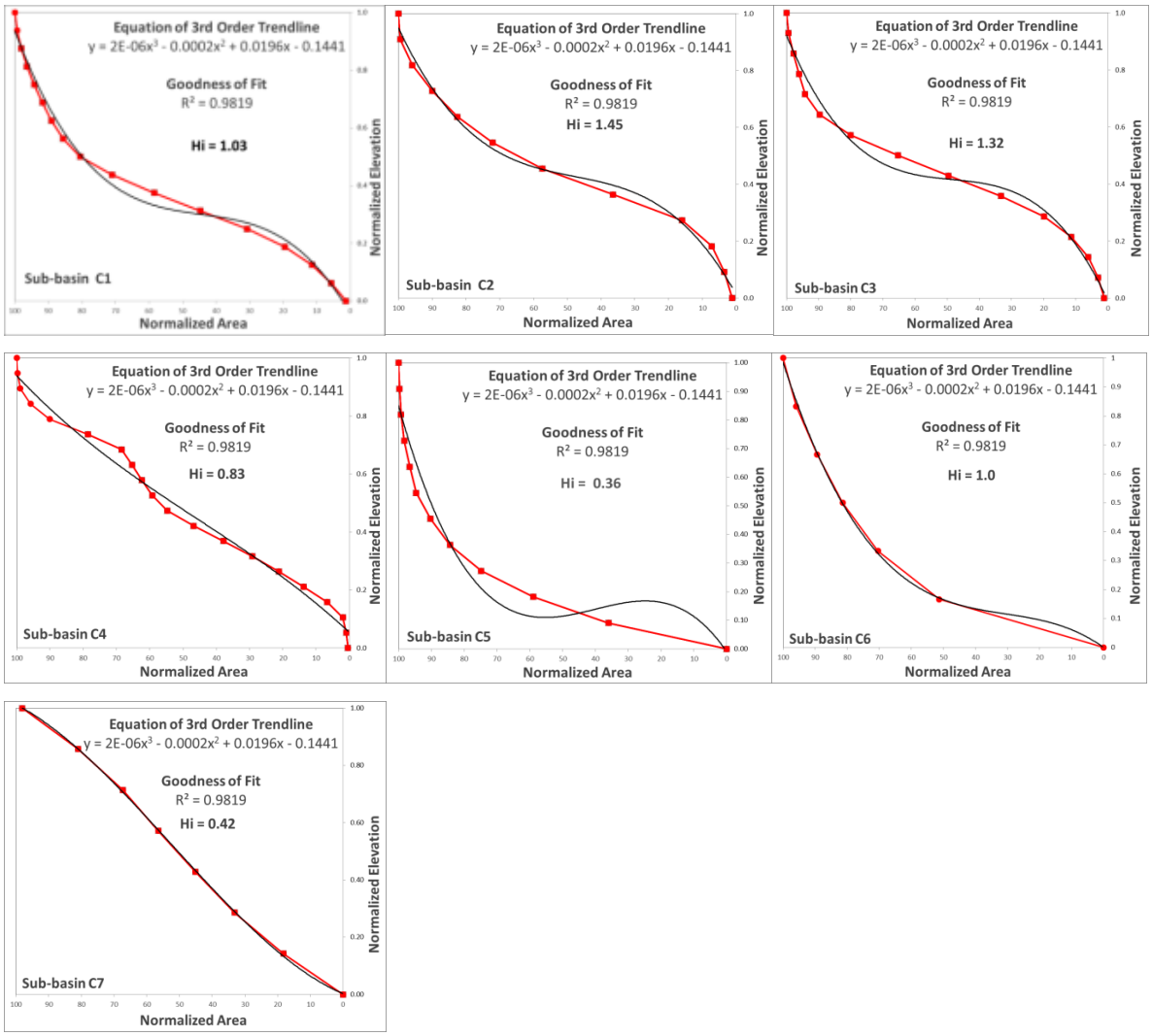

Figure 13 Sub-basins hypsometric curves, constructed in an XY scatter chart, and fit a trendline to it, based on normalized data.

All the curves present the same upper section with high gradient. The reaming sections of the curves progressively change from concave in westernmost river to convex in easternmost one. This eastward steepening in the lower sections of hypsometric curves might be related to the captures processes of the catchments previously draining to the North into the Amato River.

As this process advances over time, different curve shapes give an idea of relative chronology of this piracy process.

Assuming that lithology does not play a unique role in making differences among hypsometric curve shapes, and that climate is homogeneous all over this region, tectonic activity influences the evolution and the landform.

VALUE	COUNT	Minimum Elevation	BINS (Break Values)	BIN LABELS	FREQUENCY	Pixel Area (m2)
0	2	0m	100	1-100	23759	1600
1	7		200	101-200	25752	
2	11	Maximum Elevation	300	201-300	16352	Total Pixels
3	35	1435m	400	301-400	11338	182938
4	47		500	401-500	5002	
5	78	Input Data Range	600	501-600	8112	Total Area (m2)
6	37	A6 to A1479	700	601-700	11914	292,700,800
7	37		800	701-800	15635	
8	50	Bins Needed	900	801-900	18667	Total Area (km2)
9	80	15	1000	901-1000	17777	292.70
10	91		1100	1001-1100	13165	
11	147	Bin Interval	1200	1101-1200	10704	
12	171	100m	1300	1201-1300	3490	
13	132		1400	1301-1400	1225	
14	313		1500	1401-1500	46	

AREA BY BIN	SUM AREA	PERCENT AREA	CUM AREA IN PERCENT		Chart X	Chart Y
38014400	292700800	12.987	12.987		12.987	0.000
41203200		14.077	27.064		27.064	0.071
26163200		8.939	36.003		36.003	0.143
18140800		6.198	42.201		42.201	0.214
8003200		2.734	44.935		44.935	0.286
12979200		4.434	49.369		49.369	0.357
19062400		6.513	55.882		55.882	0.429
25016000		8.547	64.428		64.428	0.500
29867200		10.204	74.632		74.632	0.571
28443200		9.717	84.350		84.350	0.643
21064000		7.196	91.546		91.546	0.714
17126400		5.851	97.397		97.397	0.786
5584000		1.908	99.305		99.305	0.857
1960000		0.670	99.975		99.975	0.929
73600		0.025	100.000		100.000	1.000

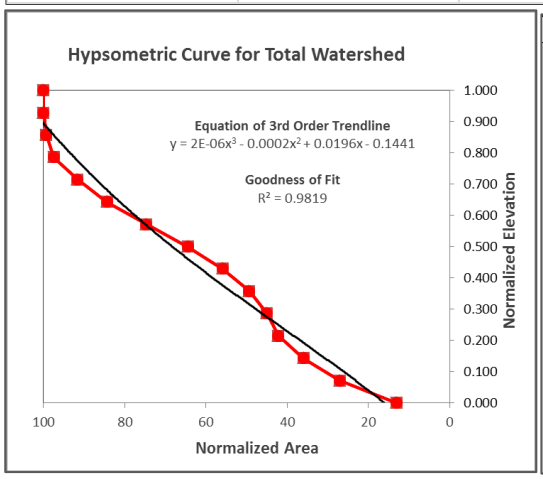

Normalizing Binned Values (only Elevation shown here)			
A = MinValue =>	100	Input x Values	Normalized Elevation
B = MaxValue =>	1500	100	0.000
a = Norm Scale Min =>	0	200	0.071428571
b = Norm Scale Max =>	1	300	0.142857143
B-A =>	1400	400	0.214285714
b-a =>	1	500	0.285714286
Normal. Formula =>	(x-A) / (B-A)	600	0.357142857
Formula interp =>	(x-min) / (range)	700	0.428571429
		800	0.5
		900	0.571428571
		1000	0.642857143
		1100	0.714285714
		1200	0.785714286
		1300	0.857142857
		1400	0.928571429
		1500	1

Figure 14 This assignment will test and build Excel skills oh Hypsometry. Elevation VALUE column contains DEM pixel values extracted from a single watershed. Pixel COUNT column contains the number of pixels at that same elevation in the watershed. Through a series of calculations in Excel, it will bin the data, generate hypsometric values, create a few summary statistics, convert some values.

First two columns came from .dbf export of filled DEM (integer). VALUE column is elevation in Meters. COUNT column is the number of pixels at the corresponding elevation.

BINS Break Value Using a 100m bin interval, It is needed 15 bins to cover the range of elevation data (0m-1435m). Each bin is defined by its upper limit.

BIN LABELS Labels for bin ranges.

FREQUENCY Number of pixels contained in each bin. Drag-highlight the cells in the COUNT column corresponding to the first bin range.

AREA BY BIN. The area (m2) for each Bin of elevation data by multiplying pixel area by pixel count in the bin. DEM has pixels that are 40m x 40m in size, thus area for a single pixel = 1600m2. Converting from m2 to km2 requires dividing by one million.

SUM AREA Sum of AREA by BIN values, which will be used for normalization. This value is the total area of the watershed in m2.

PERCENT AREA of bins CUM AREA IN PERCENT Cumulative, normalized area data for the watershed.

2.2. Stream Length (SL)

SL is one of the most broadly used geomorphic index to characterizes active tectonics. It is strongly dependent on stream length. The SL index shows the variation in stream power along the river reach. This index is very sensitive to changes in channel slope, thus allowing the evaluation of recent tectonic activity and/or rock resistance.

The SL index in a river reach is defined as follows (Hack,1973):

$$SL = \frac{dh}{dl} L$$

where ***dh/dl*** is the slope (***dh*** is the change in elevation and ***dl*** is the length of the reach) and ***L*** is the channel length upstream from the midpoint of the reach to the river head.

This geomorphic index is very sensitive to changes in lithology and/or tectonic uplift. Most of studies were based on comparisons of SL profiles along different rivers. However, the fact that the SL index is strongly influenced by river length makes comparing SL values in rivers of different length difficult.

Several locations along the head water regions of the river basin show anomalous SL values where the river crosses the fault planes, but in the downward part of the river, SL values are found to be distributed uniformly. The SL Index analysis was performed using 1:10.000 topographic maps and following Hack's (1973) method.

SL Index is used to detect recent tectonic activity by identifying anomalously high index values on a specific rock type.

The whole dataset was collected calculating the values along longitudinal profiles of the third order stream network and relative watershed, for 100 m long reaches, from the divide towards the valley floor. The dataset obtained was georeferenced and processed with GIS software in order to obtain a map by using zonal statistic interpolation (Tab.5). A map, with a resolution of 1 Km, was produced to show the spatial distribution of the SL parameter. In the SL Index map the values are grouped in 9 classes. The anomalous SL values that are observed in uniform lithological conditions maybe are due to tectonic activities according Keller and Pinter (2002).

The SL index value increases as rivers and streams flow over an active uplift, and had lesser values when they are flowing parallel to features such as valleys produced by strike-slip faulting.

A high value of SL index also expressed lithological changes in metabasites, serpentinites, phyllites, orto- and para-gneisses. The outcropping rocks show a resistant behaviour, even if weathering throughout schistosity and jointing leads to the formation of granular layers that turn out to be meccanically soft and highly erodible.

Calulated Slope	Average Slope	REACH LENGHT	CUM LENGHT	HALF L (m)	LENGHT (L) (m)	Elev MAX	Elev min (m)	Delta h (m)	SL
13.5	0.135	238.7	238.7	119.4	119.4	915.0	900.0	15.0	**16.1**
7.6	0.076	824.2	1062.9	412.1	650.8	900.0	850.0	50.0	**49.5**
3.9	0.039	1983.0	3046.0	991.5	2054.4	850.0	800.0	50.0	**80.1**
4.7	0.047	3469.7	6515.7	1734.9	4780.8	800.0	750.0	50.0	**224.7**
7.1	0.071	3693.1	10208.8	1846.5	8362.2	750.0	700.0	50.0	**593.7**
7.6	0.076	3641.2	13849.9	1820.6	12029.3	700.0	650.0	50.0	**914.2**
5.5	0.055	4398.19	18248.1	2199.1	16049	650	600	50	**882.696**
6.8	0.068	3906.77	22154.9	1953.39	20201.5	600	551	49	**1373.7**

x-DISTANCE	SLOPE(S)	REACH LENGHT (m)	CUM LENGHT (m)	HALF L (m)	LENGHT (L) (m)	Elev MAX (m)	Elev min (m)	Delta h (m)	SL
			0						0
2420	0.009979841	3507.07	3507.07	1753.535	4173.535	185	150	35	41.65
2420	0.033181142	1506.88	5013.95	753.44	6680.51	150	100	50	221.67
2420	0.021112101	2368.31	7382.26	1184.155	8618.105	100	50	50	181.95
2420	0.015003244	2666.09	10048.35	1333.045	11135.305	50	10	40	167.07

Table 3 SL value from C1 Sub.basin.

Longitudinal profiles – SL Index in sub-basin C1

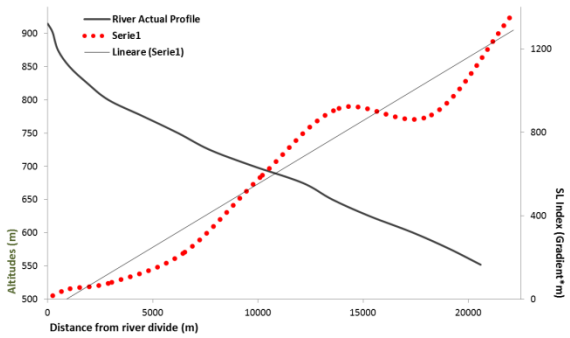

Longitudinal profiles – SL Index in sub-basin C2

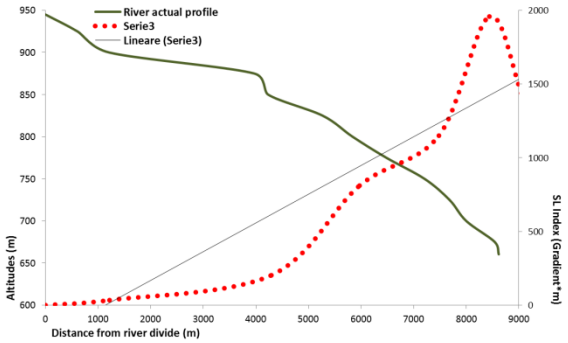

Longitudinal profiles – SL Index in sub-basin C3

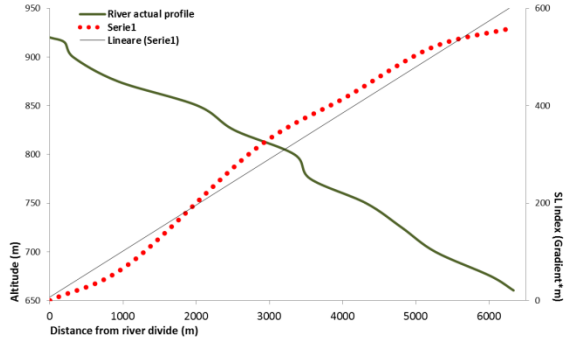

Longitudinal profiles – SL Index in sub-basin C4

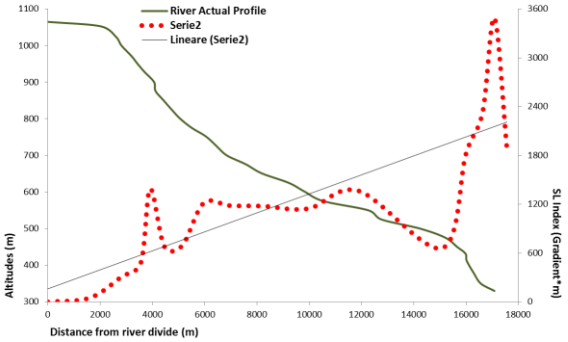

Longitudinal profiles – SL Index in sub-basin C5

Longitudinal profiles – SL Index in sub-basin C6

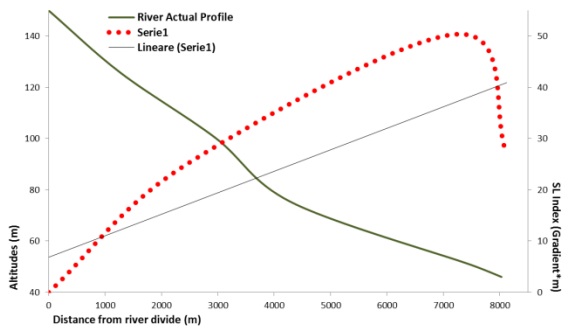

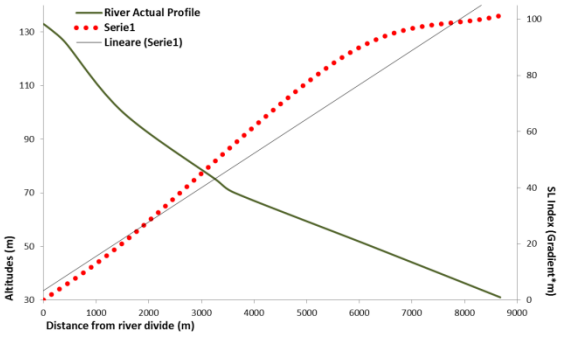

Longitudinal profiles – SL Index in sub-basin C7

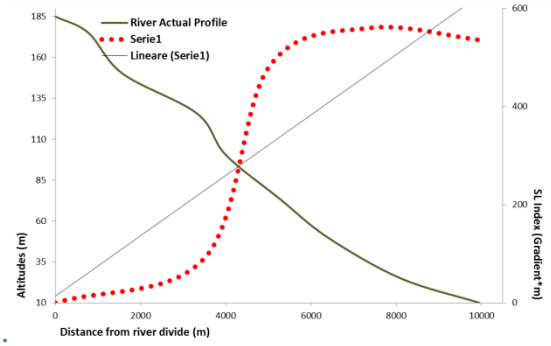

Table 5 Longitudinal river profiles in the NE border of Catanzaro Straight and the measured SL index

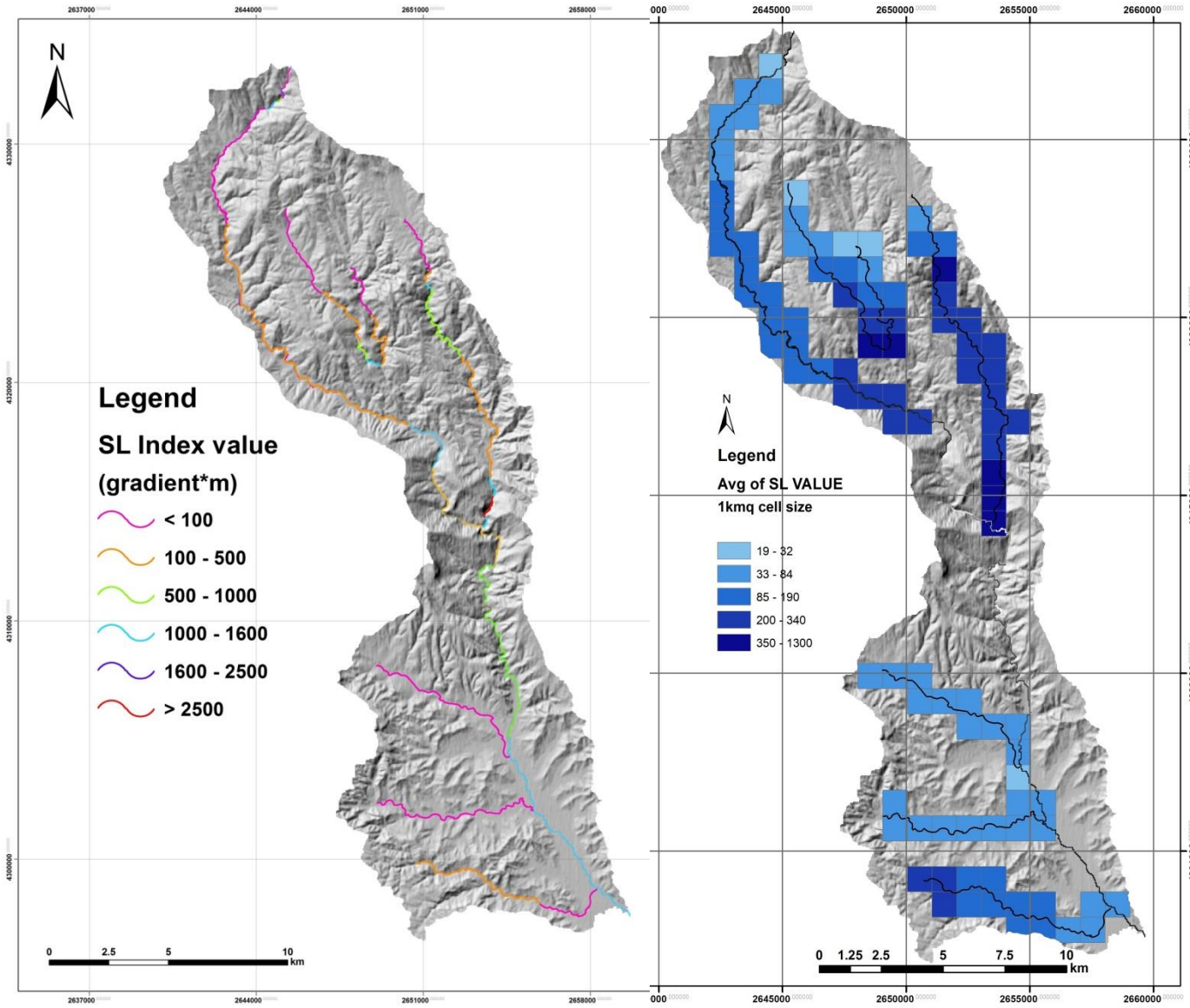

Figure 15 SL Index map and its relative anomalies

In detail, the highest values are located along both flanks of the Gimigliano town, where the SL (Fig. 15; Tab 3-5). Index reaches the maximum value of 440m in correspondence with a deep seated landslide affecting its south and north-eastern slope. Anomalous high values are also recorded along the middle sector of the Melito River.

Immediately downstream, the SL Index values increase to approximately 300 m in correspondence with a NW–SE trending fault and landsliding.

2.3. Index of drainage basin shape (Bs)

The index reflects differences among Relatively young elongated drainage basins with high values of Bs associated with relatively higher tectonic activity, and more circular basins with low values

generally associated with low tectonic activity. The elongated shapes are transformed into circular basins, as tectonic activity reduces with time and continued topographic evolution (Bull and McFadden, 1977)

Horizontal projection of basin shape may be described by the elongation ratio, Bs (Cannon, 1976; Ramírez-Herrera, 1998) expressed by the equation:

$$Bs = Bl/Bw$$

where Bl is the length of the basin measured from the headwater to the mouth and Bw is the width of the basin measured at its widest point.

Rapidly uplifted mountain fronts generally produce elongated, steep basins; when the tectonic activity is diminished or ceases, widening of the basins occur from mountain front up (Ramírez-Herrera, 1998).

The values of basin shape (Bs) vary greatly among basins. The low value of Bs in basins 1 and 9 (1.32 and 1.22 respectively) shows the relatively circular shape of mentioned basins. The highest value of Bs is associated with basin 4 where its length is 4.76 times longer than its maximum width. Basins 10, 8, 13, 11 and 5 have high values of Bs indicating elongated basins: here, drainage basin widths are much narrower near the mountain front.

The basin length to mean width ratio (Bl/Bmw) is also low in basins 1 and 9 (1.56 and 1.37 respectively) demonstrating their circular shape. The high values of Bl/Bmw ratio in basins 4, 10, 8, 6 (8.29, 4.9, 4.71 and 4.15 respectively) show the higher length compared to mean width of mentioned basins. Here the energy of the stream has been directed primarily to down cutting.

The Bl/Bmw ratio in other basins ranges from 2 to 4 implying the less elongated shapes.

Therefore, Bs may reflect the rate of active tectonics. Bs was computed using the 5 m resolution DEM and classified into three classes (from lower values to higher):

class 3 (1.77e3.22); class 2 (1.21e1.76) and class 1 (1.11e1.20). Bs ranges from 1.11 (sub-basin 18) to 3.22 (sub-basin 7). The distribution of the values were computed in GIS, with raster grid network of 10 km regular square, using Raster Interpolation Tools. (Fig. 18; Table 4 a-b).

More than two-thirds of the studied sub-basins belong to classes 1 and 2 and are elongated with higher Bs values as compared to class 3 with less Bs values and are nearly circular shapes All the sub-basins of class one are located at the middle part except two sub-basins (Nr. 6 & 2) which lie in the downstream part of the basin. About 90% of the studied sub-basins belong to classes one and two and are elongated with higher Bs values as compared to those belong to class three (which show less Bs values and are nearly circular in shape).

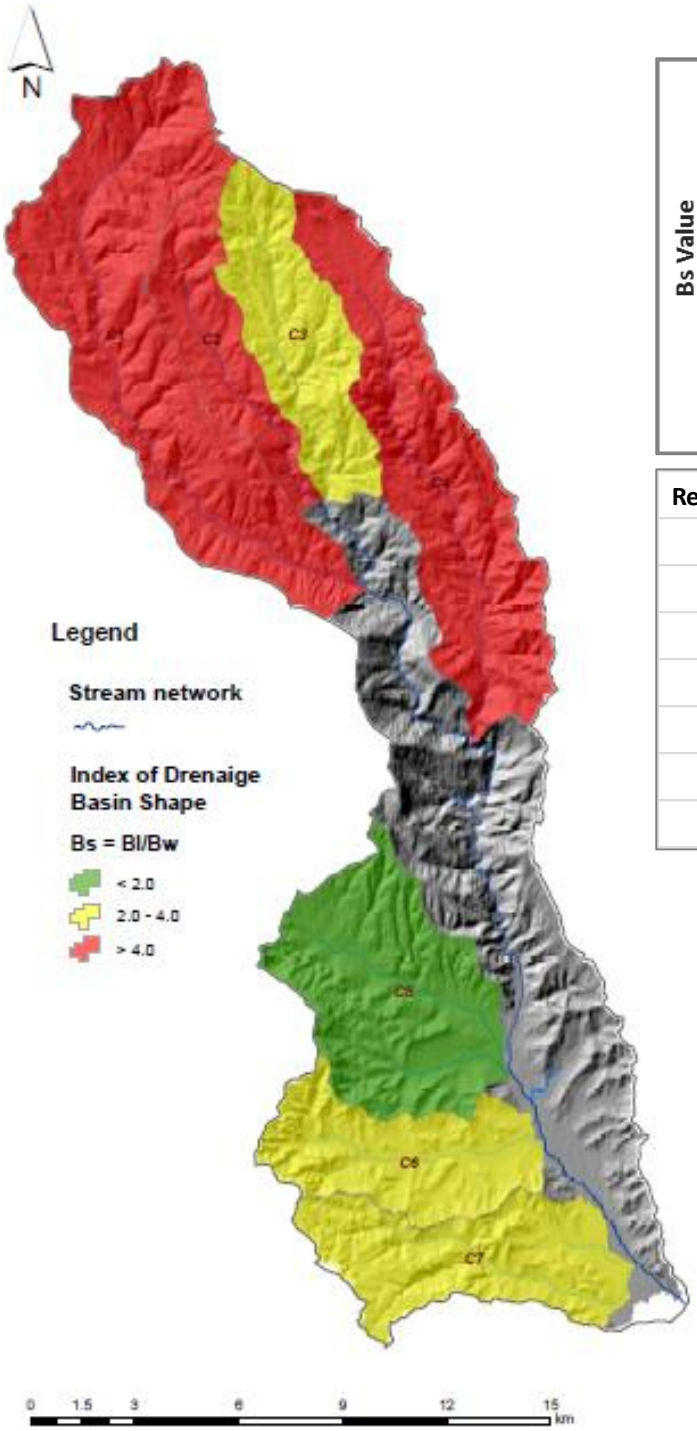

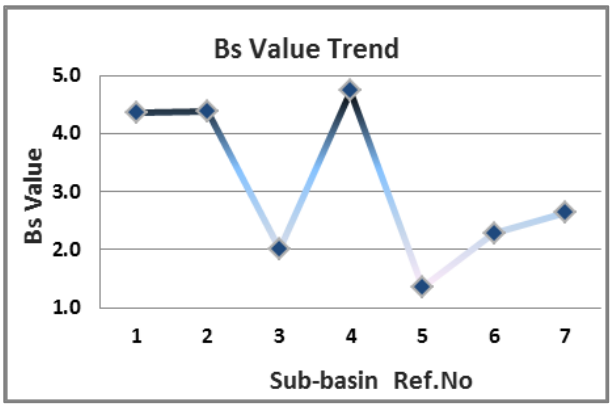

Ref. No.	Bl (m)	Bw	Bs	Class
1	22154.88	5090.1302	**4.35**	**3**
2	9084.817	2072.2888	**4.38**	**3**
3	6318.66	3148.6428	**2.01**	**2**
4	17558.75	3708.949	**4.73**	**3**
5	8164.907	6023.7425	**1.36**	**1**
6	9107.719	3988.9848	**2.28**	**2**
7	10048.35	3804.3614	**2.64**	**2**

Figure 16 Bs Index Map.

Table 6 a-b Value of Bs (drainage Basin shape index) in the analysed basins or sub-basins (Bl: length of the basin measured from the headwaters to the mouth; Bw: width of the basin measured at its widest point.

2.4. Asymmetric Factor *AF*

The asymmetric factor (*Af*) of catchments was used to detect possible tectonic tilting at the scale of the whole range. The Af (Keller and Pinter, 2002) is defined as :

$$Af=Ar/At\ 100$$

where Ar is the area of the basin to the right (facing downstream) of the trunk stream and At is the total area of the drainage basin.

If a basin has developed under a stable conditions with little or no tilting, the Af is close to 50; on the contrary, values of Af above or below 50 indicate that the basin is asymmetric and mat result from basin tilting, either from active tectonics or lithologic structural control differential erosion.

In order to avoid possible confusions among the catchments tilted on right or left downstream side, Af values were expressed as |Af-50|, which represent the amount of difference between the neutral value of 50 and the observed values, in absolute value.

In order to evaluate distribution *AF* absolute values were interpolated in a network grid of 1 km regular square divided in three classes; from values that represent symmetric basins to values that represent strong asymmetric basins, for the whole area, sub-basins, and to evaluate ….

In this case study it ranges from 0.1 to 16.6 (Fig.19, Tab 7).

Thus, in the study area Af values in the northeast portion present a pattern with contrary asymmetries at both sides of Corace River (main stream network), then coincide in with the …

In the south part there is not defined pattern in Af values one of the sub-basin, C5, is almost symmetric, the last two are gentle asymmetric, with Af value 6.8.

Structural control of the schistocity orientation or bedding may play a significant role in the development of basin asymmetry. Inclination of schistocity or bedding allows for preferred migration of the valley in the down-dip direction, producing an asymmetric valley. In order to incorporate this influence, it was ignore those values for which rock structure is an obvious factor.

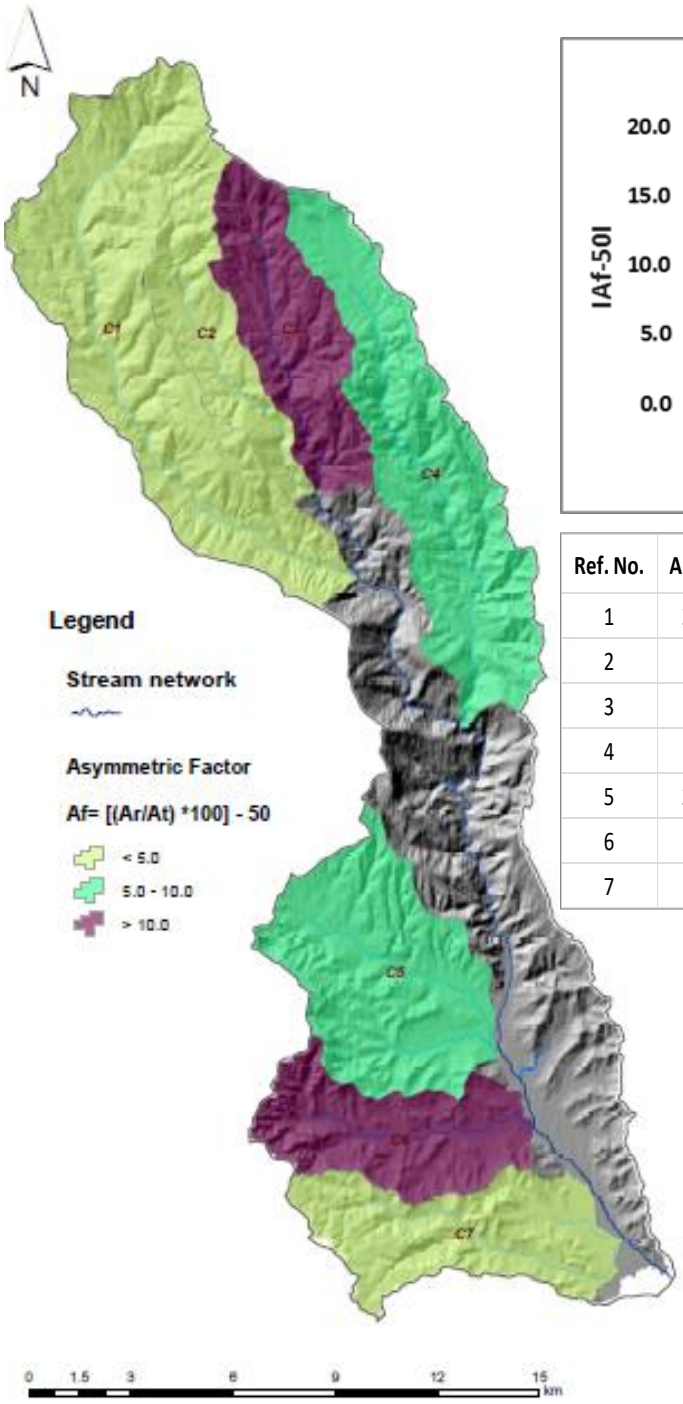

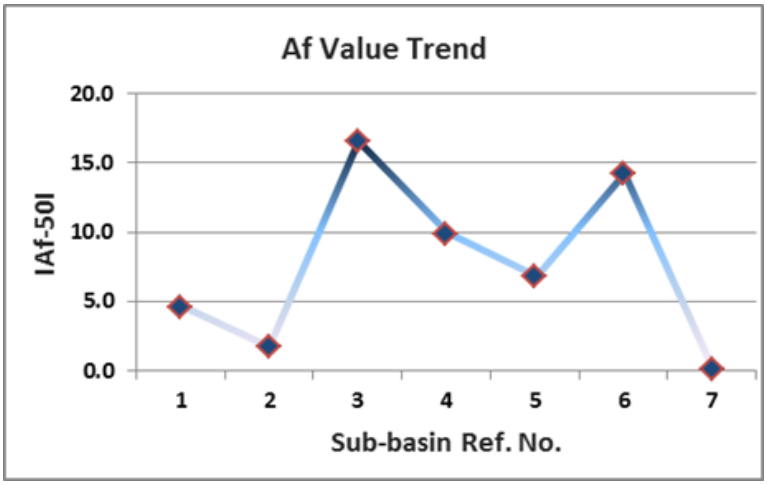

Ref. No.	Ar (km²)	At (km²)	Af	|Af-50|	Lithological control	Class
1	26.50	58.39582	45.4	**4.6**	no	**3**
2	8.32	16.08145	51.7	**1.7**	no	**3**
3	7.72	23.09691	33.4	**16.6**	no	**2**
4	16.63	41.47968	40.1	**9.9**	no	**2**
5	20.11	35.37394	56.8	**6.8**	no	**2**
6	14.54	22.63492	64.2	**14.2**	no	**1**
7	12.78	25.62049	49.9	**0.1**	no	**3**

Figure 17 Af Index Map

Table 7 Asymmetry factor (Af) values of the different basins of the study area. (Ar: surface of downstream right margin of the basin; At: total surface of the basin. Af-50 is Af absolute value minus 50, that represent no tilting value.

2.5. Valley floor width-to-height ratio (Vf)

The Valley floor width-height (*Vf*) ratio tells a few things about a mountain range front.

Historically used to differentiate between valleys carved by glaciers (broad, U-shaped) and those carved by streams (tight, V-shaped), this particular geomorphic index is now used by some to identify portions of a range front that experience more tectonic activity than others.

Imagine, for example, a range front untouched by glaciers and exposed to the same climate along its length. Now, suppose that this range front is structurally-controlled, and that the bounding fault(s) are thought to be active.

Faster uplift requires higher concomitant incision. Hence, slow moving or tectonically inactive portions of a range front will tend to have broader, shallower valleys, and faster, active portions will tend to have narrower, deeper valleys.

Effectively, these data may be obtained by:

- constructing a topographic cross section across each valley in question
- taking the highest elevation on right and left side
- taking the lowest elevation (the valley floor)
- measuring the width of the valley floor, in between where topography starts to noticeably slope upwards on either side

Narrow, deep valleys will have lower values for *Vf*. Broad, shallower valleys will have larger values.

I've tried to come up with a method to automatically do this on a larger scale in GIS, but calculation of this particular metric appears to be relatively simple and quick. Additionally, *Vf* doesn't seem to have a terribly great significance on a huge scale.

The Valley Width-to-Height Ratio (*Vf*) allows comparison of erosional patterns between watersheds. V-shaped valleys are common in areas of active uplift and deep, linear stream incision (low Vf values, often close to 0). U-shaped valleys are representative of formerly glaciated or tectonically stable areas where stream valley bottoms tend to be wider (higher Vf values).

The Valley Width-to-Height Ratio (*Vf*) allows comparison of erosional patterns between watersheds. In this case sub-basins are the unit of measure; one *Vf* value per each watershed.

This index is defined as:

$$Vf = 2Vfw/[(Eld - Esc) + (Erd - Esc)]$$

Where *Vf* is the ratio of valley floor width to valley heigh; *Vfw* is the width of the valley floor; *Eld* is the elevation on the divide on the left side of the valley; *Erd* is the elevation of the right side and *Esc* is the average elevation of the valley floor.

The four inputs to the index are acquired from a DEM and/or aerial photos. Data is collected at a single cross section for each drainage.. Because uplift is associated with incision, the index is thought to be a surrogate for active tectonics where low values of Vf are associated with higher rates of uplift; but in an equilibrium state, incision and uplift are nearly matched.

The obtained values were classified into three categories: <0.5; 0.5-1.5; 1.5-2.5;>2.5. Relatively young drainage basins in active tectonic areas tend to be elongated in shape normal to the mountain topographic slope. For each of the selected basin, the requisite valley width and height data were obtained along valley cross-sections perpendicular to the drainage basin axis and calculated the Vf (Figure 6). The values were classified into three categories: Vf≤0.39 class 3; Vf >0.55 Vf<1.05 class 2; and Vf >1.2. class1 (Tab. 8 a-b).

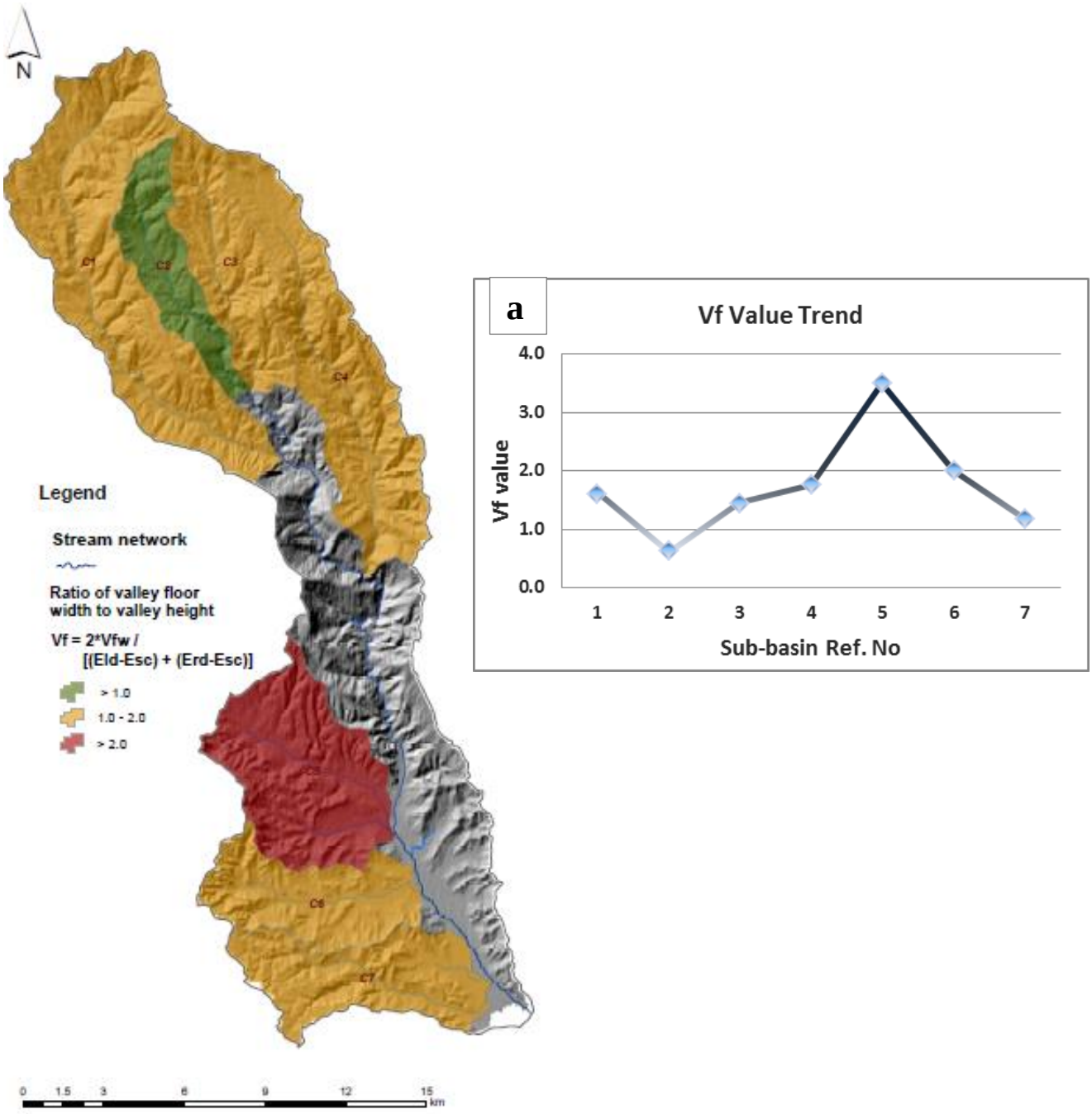

Figure 18 Vf Index Map

Ref. No	Lithology of the valley floor	Basin square (km2)	Vf	Vfw	Eld	Erd	Esc	Class
C1	Schistos and phyllites	58.40	1.6	120	785	865	750	2
C2	Schistos and phyllites	16.08	0.6	140	980	1090	808	1
C3	Schistos and phyllites	23.10	1.4	200	948	890	780	2
C4	Scisti e filladi, gneiss, Conglomerates and sandstones	41.48	1.8	50	810	805	779	2
C5	Argille,Sabbie e Arenarie	35.37	3.5	577	340	250	130	3
C6	Clay and sandstones	22.63	2.0	420	290	240	55	2
C7	Clay and sandstones	25.62	1.2	150	210	250	101	1

Table 8 a – b Vf Value Distribution.

2.6. Mountain front sinuosity (Smf)

The S*mf* index reflects a balance between the tendency of stream and slope processes to produce an irregular (sinuous) mountain front and vertical active tectonics that tends to produce a prominent straight front. Thus, mountain fronts associated with active uplift are relatively straight, but if the rate of uplift is reduces or ceases, erosional processes will begin to form a sinuous front that becomes more irregular with time.

When the values of S*mf* are low, suggesting active tectonics, whereas high values suggest relative tectonic stability.

Mountain front sinuosity, like stream gradient index, sl, is a valuable reconnaissance tool whe evaluating effects of active vertical tectonics. The S*mf* index is particularly attractive because it can be quickly and easily measured from aerial photographs, satellite imagery, or topographic maps.

This index has been used to evaluate the relative tectonic activity along mountain fronts (Bull and McFadden, 1977; Keller and Printer, 2002; Silva et al., 2003). In active mountain fronts, uplift will prevail over erosional processes, yielding straight fronts with low values of S*mf* . On the contrary, in less active fronts the erosional processes will generate irregular sinuous fronts, with high values of S*mf* index lower than 1.4 are indicative of tectonically active fronts, while values higher than 3 are related to inactive fronts (Keller, 1986; Silva et al.,2003). Theoretically, if S*mf* is close to 1, mountains fronts show straight that associated with active tectonic and uplift (Keller and Pinter, 1996).

Bull (1977) defined Mountain-front sinuosity S*mf* as:

$$Smf = Lmf / Ls$$

Fig

3. Evaluation of Impact Factor of Active Tectonics (IFAT)

These studies focused the assessment of active tectonics. Some previous studies on relative tectonic activity based on geomorphic indices tends to focus on a particular mountain front or area (Bull and McFadden, 1977; Rockwell et al., 1985; Azor et al., 2002; Molin et al., 2004) and not an aerial regional assessment of active tectonics. In this case six geomorphological parameters were used to evaluate the impact of active tectonics in a wider area, considering also mountain fronts. The average of the six measured geomorphic indices was used to evaluate the distribution of Impact Factor of Active Tectonics into Corace River Basin.

The values of the index were divided into four classes to define the degree of active tectonics: 1—low (1.0≤Iatb1.5); 2—moderate (1.5≤Iatb2.0); 3—high (2.0≤Iatb2.5); and 4—very high (2.5≤Iat), as showed in Figure 21 and Figure 22.

In order to evaluate the landscape in terms of potential impact factor of tectonic activity, indices along a particular mountain front or area are discussed and a judgment. (Bull and McFadden, 1977; Rockwell et al., 1985; Azor et al., 2002; Molin et al., 2004).

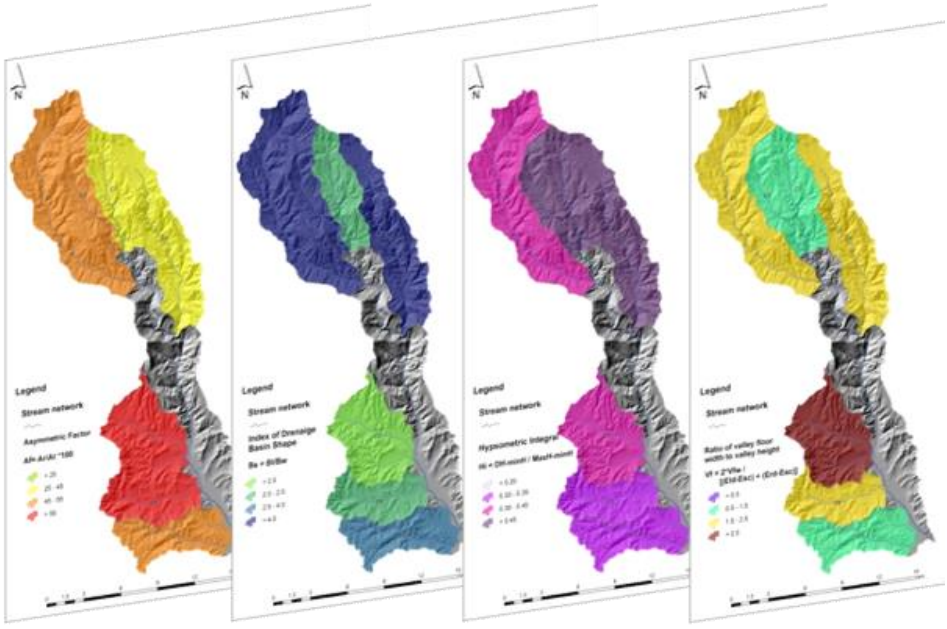

Figure 19 Merging of each index maps.

Previously indices calculated were divided into three classes, arbitrarily with class one being low activity and class three being high activity. The boundaries of the various classes change for what index is being evaluated; and for this purpose boundaries have been selected generally agree with changes in the range of the values of the various indices.

The distribution of the four classes is shows the result of the classification for each sub-basin. About 1% of the study area (about 50 km2) belongs to Class 1; 20% (1050 km2) to Class 2; 67% (3580 km2) to Class 3; and 12% (660 km2) to Class 4.

The high class values (HIGH tectonic activity) for IFAT mainly occur in the north to northwest of the basin area while the rest of the study area has classes of IFAT suggesting moderate to high tectonic activity.

The distribution of the indices describes areas associated with different mountain fronts and suggests a import role of tectonic activity. Within the study area, about 45% (201 km2) is class 1 (very high relative tectonic activity) as measured by IFAT; 22% (99 km2) shows high relative tectonic activity as measured by IFAT (class 2); 12% (53 km2) has moderate values of tectonic activity in terms of IFAT (class 3); and 21% (96 km2) has the lowest values of relative tectonic activity (class 4) based upon IFAT (Fig.22)

Thus, two-thirds of the study area is classified into classes 2 or 1 of high to very high tectonic activity in terms of the apparent geomorphic response. In different tectonic environments with greater rates of active tectonics, the values of indices would differ as well as their range in value.

However, the methodology we outline would provide an index based on area that estimates relative tectonic activity as it has for the study area in Catanzaro Basin.

A map showing relative tectonic activity of the landscape it was produced. This method has been linked to landslide susceptibility mapping (El Hamdouni, 2001) in this landscapes with widespread evidences of recent active tectonics.

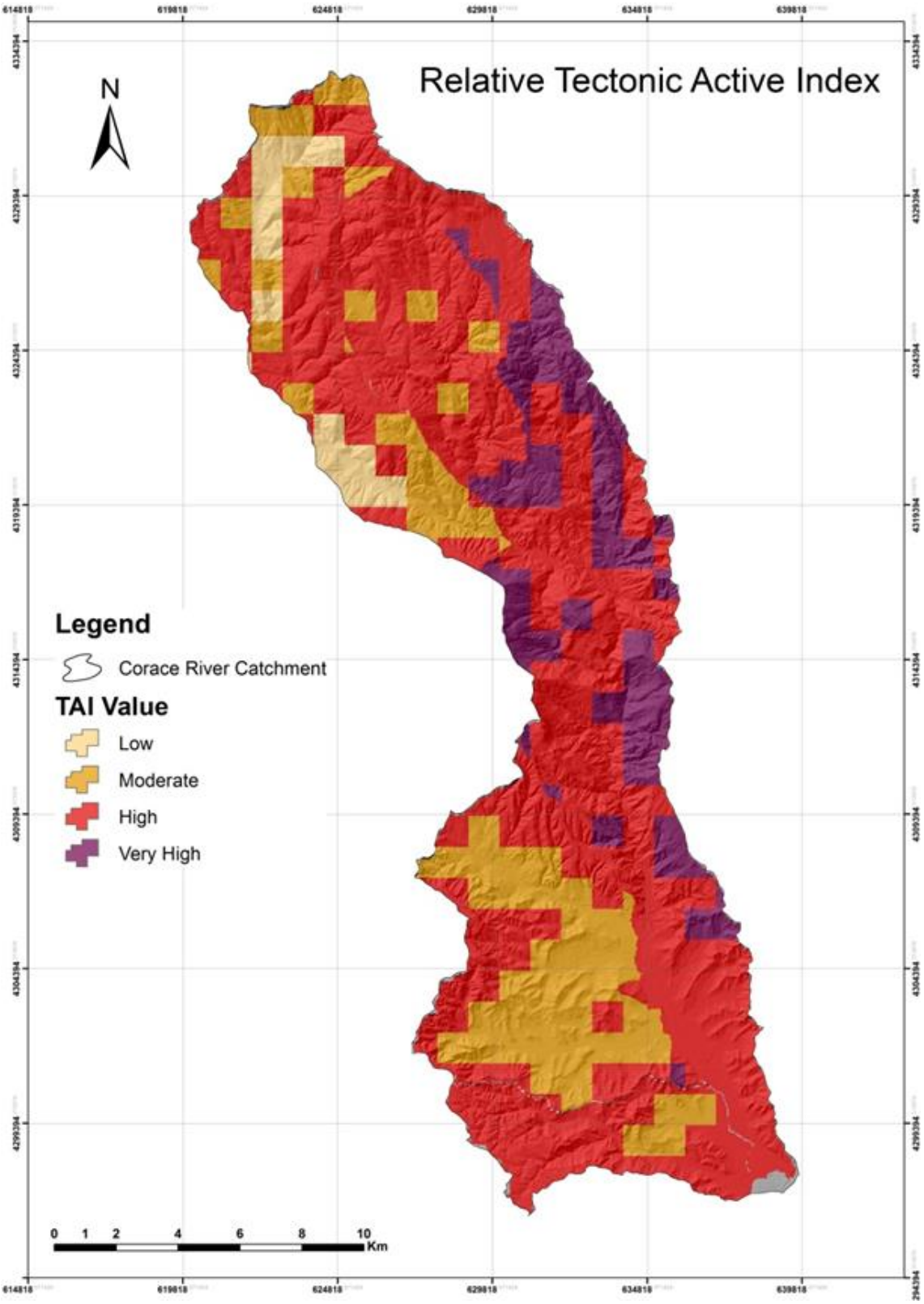

Figure 20 IFAT is obtained by the average of the different classes of geomorphic indices and divided into four classes,TAI Value 4 very high tectonic activity class 3 high tectonic activity class 2 moderately active tectonics class 1 low active tectonics.

Chapter two

Landslide inventory map and

Determinant factors in landslide susceptibility evaluation

Introduction

The concept of landslide "susceptibility" was originally design in the USGS to indicate "how prone to generate a landslide is a geological unit" (Brabb et al., 1972); this can be measured from the correlation between determining factors together with the spatial distribution of the movements (Brabb, 1984).

The main steps for this kind of analysis were

- a collection of information about historical or antecedent events;
- compilation of a landslide inventory from field and aerial photography surveys;
- GIS (ArcGIS, ESRI) implementation using a DEM and detailed thematic maps; and analysis of landslide determinant factors.

This area is historically threatened by slope failure phenomena but a comprehensive investigation of the proneness to landslide phenomena above all in Gimigliano municipality of the whole Corace. Basin Catchment has not previously been performed. The study area covers more or less 300 km2 and includes 24 small municipalities belonging to the administrative district of Catanzaro. It reachs a maximum altitude of 1143 m a.s.l., and small urban areas that are sometimes located on steep slopes.

Among the variety of existing statistical techniques for data processing of geographical information, the *matrix method* was chosen to produce a susceptibility map over the area. A best fit between the presence or absence of a landslide (dependent variable) and a set of possible causal factors (independent variables) is established on the basis of a maximum likelihood criterion, and yields an estimation of regression coefficients that are representative of the relationship between the factors and the phenomena

1. Landslide inventory map

A “landslide” is the movement of a mass of rock, debris, or earth down a slope, under the influence of gravity Landslides can involve flowing, sliding, toppling, or falling, and many landslides exhibit a combination of two or more types of movements, at the same time or during the lifetime of a landslide (Cruden and Varnes, 1996).

In order to identify geomorphologic evidences, soil erosion indications, anomalies or differences in vegetation coverage orthophotos interpretation analysis is exploited, allowing the possible identification and mapping of ground instabilities and land movements. Photointerpretation of optical aerial and satellite images represent first tool for geomorphological studies. It is a powerful tools to recognize counter slope variations as landslide indicators and to delimit the geometry of unstable areas, especially in combination with topographic maps or DEM layers facilitates. Geomorphological analysis of the land morphology temporal evolution was performed through a set of aerial photographs. Once the movements had been mapped, a field campaign was carried out in order to verify the typology of each movement and state of activity.

A system of classification based on Varnes (1978) was applied, whereby three basic movement types are distinguished: rock falls, slides and flows. Movements were considered to be complex if they resulted from a combination of two or more of the three main types. There are as many types of complex movement as there are possible combinations of simple movements.

The first stage in compiling the inventory consisted of interpreting the 1:33 000-scale stereoscopic aerial photographs provide by Military Geography Institute- IGM, that cover a time period from 1991 to 1994, and the 1: 10000 scale topographic maps provided by Regione Calabria. Once the movements had been mapped, a field campaign was carried out in order to

verify the typology of each movement and collect further data (e.g. on activity, make a photographic record, take samples, etc.). In the study arera 1989 movements were recorded: 69 rock falls, 1169 slides, 175 flows, and 643 `complex' movements. The area affected by landslides (more or less 62 km^2) represents 21 per cent of the total surface area(294 $km^{2)}$. The surface area distribution for each movement type is shown in Tab 9. Slides phenomena accounted for not only nearly 50 per cent of all the surface area affected, but also the largest of the landslides recorded (30 km^2 per movement of average area). Flows represented 5 per cent of the movements, with an average area of 3´km^2 per movement. With 28 km^2 per movement, complex movements were in second place in terms of the total surface area occupied (46 per cent) and in terms of the average area. Rock falls represented only a 0.08 per cent of the surface area of the movements, with an average area of 0.05 km^2 per movement.

With respect to studied area, (Tab.10). 1989 slope movements were registered, which have affected 21% of the total in the zone and are distributed in the following way:

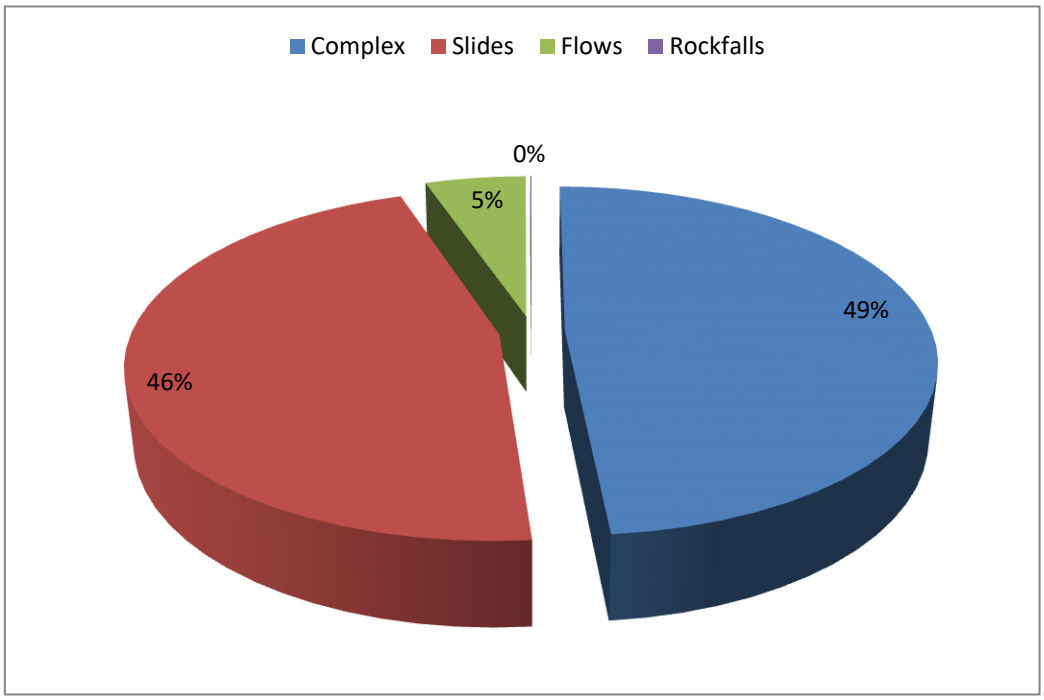

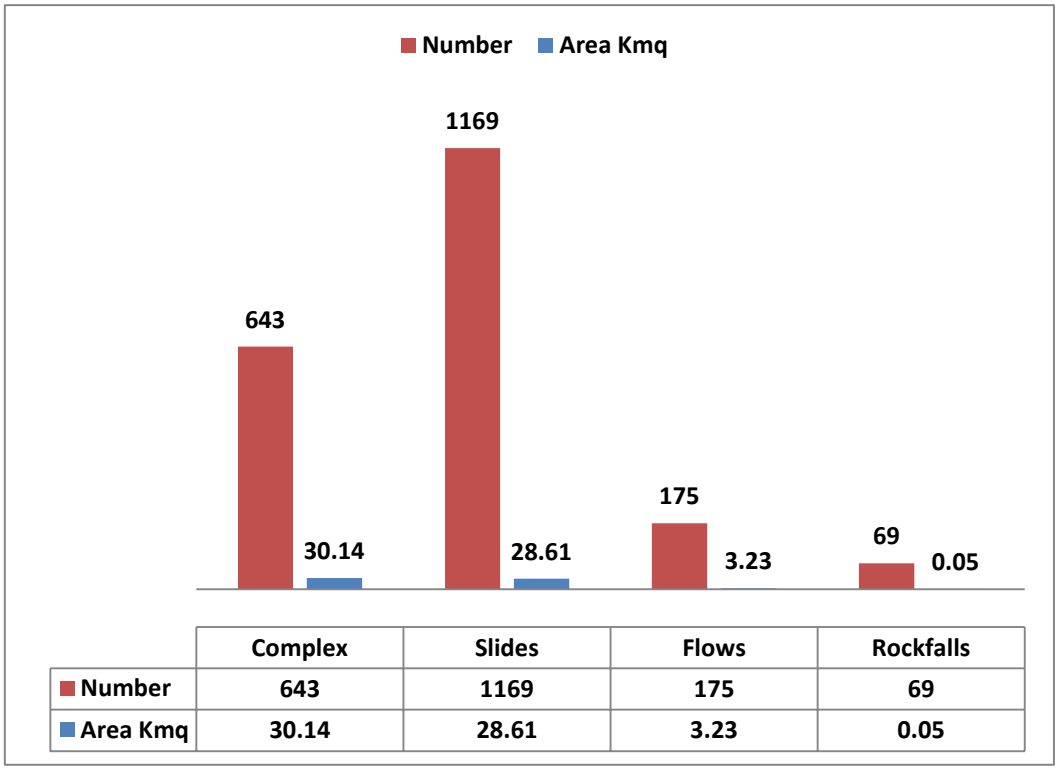

	Complex	Slides	Flows	Rockfalls
Number	643	1169	175	69
Area Kmq	30.14	28.61	3.23	0.05

Table 9 Distribution of slope movments.

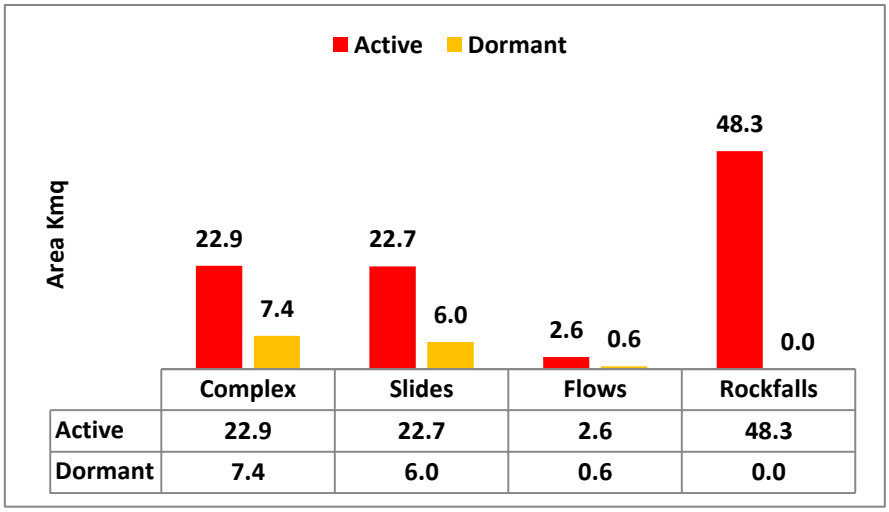

	Complex	Slides	Flows	Rockfalls
Active	22.9	22.7	2.6	48.3
Dormant	7.4	6.0	0.6	0.0

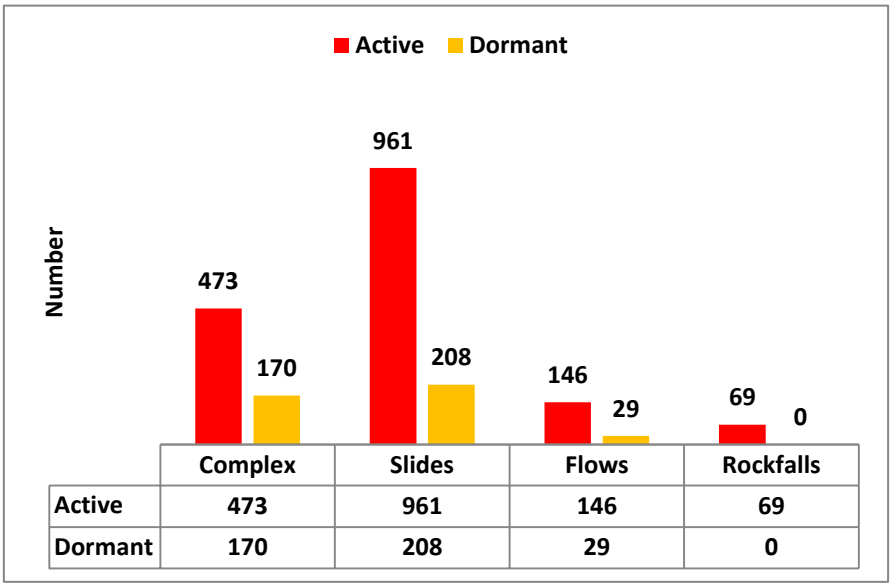

	Complex	Slides	Flows	Rockfalls
Active	473	961	146	69
Dormant	170	208	29	0

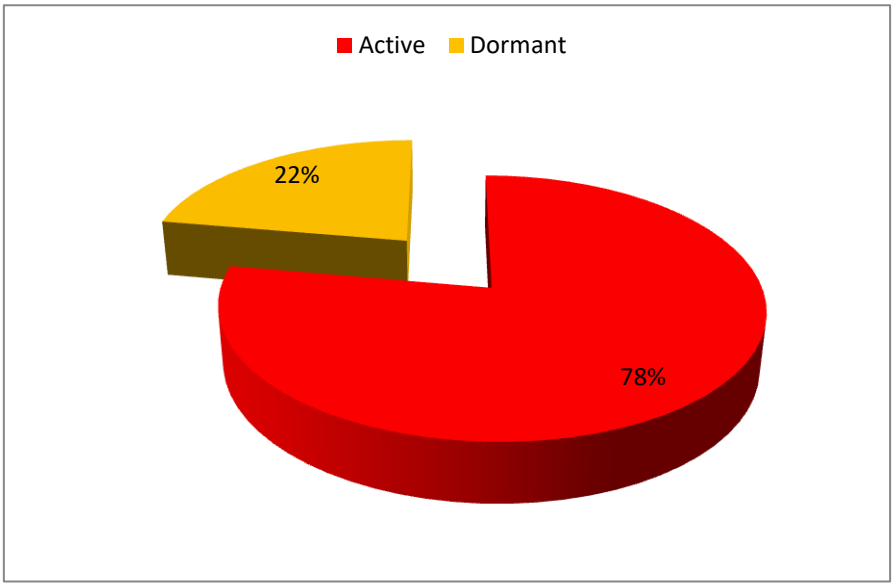

Table 10 Distribution of slope movements based on activity state.

1.1. Rockfalls

69 rock falls: fallen rock blocks or small, isolated boulders reach from escarpments evolving to massive landslides. Also, collapses of rocky material or soils can occur due to undercutting at the foot of escarpments. All of these represent little more than 0.05% of the mobilized zone. these are massive crumbling or in individual blocks generated in the carbonated escarpments of the calcareous sandstone and marble as showed in Fig. 23.

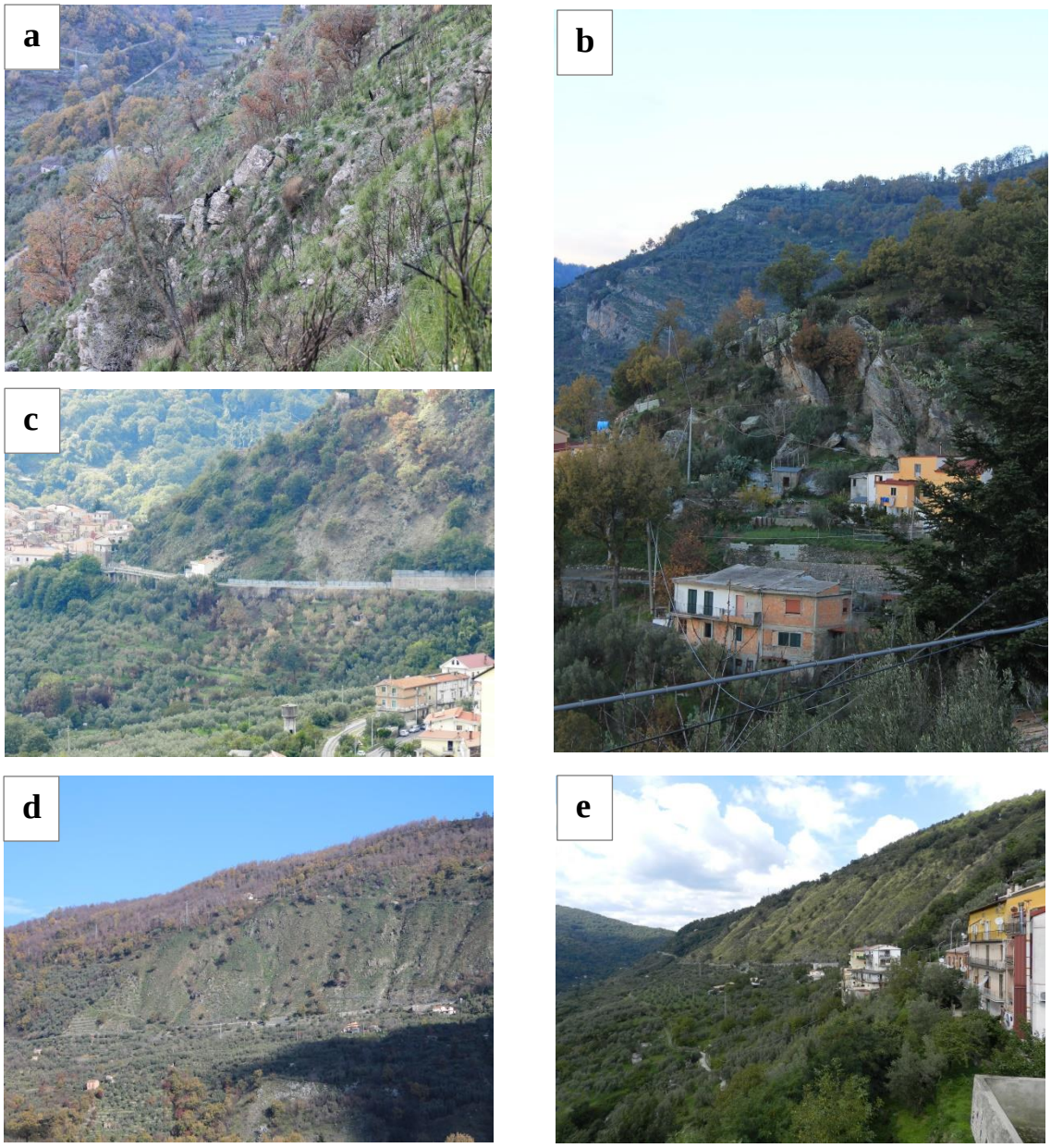

Figure 21 a-e Rockfalls landslides , that represent little more than 0.05% of the mobilized zone.

1.2. Slides

These can affect the weathered layer or the rocky mass along the discontinuities. They go from small shallow slides of small surface area (less than a hectare) to massive slides reaching hundreds of metres long. They represent about 49% of the mobilized zone. These are usually ovoid in shape, with incipient development and of variable dimensions (up to several km long and 300 m thick). They are often accompanied by rock falls or debris flow (Fig. 24

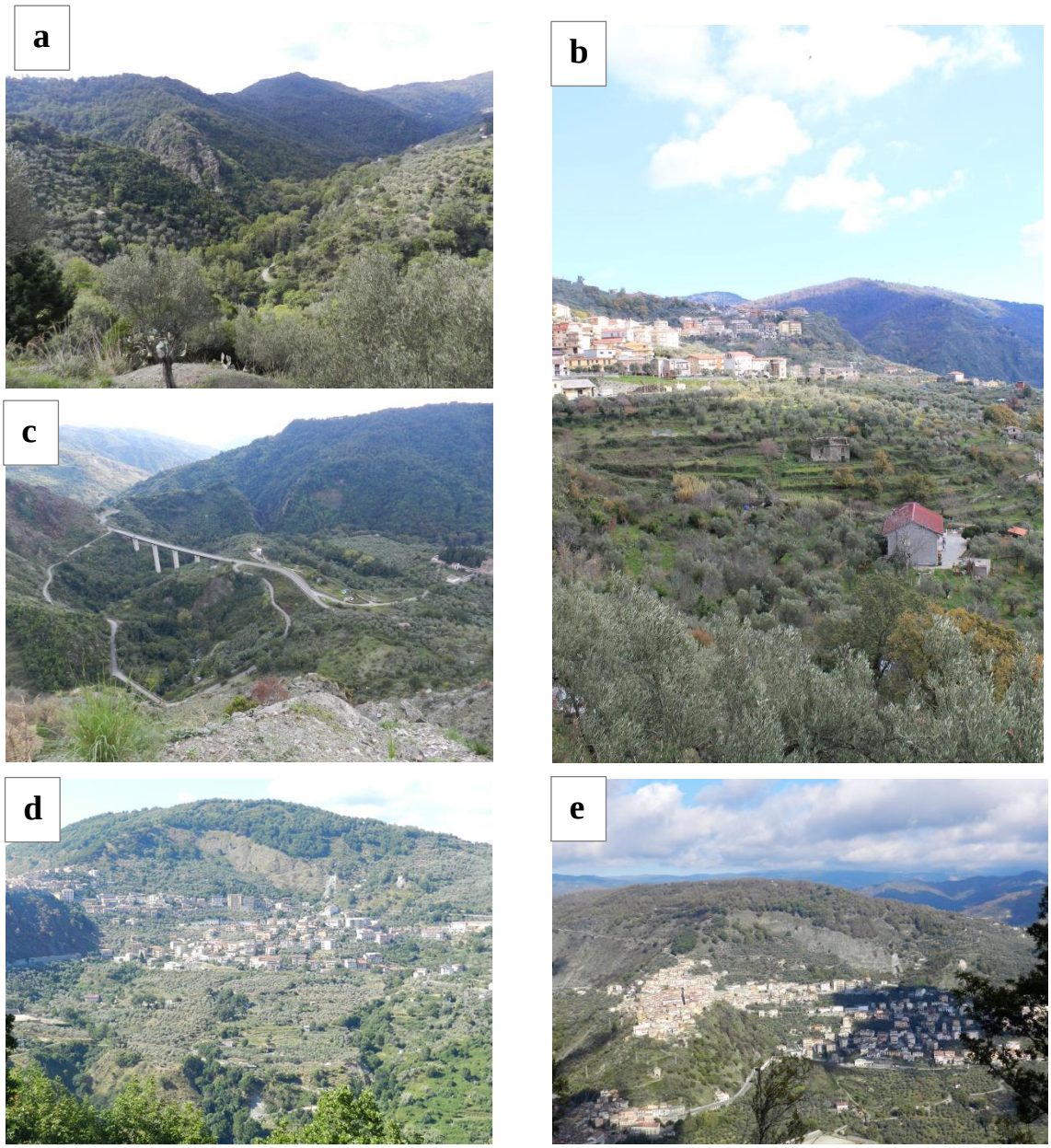

Figure 22 a-e Small shallow slides of small surface area (less than a hectare) to massive slides reaching hundreds of metres long. They represent about 49% of the mobilized zone .

1.3. Flows

Debris flows consist of carbonate-rock fragments with a low content in fine material and or metapelite (micaschist and phyllite) material from the decomposition and weathering of rock, with a greater proportion of fine materials. In this zone, more or less of 150 slope movements were registered. Soil creep areas affect soft materials (clays) and represent some 25% of the total flows area mobilized in the study area.

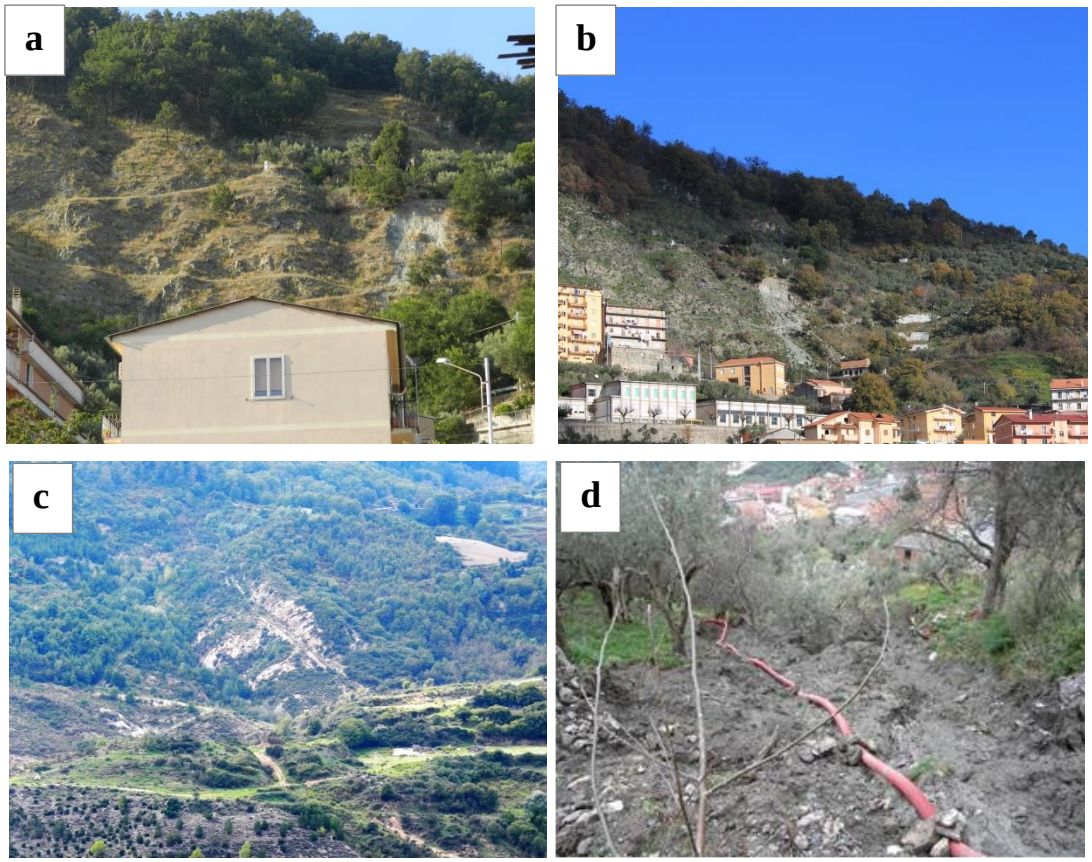

Figure 23 a-d Debris flows consist that involve carbonate-rock fragments with a low content in fine material and or metapelite (micaschist and phyllite) material from the decomposition and weathering of rock.

1.4. Complex movements

These are primarily earth flows that originated during or after rotational slides and/or rock falls. They make up more than 46% of the total zone under movement (Fig. 26).

Figure 24 Rotational slides and/or rock falls

2. Determinant factors

Determining factors were analysed some derived from the digital elevation model (DEM) such as altitude, slope, aspect, hillshade, curvature of the slope and other one obtained from thematic maps, resulting from field research or from published maps such as lithology, land cover usage, average annual precipitation, proximity to flow channel and last but not least the *impact factor of active tectonics-IFAT*.

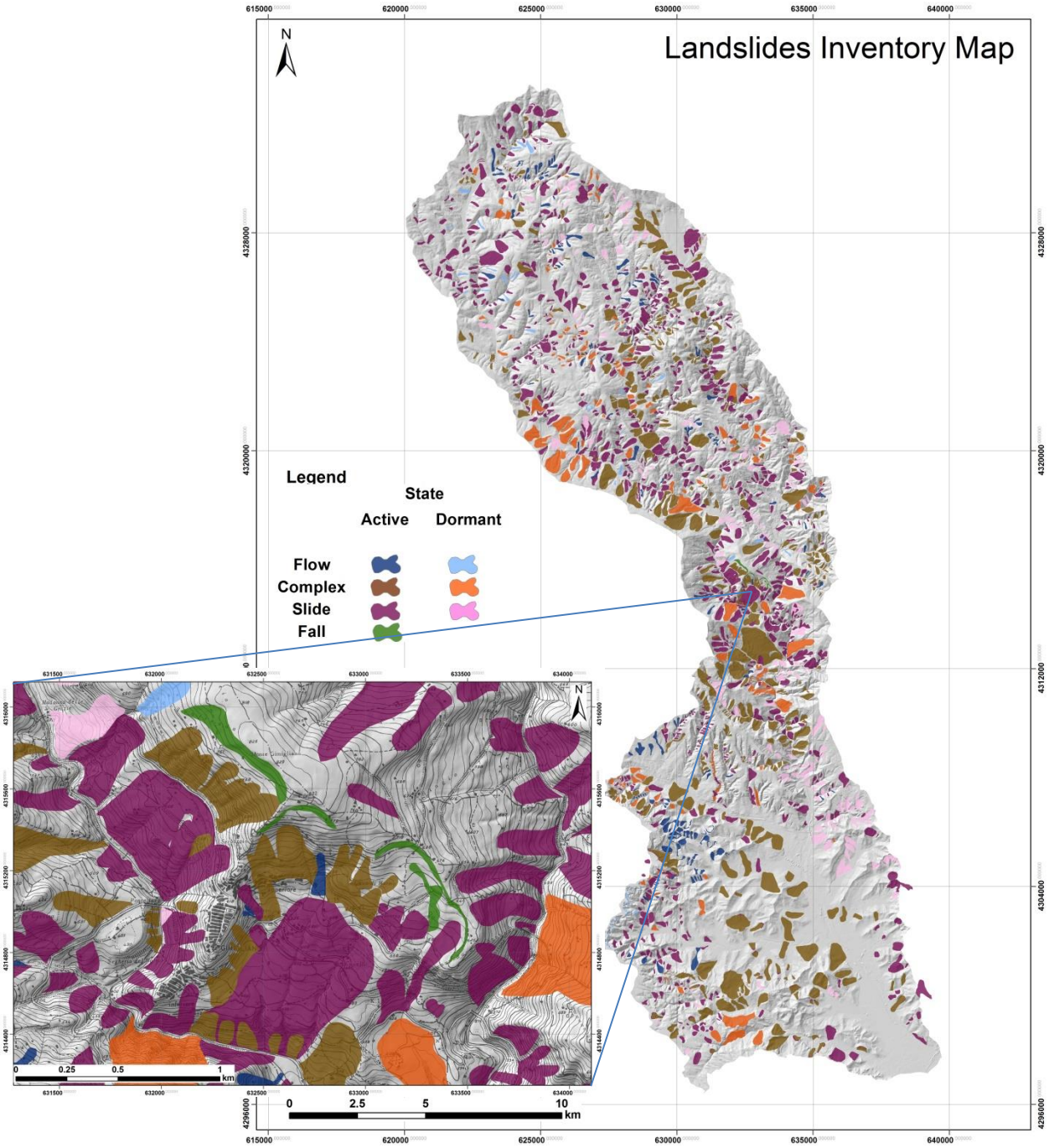

Figure 25 Landslide inventory map

2.1. Determinant factor derived from DEM

2.1.1. Digital Terrain Model DTM

A digital terrain model is a topographic model of the bare earth terrain relief, that can be manipulated by computer programs. The data files contain the spatial elevation data of the terrain in a digital format which usually presented as a rectangular grid. Vegetation, buildings and other man-made (artificial) features are removed digitally - leaving just the underlying terrain (on the other hand, Digital Surface Model (DSM) is usually the main product produced from photogrammetry, where it does contain all the features mentioned above, while a filtered DSM results in a DTM).

DTM model, related as raster data type, stored usually as a rectangular equal-spaced grid, with space (resolution) of between 5m meters, is georeferenced in UTM WGS84 33N Coordinate System. Modeling terrain relief via DTM is a powerful tool in GIS (Geographic Information System) analysis and visualization. DTM: all information are stored in a GIS databases

The different components of the digital terrain model dtm such as Digital Elevation Model dem itself and the derived models (gradients, orientation, etc.) are factors that determine instability. These components of the dtm actually come from the dem and are obtained directly, usually through the application of analysis or using other map classification and overlapping functions. The factors used in this study come directly from the DEM

2.1.2. Digital Elevation Model (DEM):

Digital Elevation Model (DEM) is a digital cartographic/geographic dataset of elevations in xyz coordinates. The terrain elevations for ground positions are sampled at regularly spaced horizontal intervals. DEMs are derived from hypsographic data (contour lines) and/or photogrammetric methods. DEMs consist of a sampled array of elevations for a number of ground positions at regularly spaced intervals.

From dem, morphological and morphometric characteristics of the terrain are obtained (slope, exposure, illumination, curvature, etc.). For the present study, digital cartographic/geographic data files are provided by Regione Calabria and have a spatial resolution of 5m.

Fig dem

From Spatial Analyst Tool , in a gis software, altitude, slope, aspect, hillshade, curvature of the slope are obtained.

2.1.2.1. **Altitude** is not commonly used as determinant factor, but it is powerfully used in mountainous areas with high slopes, as is the case at hand. The elevation map (Figure xx) consists of a reclassification of the dem, into a "raster" surface and converts it into discrete intervals of altitude, by reclassification. Due to the high topographic gradient existing in the study area, the MDE interval classification has been performed with a Natural Break Classification which is considered representative for the work scale. The minimum altitude value coincides almost with the sea level, 1.24 m asl. Fi. 25 shows the areal distribution expressed as percentage, cumulative percentage and square kilometres for each altitude interval considered. It can be verified the distribution of altitudes is quite homogeneous. The most represented section, with 32.4 % is between 800-1200 m. The average height is 567 m. more or less 43% of the area is below 800 meters and 40% above 800 meters.

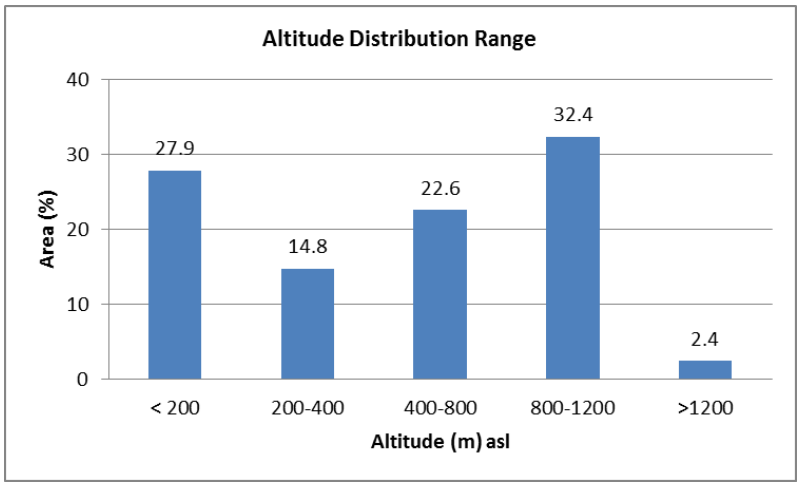

Figure 26 Altitude map Class 1 _ <200; Class 2 200-400 ; Class 3 :400-800; Class 4: 800-1200; Class 5 >1200.

Altitude (m)	%	Area (kmq)	Cumulate Area (kmq)
< 200	27.9	82.8	82.8
200-400	14.8	43.9	126.7
400-800	22.6	67.1	193.8
800-1200	32.4	96.2	290.0
>1200	2.4	7.2	297.2

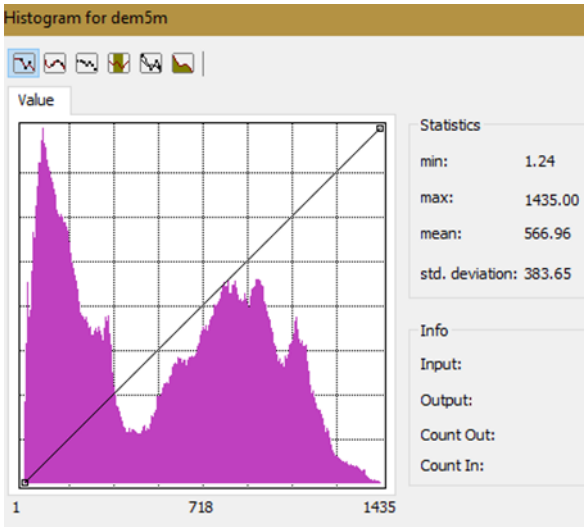

2.1.2.2. Slope

Identifies the slope (gradient, or rate of maximum change in z-value) from each cell of a raster surface Slope is the rate of maximum change in z-value from each cell. The use of a z-factor is essential for correct slope calculations when the surface z units are expressed in units different from the ground x,y units.The range of values in the output depends on the type of measurement units. For degrees, the range of slope values is 0 to 90. For percent rise, the range is 0 to essentially infinity. A flat surface is 0 percent, a 45 degree surface is 100 percent, and as the surface becomes more vertical, the percent rise becomes increasingly larger.

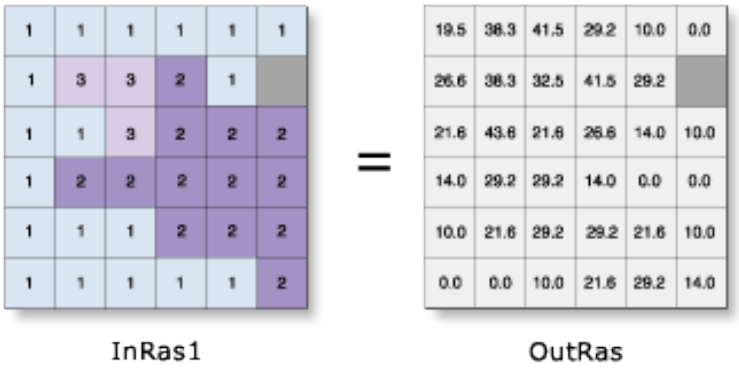

In this case following classes were obtained:(°) 0-8.4 (soft slope), 8.4-18.4 (moderate slope), 18.4-xx (strong slope), xx (very strong slope), xx ° (Vertical or subvertical slope). With these classes the map of slopes in the zone was elaborated.

Table xx shows the areal distribution expressed as percentage (%) cumulative percentage and square kilometers (Kmq) for each slope interval considered. The main feature of the area is that almost 45% of the terrain has a slope higher than 26º. Strong slopes of the area occupies ca 35 % and only 10% has a very strong slope. These zones of very strong slope coincide with the valleys embedded by where the tributaries of the Corace and Melito flow. However, in the course of this, the slope is moderate to strong. A wide area that has a gentle to moderate slope is the southern portion. It also has a moderate slope the higher areas due to certain characteristics. The average slope of the area is 20º.

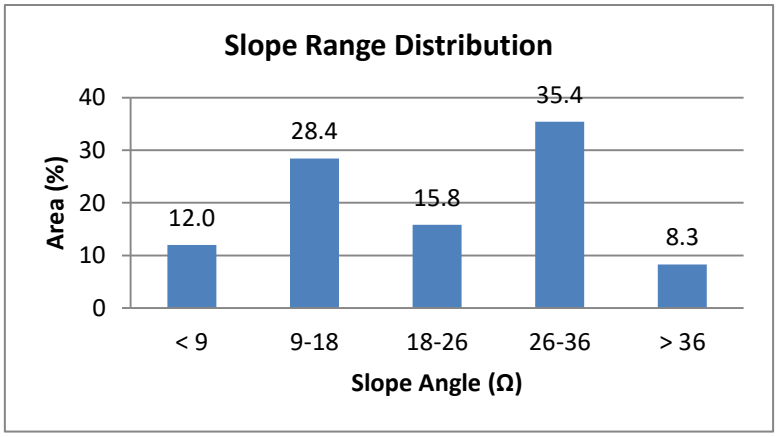

Figure 27

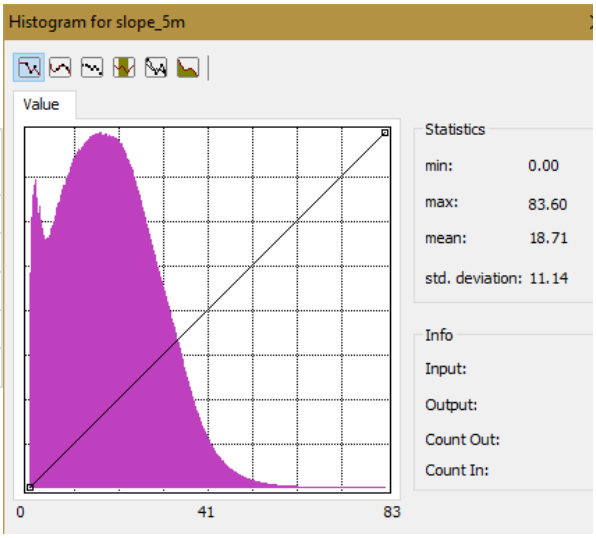

Angle (Ω)	%	Cumulate %	Area (kmq)	Cumulate area (kmq)
< 9	12.0	12.0	35.3	35.3
9-18	28.4	40.4	83.7	119.0
18-26	15.8	56.3	46.6	165.6
26-36	35.4	91.7	104.2	269.8
> 36	8.3	100	24.4	294.2

2.1.3. **Aspect:** Aspect derives from a raster surface. The aspect identifies the downslope direction of the maximum rate of change in value from each cell to its neighbors. Aspect can be thought of as the slope direction. The values of the output raster will be the compass direction of the aspect.

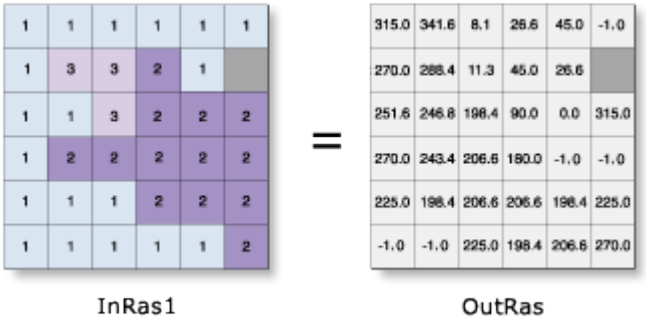

Aspect is the direction of the maximum rate of change in the z-value from each cell in a raster surface. Aspect is expressed in positive degrees from 0 to 359.9, measured clockwise from north. Cells in the input raster that are flat—with zero slope—are assigned an aspect of -1.

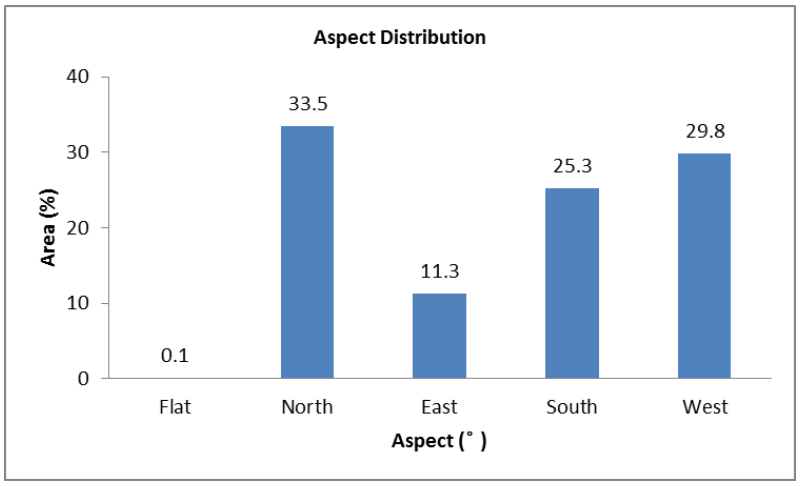

Class of Aspect	%	Area kmq
Flat	0.1	0.30
North	33.5	98.43
East	11.3	33.32
South	25.3	74.41
West	29.8	87.74

Figure 28

2.1.4. **Curvature: c**alculates the curvature of a raster surface, optionally including profile and plan curvature. The primary output is the curvature of the surface on a cell-by-cell basis, as fitted through that cell and its eight surrounding neighbors. Curvature is the second derivative of the surface, or the slope-of-the-slope.

A positive curvature indicates the surface is upwardly convex at that cell. A negative curvature indicates the surface is upwardly concave at that cell. A value of 0 indicates the surface is flat.

Units of the curvature output raster, as well as the units for the optional output profile curve raster and output plan curve raster, are one hundredth (1/100) of a z-unit. The reasonably expected values of all three output rasters for a hilly area (moderate relief) can vary from -0.5 to 0.5; while for steep, rugged mountains (extreme relief), the values can vary between -4 and 4.

The curvature values represent the morphology of the topography. A positive curvature indicates that the surface was upwardly convex at that grid. A negative curvature indicates that the surface was upwardly concave at that grid. A value of zero indicates that the surface was flat. The reason for this is that following heavy rainfall, a convex or concave slope contains more water and retains this water for a longer period.

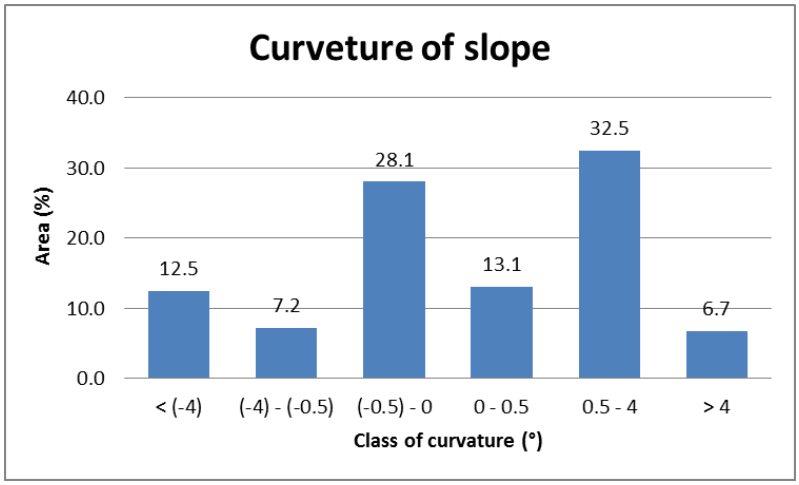

Class of curvature	%	Area (%)
< (-4)	12.5	36.6
(-4) - (-0.5)	7.2	21.2
(-0.5) - 0	28.1	82.5
0 - 0.5	13.1	38.5
0.5 - 4	32.5	95.6
> 4	6.7	19.8

Figure 29

2.2. Determinant factor obtained from thematic maps

Other factors that influence stability are those that depend on the nature of the terrain such as lithology, land use, annual average precipitation and so on.

2.2.1. Lithology

From the geological map carried out by CASMEZ of Calabrian Region the lithological maps 1: 25.000 m of the area have been obtained. The geology of the area is quite complicated since more than 40 different lithological units appear. For the analysis performed, some lithologies have been grouped, described in the corresponding section, in lithological complexes according to the behavior, geomechanical (cohesion and internal friction angle) of the materials (Tab.9).

Thus the following 10 units or lithological complexes have been differentiated:

Raste cod.	Lithology
6	Granites
9	Phyllades, Schysts
10	Marbles and Paragneiss
1	Gneiss
8	Serpentinites
11	Alluvial deposits
3	Clays
4	Sandstones and Conglometates
5	Gypsum
7	Carbonates
2	Sandstones and Conglometates

Lithology	%	Area kmq
01	0.1	0.4016
03	1.1	3.1104
06	23.1	68.1104
07	10.7	31.5872
11	1.0	3.0192
12	47.9	140.9712
15	0.5	1.3648
16	0.4	1.0304
20	0.0	0.0272
21	4.1	12.0704
22	0.3	0.7392
23	0.8	2.2256
24	3.2	9.4352
26	6.9	20.1952

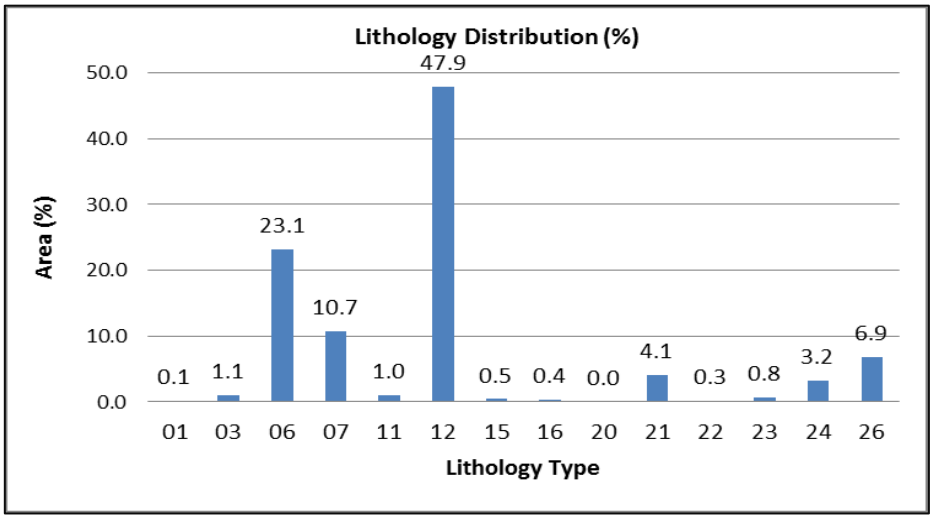

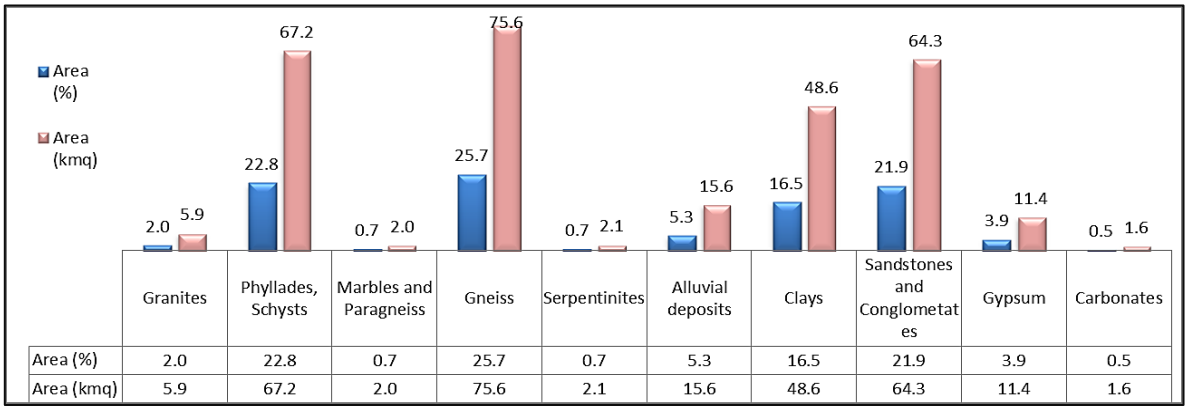

	Granites	Phyllades, Schysts	Marbles and Paragneiss	Gneiss	Serpentinites	Alluvial deposits	Clays	Sandstones and Conglometates	Gypsum	Carbonates
Area (%)	2.0	22.8	0.7	25.7	0.7	5.3	16.5	21.9	3.9	0.5
Area (kmq)	5.9	67.2	2.0	75.6	2.1	15.6	48.6	64.3	11.4	1.6

Table 11 Lithology distribution

2.2.2. Land Use Coverage

Land cover was derived from the classification of Landsat 7 (sensor ETM+) satellite data provided within the Corine Land Cover project (launched by the European Union Commission), after the validation by field survey. The spatial accuracy of these data could be related to a 1:50 000 map scale and, in order to reduce the number of variables involved in the analysis of this causal factor, the original classes of land cover were grouped into 11 classes on the basis of presumed similarities. Brief descriptions of each class has been reported**:**

Land Coverage	Area kmq	%
Heterogeneous agricultural	47.69	16.21
Arable	34.84	11.84
Shrubs and / or herbaceous	14.70	5.00
Permanent crops	41.87	14.23
Wood	141.40	48.05
Mining, landfills and construction sites	3.59	1.22
Urbanized area	5.52	1.88
Open areas with sparse or no vegetation	1.98	0.67
Meadows	0.26	0.09
Artificial green non-agricultural areas	0.18	0.06
Industrial, trade and communication networks	2.24	0.76

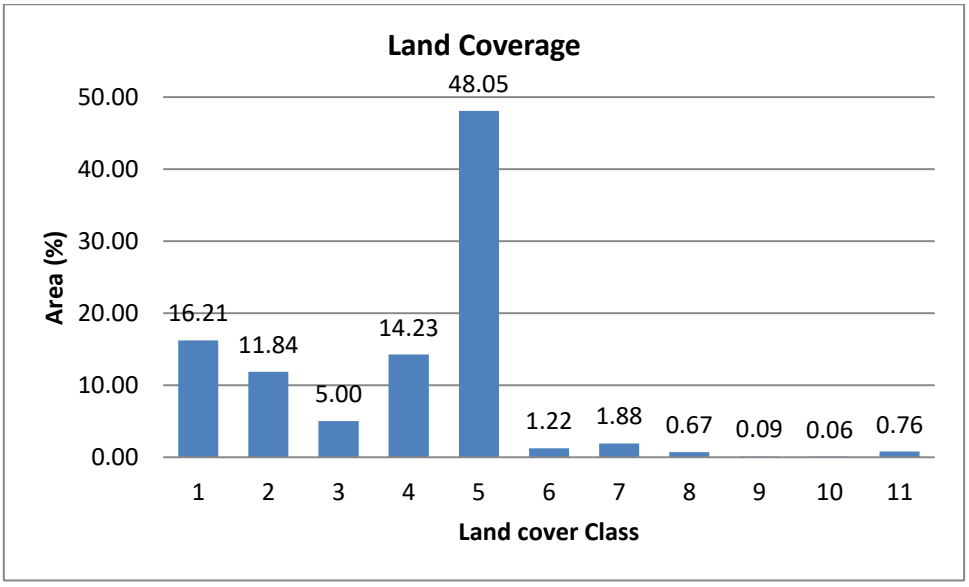

Table 12 Land coverage value distribution.

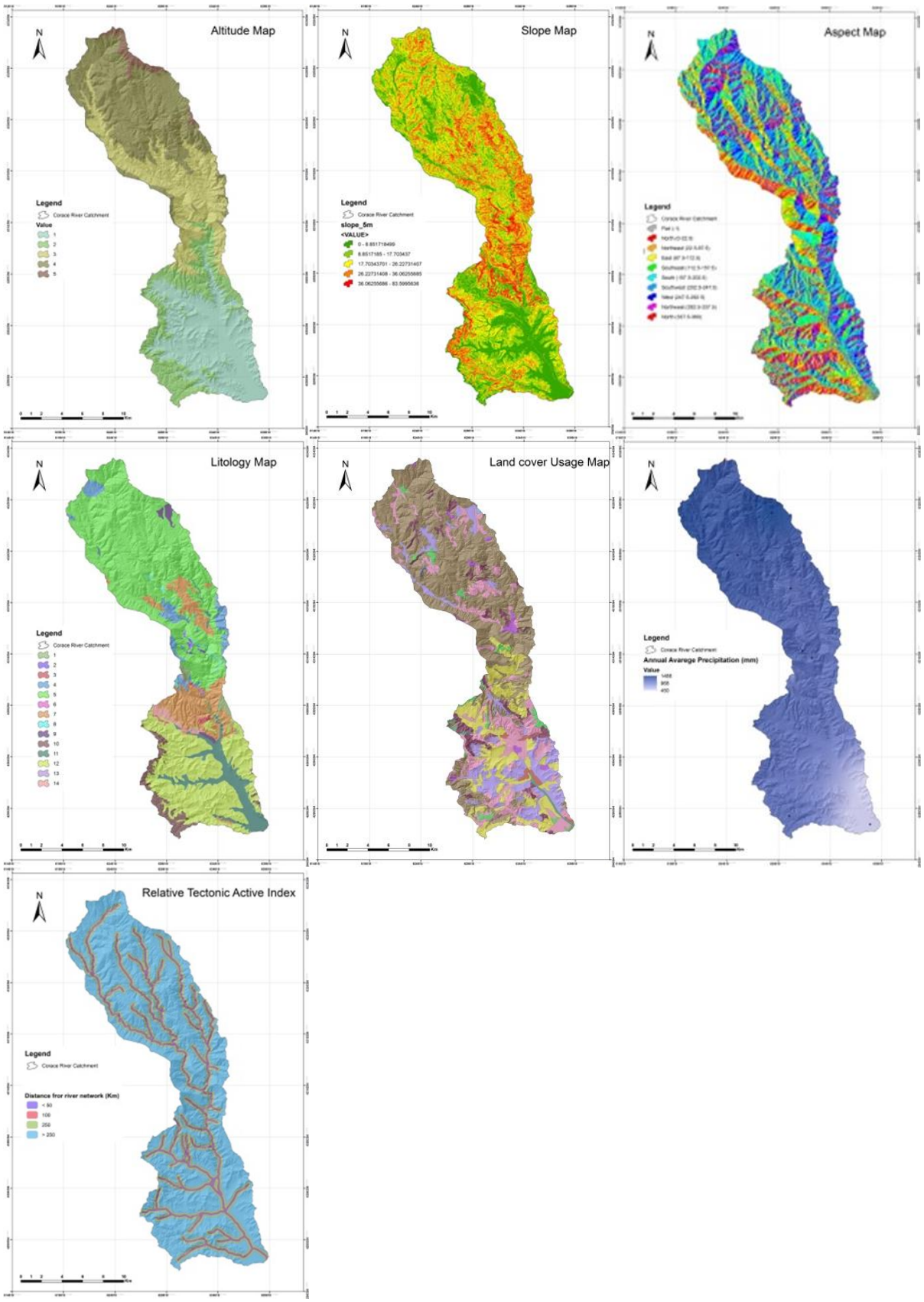

Figure 30 Geomorpholocial factor.

2.2.3. Annual Average Precipitation

The precipitation data was prepared using the last 10 years (2006–2016) of historical rainfall data. In this methodology it was used long-term precipitation for a 30 year period. An average annual rainfall contour map is mapped out from the daily rainfall data measurements. Also, the IDW method using Gis Software was used for spatial interpolation on the contour maps. IDW interpolation explicitly implements the assumption that things that are close to one another are more alike than those that are farther apart. To predict a value for any unmeasured location, IDW will use the measured values surrounding the prediction location. Those measured values closest to the prediction location will have more influence on the predicted value than those farther away. Thus, IDW assumes that each measured point has a local influence that diminishes with distance. It weights the points closer to the prediction location greater than those farther away, hence the name inverse distance weighted.

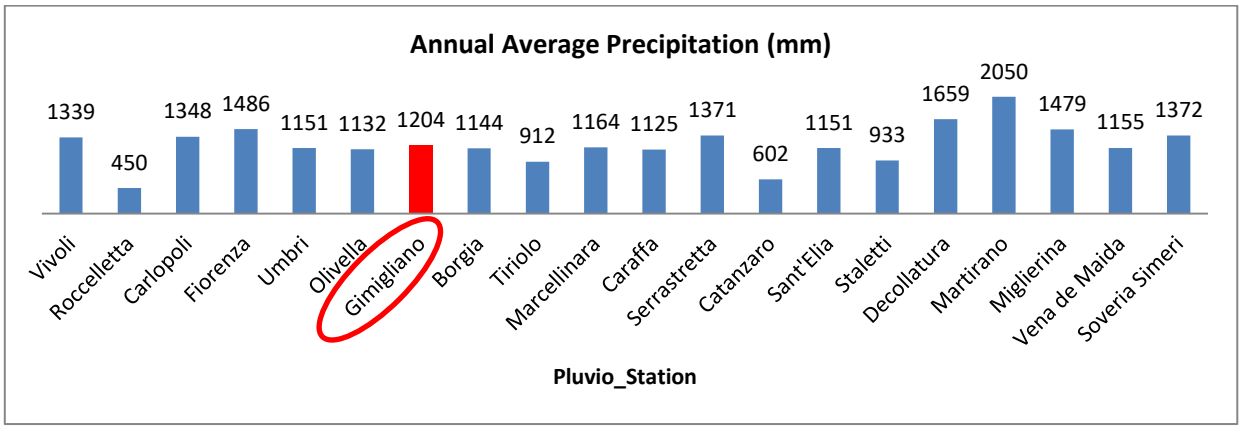

Table 13 Annual Avarage Precipitacion values.

2.2.4. Distance to drainage

The “proximity to rivers” factor would potentially include an activating mechanism related to erosion along the slope foot. Unfortunately, ephemeral watercourses are not very easily expressible in symbolic form in the vector data representing a river network, and it is very difficult to model the theory of watercourses as triggers of landslide occurrences by data in a GIS. Analysis was carried out to assess the influence of drainage lines on landslide occurrence. For this purpose, the proximity to a drainage line was identified by buffering (four buffer zone reach from < 50 m, up to > 250 m). In the case of the relationship between landslide occurrence and distance from drainage, as the distance from a drainage line increases, the landslide frequency generally decreases. At a distance of < 250 m, the ratio was > 1, indicating a high probability of landslide occurrence, and at distances > 250 m, the ratio was < 1, indicating a low probability.

2.2.5. Impact Factor of Active Tectonics IFAT

A method to evaluate an index over an area that represents impact factor of active tectonics (IFAT) it is present. The various indices is divided into three classes, with class one being high activity and class three being low activity. In order to develop an aerial index, IFAT is obtained by the average of the different classes of geomorphic indices and divided into four classes, where class 4 is very high tectonic activity class 3 is high tectonic activity class 2 is moderately active tectonics class 1 is low active tectonics. The proposed GIS methodology allows a map showing impact factor of active tectonics of the landscape to be produced. This method has been linked to landslide susceptibility mapping.

A higher frequency of landslides is related to areas with higher indexes of active tectonic in the northeaster slopes of Corace basin and also in the and the of Gimigliano village. These correlations between density of landslides and active tectonics intensity, expressed by geomorphic indexes, suggest the usefulness of the integration of the active tectonics between the main determinant factors in landslide susceptibility assessment of mountain alpine areas which may be applied to similar areas around the world.

These studies focused the assessment of active tectonics. Some previous studies on relative tectonic activity based on geomorphic indices tends to focus on a particular mountain front or area (Bull and McFadden, 1977; Rockwell et al., 1985; Azor et al., 2002; Molin et al., 2004) and not an aerial regional assessment of active tectonics. In this case six geomorphological parameters were used to evaluate the impact of active tectonics in a wider area, considering also mountain fronts. The average of the six measured geomorphic indices was used to evaluate the distribution of Impact Factor of Active Tectonics into Corace River Basin.

In order to evaluate the landscape in terms of potential impact factor of tectonic activity, indices along a particular mountain front or area are discussed and a judgment. (Bull and McFadden, 1977; Rockwell et al., 1985; Azor et al., 2002; Molin et al., 2004).

Previously indices calculated were divided into three classes, arbitrarily with class one being low activity and class three being high activity (Table 5). The boundaries of the various classes change for what index is being evaluated; and for this purpose boundaries have been selected generally agree with changes in the range of the values of the various indices.

The values of the index were divided into four classes to define the degree of active tectonics: 1—low (1.0≤IFAT>1.5); 2—moderate (1.5≤IFAT2.0); 3—high (2.0≤IFAT2.5); and 4—very high (2.5≤IFAT), as showed in Tab (da fare)and Fig.28.

The distribution of the four classes is shows the result of the classification for each subbasin. About 1% of the study area (about 50 km2) belongs to Class 1; 20% (1050 km2) to Class 2; 67% (3580 km2) to Class 3; and 12% (660 km2) to Class 4.

The high class values (HIGH tectonic activity) for IFAT mainly occur in the north to northwest of the basin area while the rest of the study area has classes of IFAT suggesting moderate to high tectonic activity (middle portion of basin).The distribution of the indices describes areas associated with different mountain fronts and suggests an import role of tectonic activity. Within the study area, about 45% (201 km2) is class 1 (very high relative tectonic activity) as measured by IFAT; 22% (99 km2) shows high relative tectonic activity as measured by IFAT (class 2); 12% (53 km2) has moderate values of tectonic activity in terms of IFAT (class 3); and 21% (96 km2) has the lowest values of relative tectonic activity (class 4) based upon IFAT

Thus, two-thirds of the study area is classified into classes 2 or 1 of high to very high tectonic activity in terms of the apparent geomorphic response. In different tectonic environments with greater rates of active tectonics, the values of indices would differ as well as their range in value.

However, the methodology we outline would provide an index based on area that estimates relative tectonic activity as it has for the study area in Catanzaro Basin.

A map showing relative tectonic activity of the landscape it was produced. This method has been linked to landslide susceptibility mapping (El Hamdouni, 2001) in this landscapes with widespread evidences of recent active tectonics.

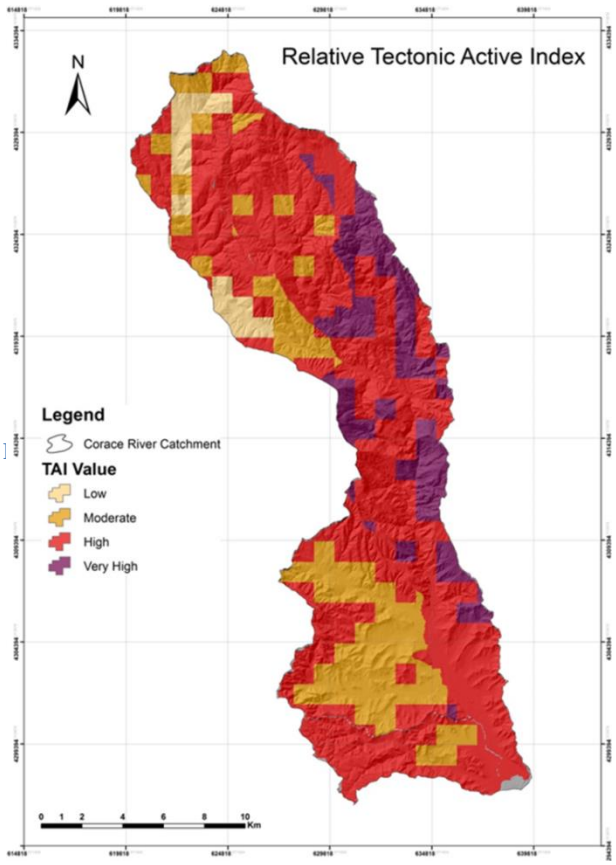

Figure 32 Impact Factor of Active Tectonics IFAT

Chapter three

Susceptibility analysis methodology

The concept of landslide "susceptibility" was originally design in the USGS to indicate "how prone to generate a landslide is a geological unit" (Brabb et al., 1972); this can be measured from the correlation between determining factors together with the spatial distribution of the movements (Brabb, 1984).

1. Matrix method

The matrix method of susceptibility analysis (DeGraff and Romesburg, 1980, with GIS development by Irigaray, 1995) is a quantitative method for establishing an instability index for a given area. The modelling was performed using the matrix method (DeGraff and Romesburg 1980) in a GIS environment (Irigaray 1995; Irigaray et al. 1999; Fernandez 2001; El Hamdouni 2001), based on the determination of all the possible combinations between the types of factors considered. The resulting landslide susceptibility map of the Corace River Basin was expressed using five classes . **Landslide Matrix** is constructed with each cell representing one possible combination of the classes of factors considered. been identified which can condition the appearance of landslides. From the landslide inventory, the area affected by movements can then be calculated for each combination of factors. A similar procedure is used to construct the **Management Unit Matrix**, representing the total area for each combination of factors The landslide-susceptibility matrix has the same number of combinations as the management unit matrix (Fig. 29).

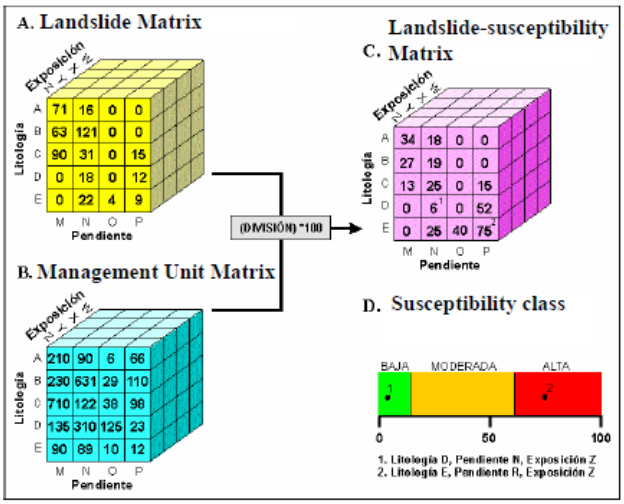

Figure 33 Illustration of the determination of landslide susceptibility by the GIS matrix method (Irigaray et al. 1999). In this example, determining factors used are bedrock, aspect and slope. A, B, C... represents the classes of these factors. Cells represent all the possible combinations of factors. The number inside the cells represents: in the landslide matrix, the surface area of each combination affected by the movements; in the management unit matrix, the total surface area of each combination; and in the landslide-susceptibility matrix, the percentage of slope movement of each combination. Finally, the results are classified in different classes of susceptibility.

The value of each cell in this new matrix is obtained by dividing the values from the landslide matrix by those from the management unit matrix. On the landslide-susceptibility matrix, value of 0 was assigned to combinations that are not associated with landslides; on the contrary the remainder will have values of >0, up to a maximum of 1 (or 100 per cent, if expressed as a percentage).
The ‘‘Landslide Matrix’’ was built from the inventory of rupture zones of the slope movements, calculating the surface area affected by the movements in each combination of factors. In the ‘‘Management Unit Matrix’’, the total surface area of each combination of factors was calculated. Finally, in the ‘‘Landslide-Susceptibility Matrix’’ the value of each cell was determined by dividing those corresponding to the landslide matrix by those of the management unit matrix. The landslide-susceptibility matrix values constitute the proportion of slope movements with respect to the total area and represent the relative susceptibility of each combination of factors. Finally, the values obtained are visualized showing 5 susceptibility levels (very low, low, moderate, high, very high (Irigaray 1995) using the natural-breaks method. class breaks are determined statistically by finding adjacent feature pairs, between which there is a relatively large difference in data value.

Susceptibility maps of slope movement were drawn, although here only the accumulated results for all the inventory of landslides an example of landslide-susceptibility map classified in five levels (very low, low, moderate, high, very high) established by the natural-breaks classification are illustrated. The extent of each susceptibility level depends on the zone studied and the type of process considered, but in general the low and very low susceptibility levels represent more than 50% of the surface area studied. If moderate susceptibility is also added, this percentage rises to more than 85%. These values indicate that these maps are not conservative, but rather that they limit the zones of maximum susceptibility just to the relatively reduced area where the associated combination of factors exist.

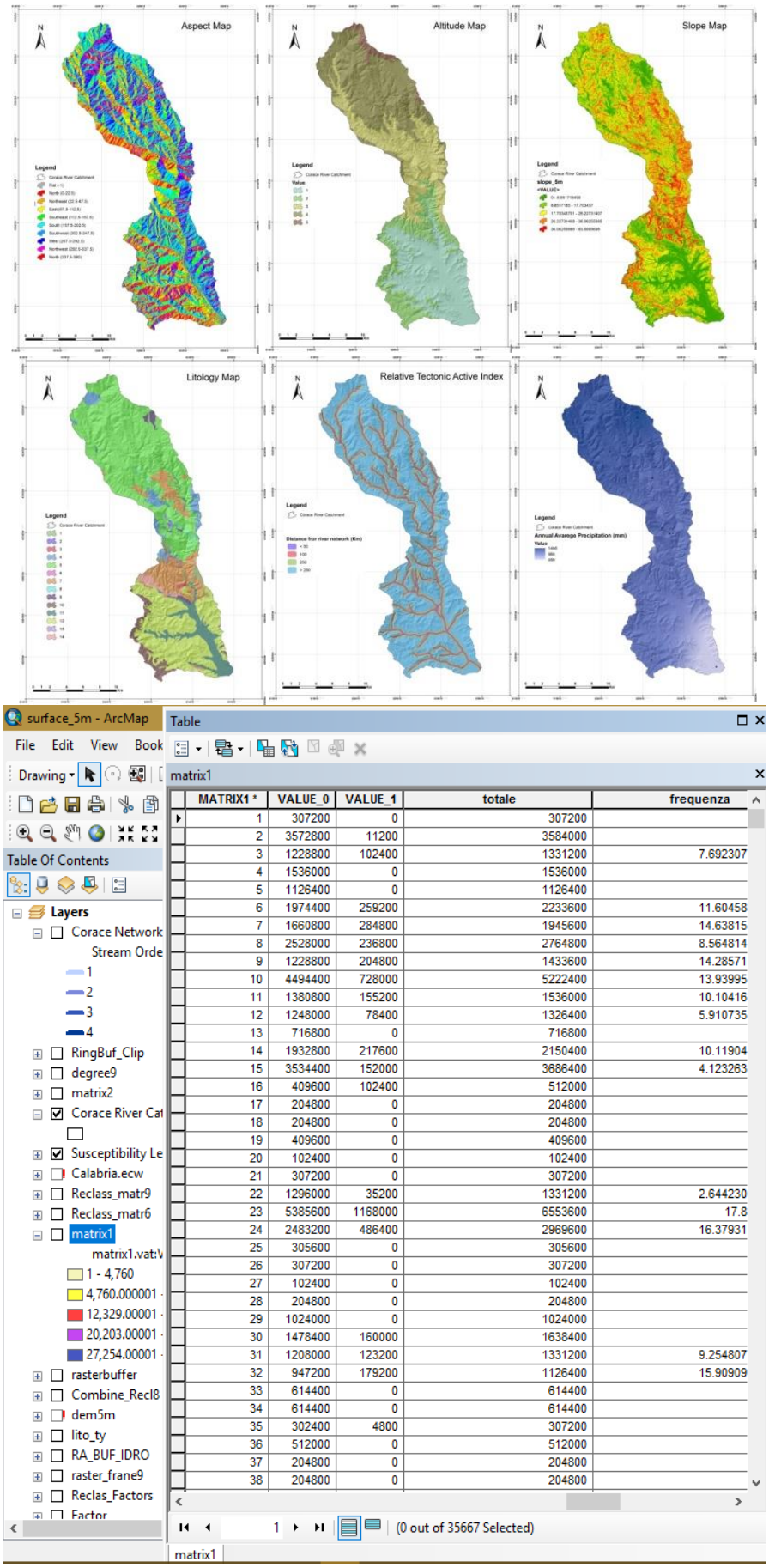

MATRIX1 *	VALUE_0	VALUE_1	totale	frequenza
1	307200	0	307200	
2	3572800	11200	3584000	
3	1228800	102400	1331200	7.692307
4	1536000	0	1536000	
5	1126400	0	1126400	
6	1974400	259200	2233600	11.60458
7	1660800	284800	1945600	14.63815
8	2528000	236800	2764800	8.564814
9	1228800	204800	1433600	14.28571
10	4494400	728000	5222400	13.93995
11	1380800	155200	1536000	10.10416
12	1248000	78400	1326400	5.910735
13	716800	0	716800	
14	1932800	217600	2150400	10.11904
15	3534400	152000	3686400	4.123263
16	409600	102400	512000	
17	204800	0	204800	
18	204800	0	204800	
19	409600	0	409600	
20	102400	0	102400	
21	307200	0	307200	
22	1296000	35200	1331200	2.644230
23	5385600	1168000	6553600	17.8
24	2483200	486400	2969600	16.37931
25	305600	0	305600	
26	307200	0	307200	
27	102400	0	102400	
28	204800	0	204800	
29	1024000	0	1024000	
30	1478400	160000	1638400	
31	1208000	123200	1331200	9.254807
32	947200	179200	1126400	15.90909
33	614400	0	614400	
34	614400	0	614400	
35	302400	4800	307200	
36	512000	0	512000	
37	204800	0	204800	
38	204800	0	204800	

Figure 34 How to create a Susceptibility map in a GIS Software..

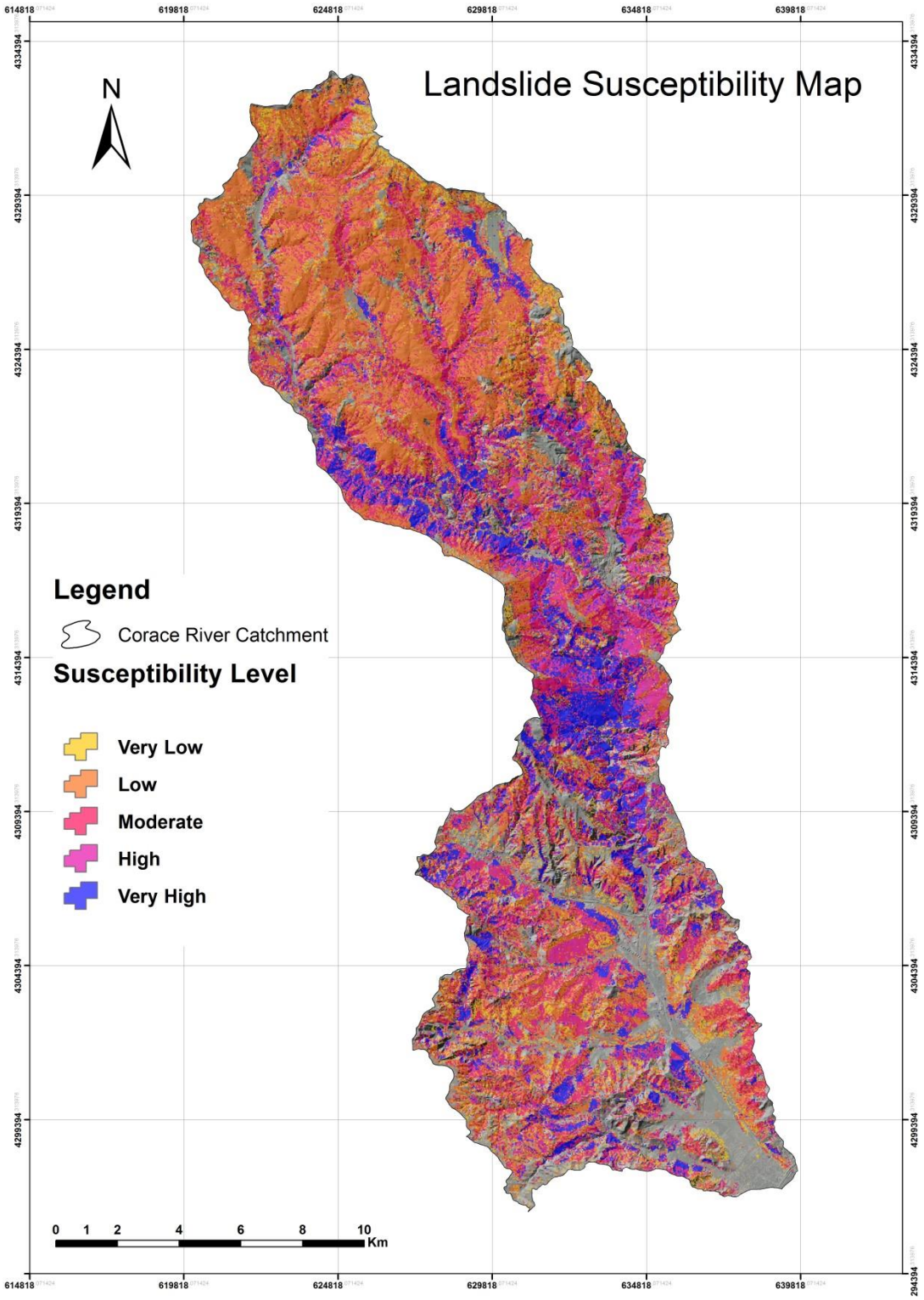

Figure 35 Landslide Susceptibility Map of Corace River Basin, obteined by matrix method.

2. Validation of susceptibility map

The landslide susceptibility analysis result was validated using known landslide locations. Validation was performed by comparing the known landslide location data with the landslide susceptibility map. Each factor used and frequency ratio was compared. The rate curves were created and its areas of the under curve were calculated for all cases. The rate explains how well the model and factor predict the landslide. So, the area under curve in can assess the prediction accuracy qualitatively. To obtain the relative ranks for each prediction pattern, the calculated index values of all cells in the study area were sorted in descending order. Then the ordered cell values were divided into 100 classes, with accumulated 1% intervals. For example, in the case of frequency ratio model, 90 to 100% (10%) class of the study area where the landslide susceptibility index had a higher rank could explain 36% of all the landslides. In addition, the 80 to 100% (20%) class of the study area where the landslide susceptibility index had a higher rank could explain 55% of the landslides. In the case of logistic regression model, 90 to 100% (10%) class of the study area where the landslide susceptibility index had a higher rank could explain 39% of all the landslides. In addition, the 80 to 100% (20%) class of the study area where the landslide susceptibility index had a higher rank could explain 57% of the landslides. To compare the result quantitative, the areas under the curve were recalculated as the total area is 1 which means perfect prediction accuracy. So, the area under a curve can be used to assess the prediction accuracy qualitatively. In the case of all factor and logistic regression model used, the area ratio was 0.8001 and it could say the prediction accuracy is 80.01%. In the case of all factor and frequency ratio model used, the area ratio was 0.7842 and we could say the prediction accuracy is 78.42%. Overall the case of all factor and logistic regression model used showed a higher accuracy than cases of each factor and logistic regression used and all factor and frequency ratio model used.

2.1. Degree of accuracy

$$Mi / ti$$

mi represents the area, in km^2 , of the observed movements lies in different levels of susceptibility and *ti* as well as the total area in km classified with a certain level of susceptibility

$\Sigma\ mi / ti * 100$ is that best defines the degree of accuracy (Baeza, 1994)(Tab.12).

Área movilizada en cada uno de los niveles de susceptibilidad y area total de casa nivel					
	Very Low	**Low**	**Moderate**	**High**	**Very high**
ti (kmq)	0.265	1.4691	0.7898	0.520425	0.488825
mi (kmq)	0.005975	0.182725	0.2027	0.203525	0.351675
mi/ti	0.02	0.12	0.26	0.39	0.72
degree of adjuste	**1.49**	**8.21**	**16.95**	**25.83**	**47.52**

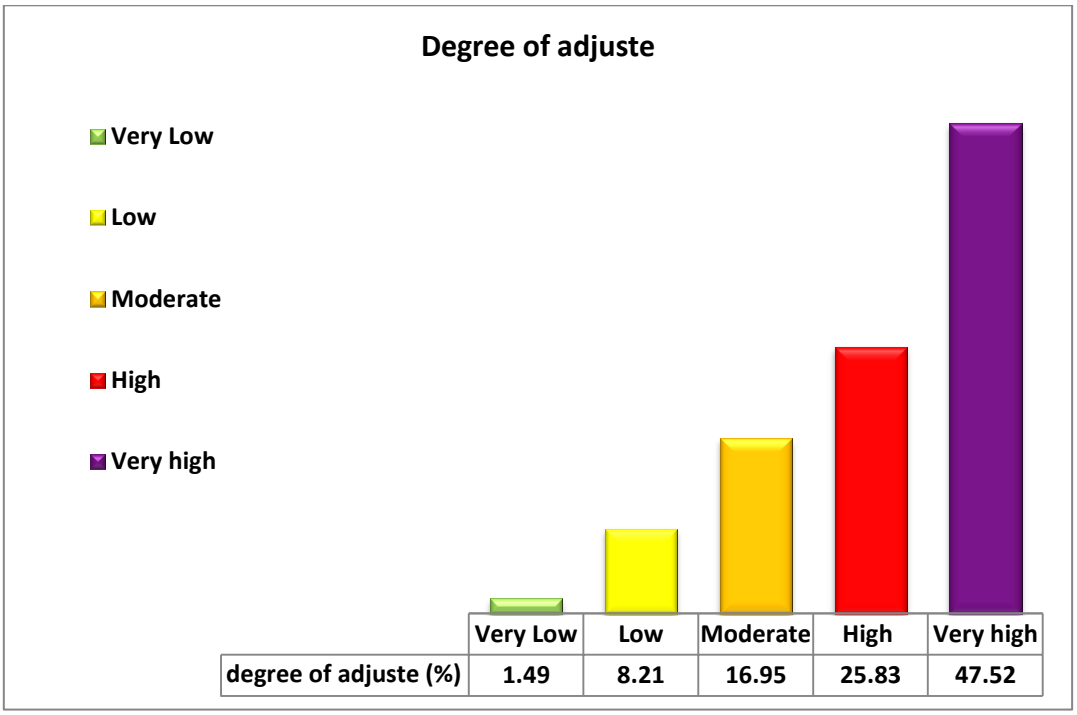

Table 14 Susceptibility Validation by degree of accuracy.

Third section

SAR Interferometry observations: analysis and measuring of ground displacements

Landslide events are complex geological and geomorphological processes due to a different factors and therefore it is very difficult to classify the existing one and predict the future occurrences. Aim of third section is the utilising of remote-sensing data to detect and map landslides, to assess their activity and velocity. Also, to determine the spatial-temporal variation of landslides and related consequences. In addition to seismic displacements, volcanic inflation or subsidence (Massonnet et al., 1994), large landslides (Fruneau et al., 1996), and the details of glacial flow (Dowdeswell et al., 1999; Mohr et al., 1998) can be observed and depicted through radar interferometry. Unlike most other geodetic techniques, radar interferometry can be done remotely, and it provides regionally extensive, high-resolution maps of interference patterns resulting from surface displacements. Although radar interferometry will have restricted applicability in highly vegetated regions, it can be extremely useful for quantitative analysis of deformation in remote, relatively arid areas.

InSAR techniques may improve towards to high robustness for landslides movement monitoring and it may be used as new methods for landslide mapping and inventory.Radar Interferometry A new geodetic technique for measuring ground displacements over larger areas has been developed based on radar interferometry.Radar interferograms for use in tectonic studies are probably best suited for arid settings where seasonal changes in vegetation and moisture are minimal. The greatest research attribute of radar interferometry lies not in its resolution (which is considerably less than that achieved through extensive GPS measurements), but rather in the tremendous spatial coverage it provides.

Using synthetic aperture radar (SAR) carried aboard satellites at 785 km altitude, radar pulses are transmitted along west-pointing ray paths at an angle of 23° from the vertical. Based on the return signal, the distance from the satellite to the ground is calculated, and a phase shift due to the ground reflection is recorded. If two images are used to construct the topography of a region, then a third image can be used to determine ground deformation with respect to that topography along the "look" direction of the radar. Alternatively, if a detailed digitized topography already exists for the area, then the differences between two images can define the ground deformation.

Chapter One

SAR Interferometry observations: analysis and measuring of ground displacements

Introduction

SAR interferometry technique has become a powerfully used technique for detecting, measuring topography and monitoring ground displacement. Syntetic Aperture Radar (SAR) images contain both the intensity and the phase information of the return signals from the earth surface. (Fig. 1) SAR interferometry (InSAR) is a technique in which two SAR images of the same area of the earth taken from slightly different satellite positions are used to generate an interferogram which represents the phase difference between the return signals in the two images (Hassen, 2001;Massonnet and Fierg, 1998; Rosen et al., 2000).

Ground displacements were evaluated by radar satellite-based sensor geomorphological evidences with the known geomorphological features. Based on the analysis linear deformation velocity maps and the ground deformation has been analysed over a catchment Corace River basin , located in the Catanzaro Stretta, focusing on Gimigliano Municipality.

Regarding the active tectonic factor, the GIS analysis provides a significant correlation landslides occurrences . In general the observed instable zones are related to steep slopes in under excavated rivers resulting from deforestation, soil erosion and active tectonics. A higher frequency of landslides is related to areas with higher indexes of active tectonic in the eastern slopes of Corace Basin and also in, with high to very high of the active tectonic indexes values correspondence of Gimigliano Village. A higher frequency of landslides is related to areas with higher indexes of active tectonics in the northeaster slopes of Corace basin and most of all in the Gimigliano village. These correlations between density of landslides and active tectonics intensity, expressed by geomorphic indexes, suggest the usefulness of the integration of the active tectonics between the main determinant factors in landslide susceptibility assessment of mountain alpine areas which may be applied to similar areas around the world.

Interferometric Synthetic Aperture Radar (InSAR), also referred to as SAR Interferometry, is the measurement of signal phase change, or interference, over time. When a point on the ground moves, the distance between the sensor and the point on the ground also changes and so the phase value recorded by a SAR sensor flying along a fixed orbit will be affected, too.

The two main fields of application of InSAR data are: a) reconstruction of digital elevation models of large areas; b) detection and monitoring of surface deformation phenomena and, in general c) measurement of displacement rates of objects on the ground.

Geomorphologists exploit images taken by Synthetic Aperture Radar (SAR) sensors primarily to measure surface deformations, and to construct time series of surface deformations, at single points (Ferretti et al., 2000, Berardino et al., 2002, Mora et al., 2003, Usai and Least, 2003, Werner et al., 2003, Canuti et al., 2004, Hooper et al., 2004, Lanari, 2004, Crosetto et al., 2005, Farina et al., 2006, Hooper et al., 2007, Cascini et al., 2009, Guzzetti et al., 2009b, Cascini et al., 2010 and Cigna et al., 2011).

1. Brief overview of SAR technique

Satellite continuously emits millions of radar signals toward the Earth's surface along the radar beam's line of sight (LOS). The angle at which the sensor is pointed toward the Earth's surface is referred to as the off-nadir angle (or look angle). The off-nadir angle ranges from values of 20° to 50° according to the satellite platform. (Fig.38) This ability to vary the off-nadir angle is important to adjust it in case of hilly or mountainous terrain (potential impediments to InSAR), if the relationship between viewing geometry and terrain slope is not optimal.

Radar signals are characterized by two fundamental properties: amplitude and phase. Amplitude is related to the energy of the backscattered signal. Phase is related to the sensor-to-target distance. It is this specific property of the radar signal that is used in estimating displacement in interferometric applications.

SENTINEL-1 satellite is potentially able to map the global landmasses in the Interferometric Wide swath mode once every 12 days, in a single pass (ascending or descending). Each SENTINEL-1 satellite will be in a near-polar, sun-synchronous orbit, with a 12-day repeat cycle and 175 orbits per cycle. In this regard, Sentinel-1 satellites will provide new high-quality data (i.e. improved SAR data availability, larger coverage and shorter temporal sampling).

The contribution of satellite SAR Interferometry in landslide risk mitigation is well-known within the scientific community. In fact, many encouraging results have been obtained, principally, in areas characterized by high coherence of the images (e.g. due to rock lithology or urban environment setting).

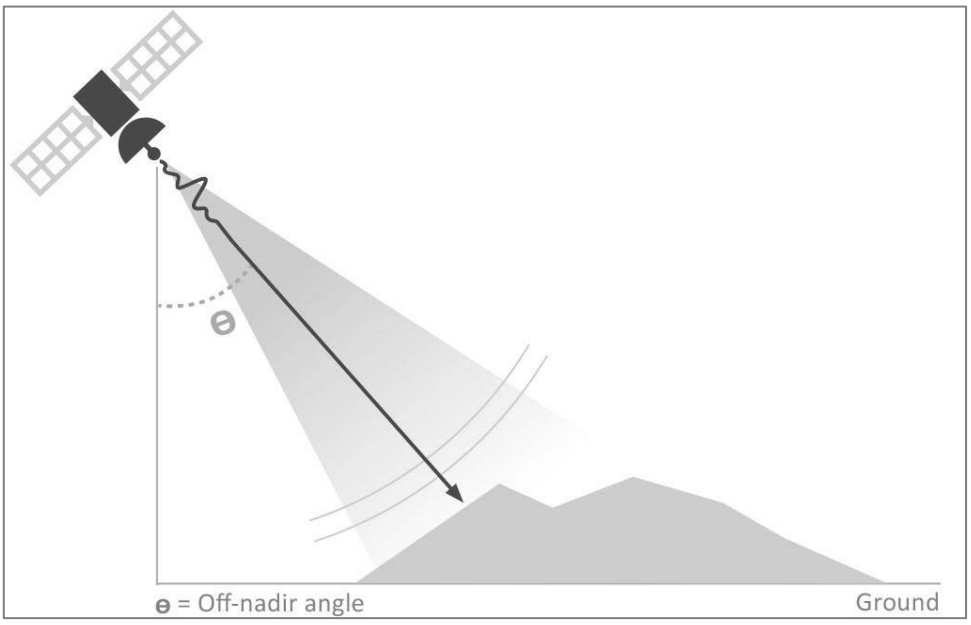

Figure 36 SAR image acquisition

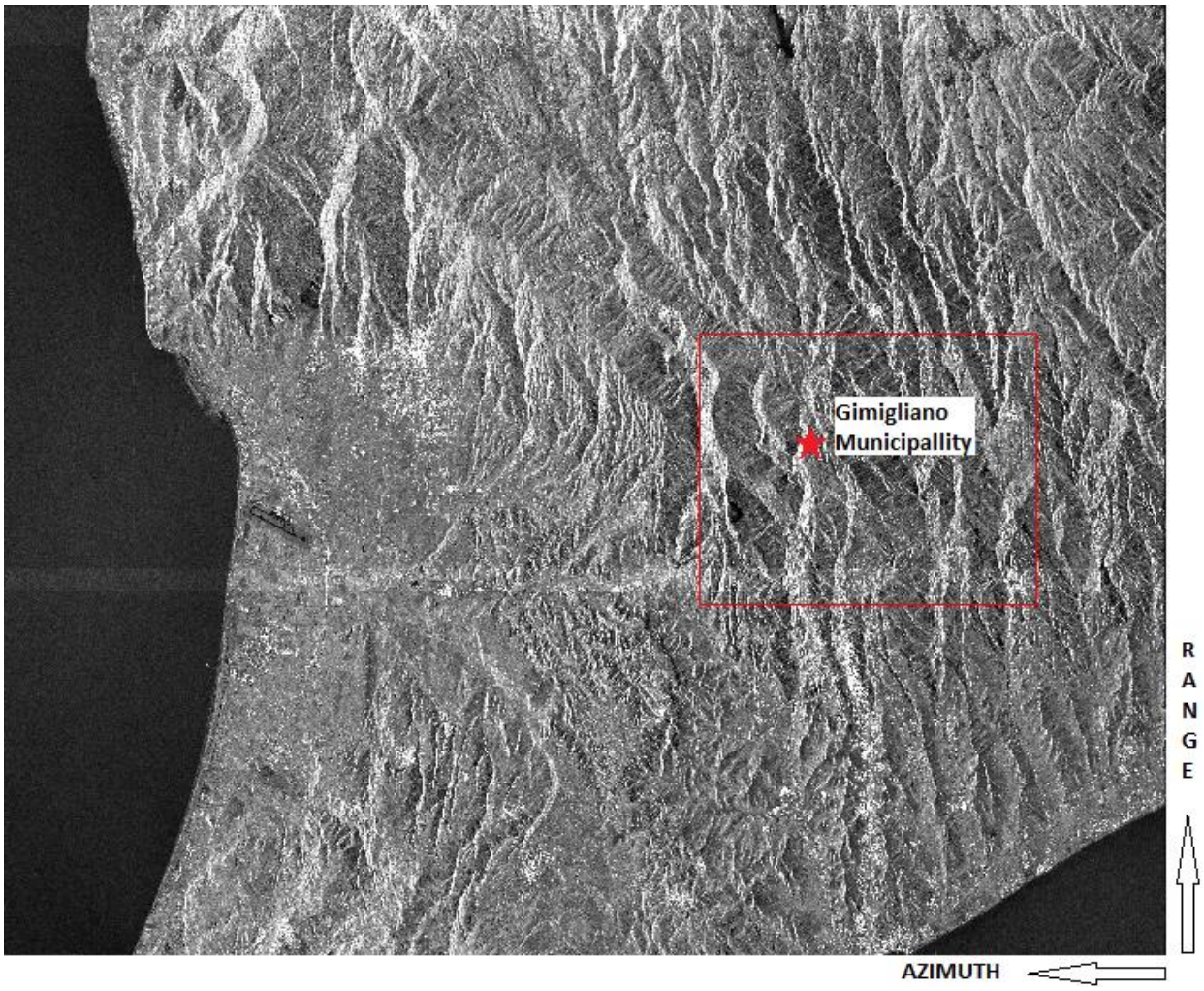

Figure 37 Sentinel 1 SAR Image . Brighter levels correspond to stronger backscattered radiation. The coastline along the Tyrrhenian Sea is clearly visible (the sea is dark due to the almost specular reflection of electromagnetic waves). Urban areas can be identified as bright spots on the image (strong backscattering from buildings). It should be noted that positive slopes of Monte Tiriolo and Monte Gimigliano (in the upper flanks on the image) are shortened with respect to the flanks descending to the sea. At the same time, the shortened flanks appear brighter on the image.

The change in signal phase (Δφ) is expressed by the equation below:

$$\Delta\varphi = \frac{4\pi}{\lambda}\Delta R + \alpha$$

Where λ is the wavelength, ΔR is the displacement in the Line Of Sight (LOS) and α is a phase shift due to different atmospheric conditions at the time of the two radar acquisitions (Fig.39)

1.1 Differential Synthetic Aperture Radar interferometry (DInSAR)

Differential Synthetic Aperture Radar interferometry (DInSAR), a technique capable of generating wide-area maps of ground surface deformations measured with millimeter precision (e.g. Gabriel et al., 1989; Ferretti et al., 2000a), has recently attracted much attention of researchers and practitioners involved in landslide monitoring and hazard assessment. This has been stimulated by some successful case studies, which indicated the potential of DInSAR in the detection of landslide movements (e.g. Fruneau et al., 1996; Rott et al., 1999; Kimura and Yamaguchi, 2000; Nagler et al., 2002; Berardino et al., 2003; Colesanti et al., 2003a; Singhroy and Molch, 2004; Strozzi et al., 2005; Bovenga et al., 2006-this issue), as well as through a series of workshops and demonstration projects supported by space agencies e.g. European Space Agency's (ESA) projects MASMOV, ALPS, SLAM (see http://dup.esrin.esa.it).

Analysis of single SAR images is not useful, since it is not possible to distinguish and separate different phase contributions related to object reflectivity, topography, atmosphere and noise inherent of any acquisition system. In particular, the application of multi-interferograms SAR Interferometry (PSI) techniques to the study of slow-moving landslides is a relatively new and interesting issue.

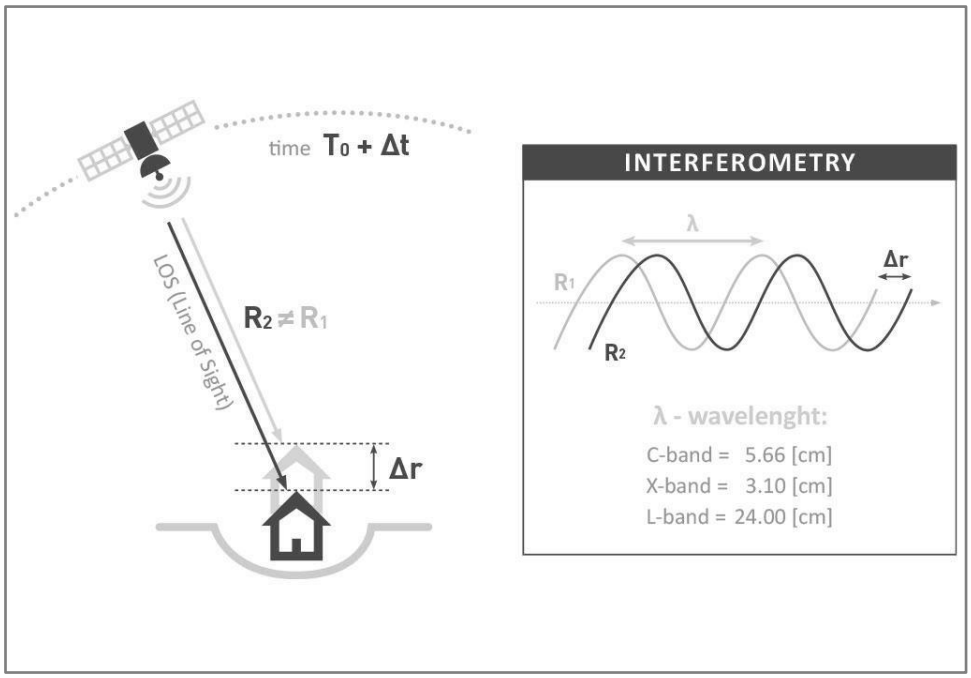

Figure 38 Basic concept of interferometric analyses.

Multi-interferograms SAR Interferometry (PSI) techniques have been implemented to exploit information contained in the phase values of SAR images: the PSI approach, is based on the use of a long series (the larger the number of images, the more precise and robust the results) of co-registered, multi-temporal SAR imagery (Fig.40-41).
Using this methodology it is possible to evaluate the displacements occurring between different acquisitions by distinguishing the phase shift related to ground motions from the phase component, due to atmosphere, topography and noise. Through a statistical analysis of the signals backscattered from a network of individual, phase coherent targets. The availability of an historical SAR archives confers to PSI the ability to measure and monitor displacement during the time and to assess temporal variations of motion.

1.2 Persistent Scatterer Interferometry (PSI)

Persistent Scatterer Interferometry (PSI) is a powerful remote sensing technique able to measure and monitor displacements of the Earth's surface over time. Specifically, PSI is a radar-based technique that belongs to the group of differential interferometric Synthetic Aperture Radar (SAR).
PSI techniques first emerged in 1999 when the Polytechnic University of Milan (POLIMI) produced and patented its Permanent Scatterers Interferometry (or PSInSAR™) algorithm.
Cumulative displacement, to map the total displacement that has occurred from the first satellite image acquisition, to any sequential acquisition (from the second to the last) can be measured. Also the average acceleration, to highlight areas affected by increasing or decreasing rates of velocity can be calculated, in according superficial ground displacements, historically based on traditional techniques, including conventional geotechnical instrumentation, such as wire extensometers, inclinometers, GPS.
The potential of the PSI technique has been recognized since it was first proposed. In the last fifteen years, a wide range of PSI applications has been developed. PSI offers wide-area coverage associated with a relatively high spatial measurement density. This allows studying wide areas (e.g. 100 by 100 km with single frames of StripMap ERS and Envisat, 250 by 250 km with single frames of the Interferometric Wide Swath of Sentinel-1), thus getting a global outlook of the deformation phenomena in the imaged areas.

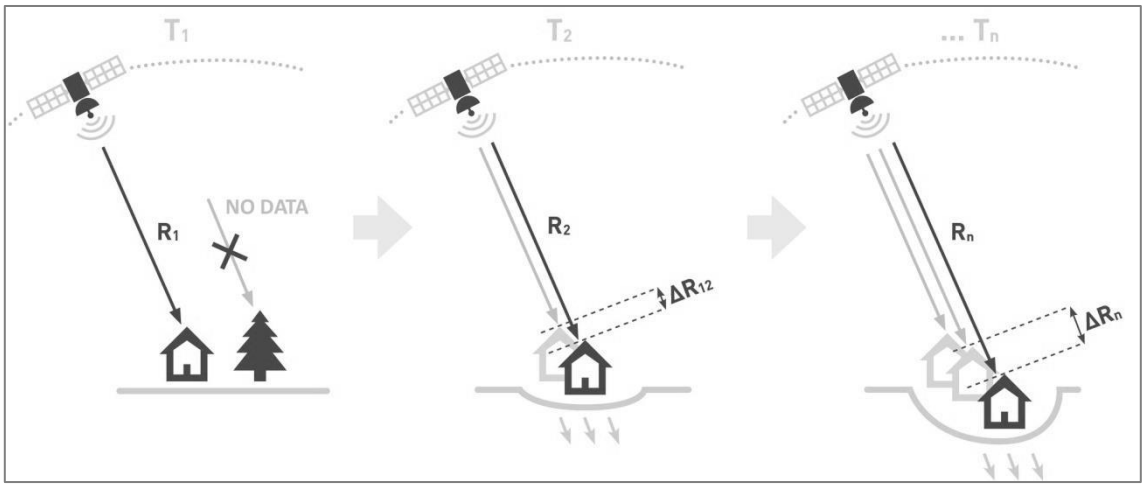

Figure 39 Basic concept of interferometric analyses: comparison of successive measurements of the sensor-target distance allows to determine relative displacements of the ground.

What is actually measured in interferometric applications is the projection of a target's motion onto the satellite's Line Of Sight (LOS). However, the LOS motion can often differ noticeably from the real value of motion, especially in cases where the ground motion is not vertical. By using both ascending and descending imageries, it is possible to obtain an accurate estimate of the true vertical and east-west components of the motion.(Fig.42)

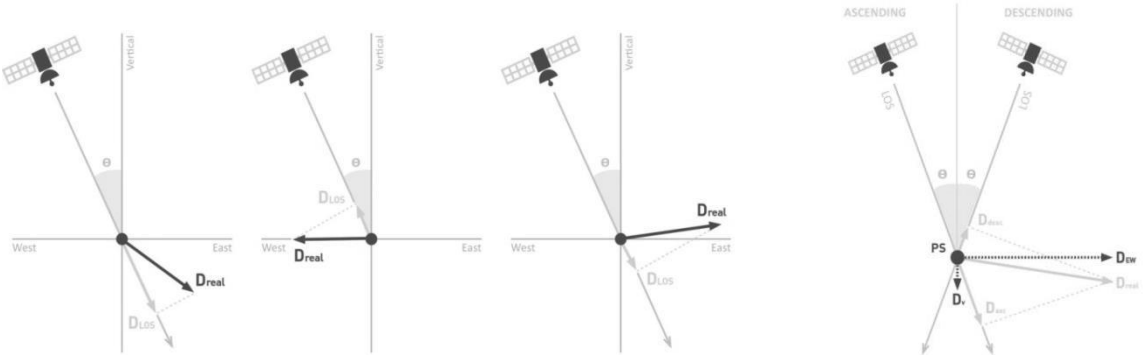

Figure 40 Simplified ascending and descending radar geometry. The ascending and descending radar LOS directions are assumed belonging to the East-Z plane. θ represents the look-angle, assumed the same for both ascending and descending geometries. The displacement vector (d) of an investigated PS, its projections along the different LOS's (dLOS Desc and dLOS Asc) and along the Cartesian axes (dz and dEast) are also shown.

However, by using ascending and descending data together, it is possible to combine the measured motion information to obtain an accurate estimate of the actual vertical motion and of the East-West component of the motion.

1.3 Sentinel 1 Images processing

ESA developed the Sentinel-1 European Radar Observatory, a polarorbiting satellite for operational SAR applications. The constellation of two C-band radar satellites will provide continuous all-weather day/night imagery for user services, especially those identified in ESA's GMES service elements programme and on projects funded by the European Union (EU) Framework Programmes. Three priorities ('fast-track services') have been identified by EU user working groups: marine core services; land monitoring; and emergency services. The first satellite was launched in 2011 aboard a Soyuz from Kourou.Sentinel-1 must maintain these quality levels in terms of spatial resolution, sensitivity, accuracy, polarisation and wavelength.

SAR interferometry can locate areas prone to landslides and monitor surface deformation to provide early warning of potential disasters and monitoring of critical infrastructure.

The SENTINEL-1 (Fig. 43) C-band SAR instrument supports operation in single polarisation (HH or VV) and dual polarisation (HH+HV or VV+VH), implemented through one transmit chain (switchable to H or V) and two parallel receive chains for H and V polarisation. .

Level-1 Single Look Complex (SLC) products consist of focused SAR data, geo-referenced using orbit and attitude data from the satellite, and provided in slant-range geometry. Slant range is the natural radar range observation coordinate, defined as the line-of-sight from the radar to each reflecting object.

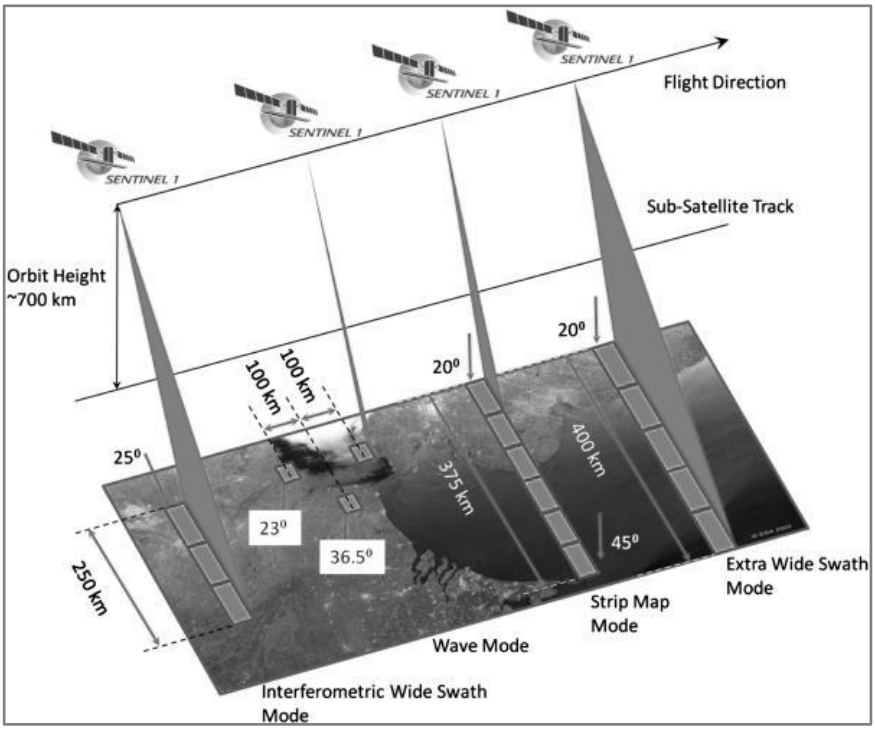

Figure 41 How to work Sentinel 1

2. Monitoring Induced Diplacement Phenomena in Gimigliano Area

Landslide events are complex geological and geomorphological processes due to a different factors and therefore it is very difficult to classify the existing one and predict the future occurrences.

The investigation has permitted to obtain an truthful deformational setting within the site-specific investigation, and to finally realize a detailed overview of the spatial distribution and temporal evolution of ground displacement phenomena in Gimigliano area in Calabria Region (Italy), by means of PSI analysis exploiting C-band data from Sentinel-1 satellite.

The deformation rates from SAR datasets were joined with available geo-information such as geological and geomorphological evidences resulting from existing auxiliary data, e.g. landslide databases, thematic maps and aerial orthophotos, and historically based on traditional geotechnical technique including conventional instrumentation, such as wire extensometers, inclinometers, GPS, too. In order to assess any temporal patterns of deformation, the present Sentinel 1 PS data were analysed and compared with historical radar measurements acquired by ESA missions archives, *i.e.* ERS, ENVISAT and TerraSAR-X satellites.

Gimigliano town is located in the Southern Calabria (Italy). The old medieval village is divided into two built-up areas (Gimigliano Superiore and Gimigliano Inferiore), which are placed almost on the same axis NNE oriented, but at different altitudes: “Gimigliano Inferiore is at an altitude of about 510 m a.s.l., while Gimigliano Superiore, is sited at 620 m a.s.l.. Both areas are located on sloping ridges of Gimigliano Mountain. The new modern Gimigliano town is built-up on the eastern lower part of the urbanized area, on an ancient landslide, defined as a complex phenomenon that is an rotational slide evolving into a flow. The landslide has an extension of 1.3 km^2 and a volume of about 10 million of cubic meters. The landslide can be defined as active, and according to the nomenclature in Cruden and Varnes,1996, the velocity ranges from slow to very slow.

Landslide occurrences represent a major threat to buildings and infrastructure, causing extensive direct damage.

The geomorphologic setting is characterized by widespread slope movements. Diffuse landslides with occasional deep-seated gravitational slope deformations have been recognized in the whole area (Fig. 44). Geological structure deeply controls geomorphological context: structural discontinuities and variation in erodibility of different lithotypes.

Figure 42 Gimigliano town: ground displacement phenomena are widespread across time up to nowadays, all over study area.

Comparison among past and recent cartographic maps suggestions that areas already affected by hydrogeological hazard and catastrophic events in 1950s have been nevertheless built-up throughout recent urban planning and unauthorized private enterprises.

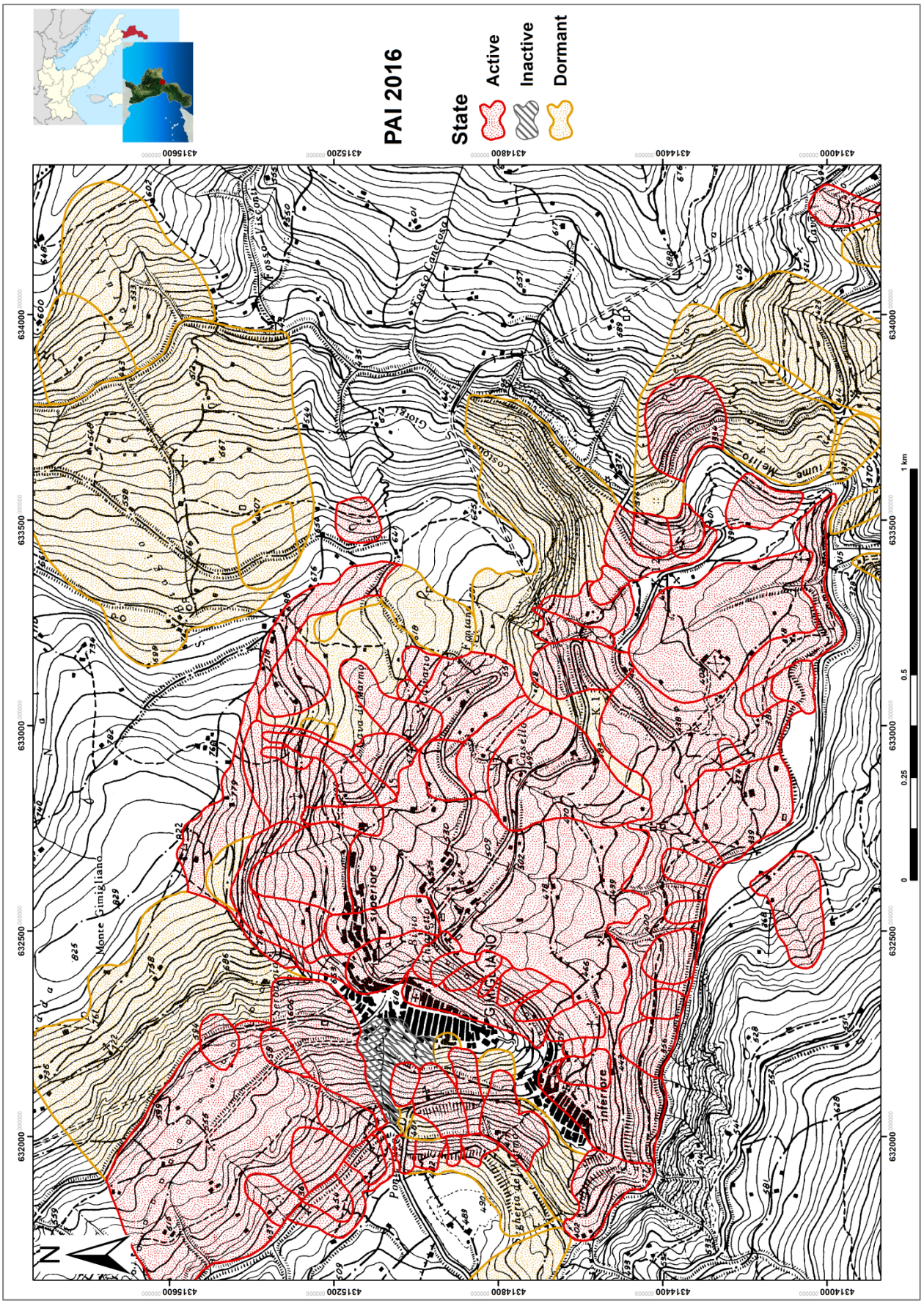

Figure 43 IGM Cartographic Map, Scale 1.1000 (1954) and Inventory Map derived from PAI, suggest that the area was already affected by hydrogeological events.

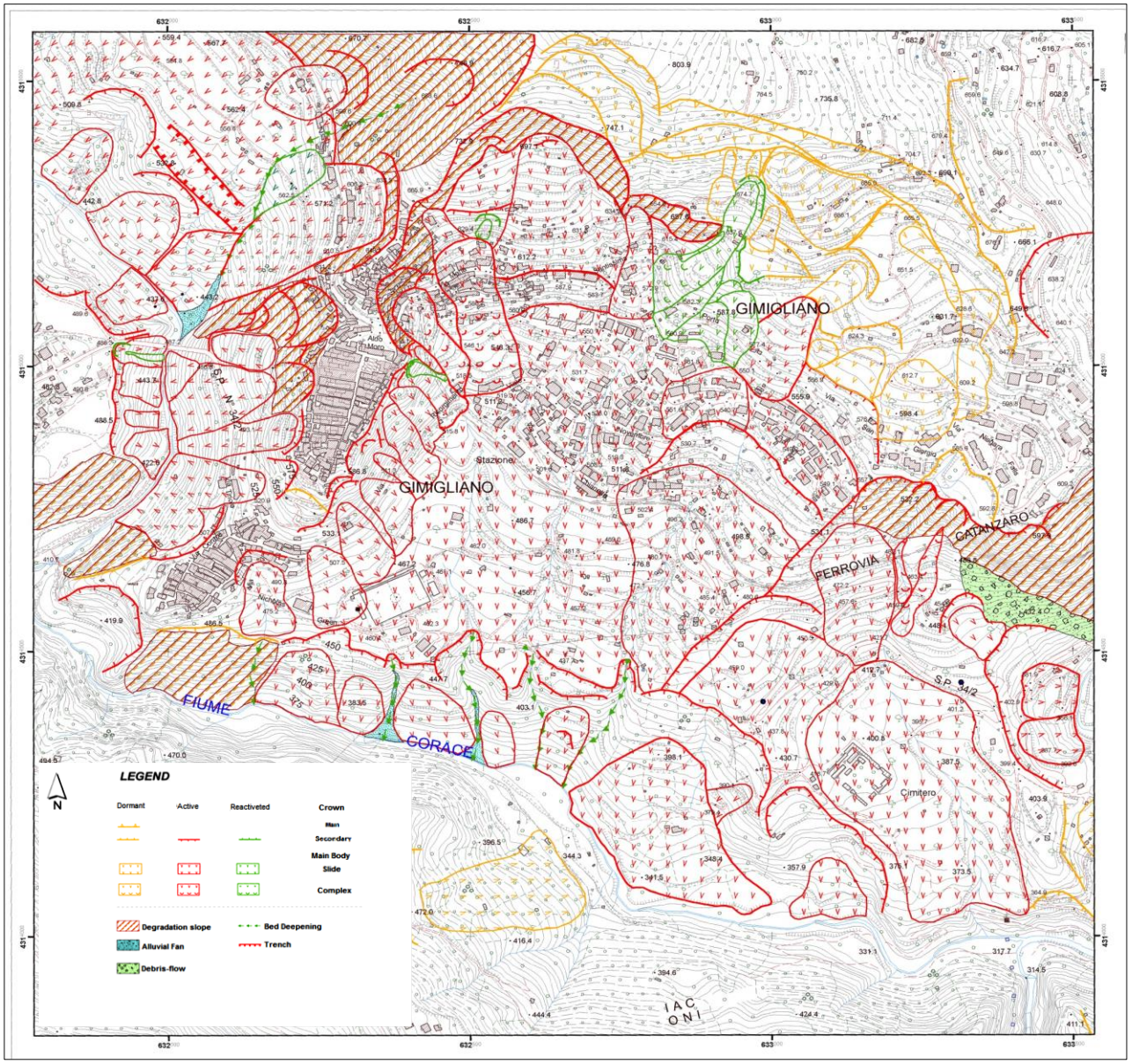

Figure 46 a-b Inventory Landslides Map

Characterization and monitoring Gimigliano landslides have been carried out by using long stacks of satellites Synthetic Aperture Radar (SAR) images and PSI analysis has been carried out exploiting of Sentinel-1 SAR images spanning from October 2014 to October 2016 in ascending and descending orbits. Radar data acquired are combined with geological and geomorphological evidences resulting from the auxiliary data such as aerial orthophotos referred to different dates and landslide databases.

Results coming from PSI, inventories, topography and aerial imagery analysis are finally validated with recent field checks and *in situ* observations and all data are implemented in a Geographic Information System (GIS) environment, which allows to suitably to store, manipulate, analyse, manage, and present spatial or geographic data collected.

3. Data and Methodology

Data processing and analysis were treated by means of a new approach to Persistent Scatterer Interferometry implemented by remote sensing department, Geomatics Division of CTTC, Centre Tecnològic de Telecomunicacions de Catalunya (CTTC).

According to linear deformation velocity maps and the ground deformation occurrences over a site of Corace River , in the Catanzaro Stretta, specifically in Gimigliano Municipality has been analysed.

The elaboration is comparted in different sections:

1. Sentinel 1 processing: from the images download to the interferogram generation in which explains all the necessary steps to get a set of interferograms. All the step of the image processing are applied by executing scrips elaborated in Linux Coding.
2. Velocity and topographic error estimations, in which explains how to process the interferogram in order to have a cleaned, unwrapped, and then geocoded result over a subset points. The linear velocity of deformation and residual topographic error RTE are estimated. If image dataset is lower than 20-25 images the estimates velocity could be not correct. However, the RTE estimation is more robust, so it can be used only the output RTE map.
   In this specific case 34 images in ascending geometry and 21 in descending geometry are available, .
3. The topographic error, thermal dilation and the linear velocity of deformation are estimated from a stack of differential interferometric wrapped phases (551 interferograms obtained from ascending images and 182 from descending ones)

In order to visualize the outputs in Envi , vectorial files are converted to raster files. It is also possible visualize them in Google Earth or in a GIS Software.

4. Geocoding assigns to each line-column position of a vector the corresponding WGS84 and UTM-WGS84 coordinates. The geocoding utilize the orbit information and the DEM.

Selection of SAR images suitable for interferometry use is the first step to be carried out for any interferometric processing. It is a key step, since the criteria adopted for selection of the images have strong impact on the quality of the final results. These criteria depend upon the specific application for which the SAR interferometric images are required.

A total of 55 Interferometric Wide swath (IW) Single Look Complex (SLC) Sentinel-1 images from the ESA archive (31 in ascending geometry and 24 in descending geometry), ranging the period from October 2014 to October 2016 was collected in this study.

A list of Sentinel 1 images acquired over a certain area is easy to obtain, thanks to the Sentinel Scientific Data Hub, on the website http://scihub.copernicus.eu/dhus/#/home (Fig.10). Download of

two images concurred is allowed. Frequently download of the images fails or has a problem; in those case file .zip maybe it is corrupted.in this case it was necessary to repeat download operation.

This data hub allows the user to perform fast inventory searches on the major ESA-supported missions, by means of a user-friendly graphic interface. All images acquired over the area of interest can easily be identified, drawing a polygon of the area of interest and/or by selecting advanced search criteria.

SLC product type was selected and the relative orbit of the frame interested is number 138, in ascending and number 57 in descending orbit.

Each images covers approximately a spatial resolution of 3 x 20 km in range and azimuth, respectively. The processing was performed burst-wise over the multi-looked interferograms (1 in azimuth and 5 in range). Then precise orbits have to be periodically downloaded and updated , especially before doing precise orbits extraction. The precise orbits are available only after 15 days the image data acquisition.

Before starting processing necessary file is required: a DEM in order to remove the topographic component in following processing. The elevation models derived from the SRTM data are used in geographic information systems. (Fig.11). It can be downloaded freely over the Internet, and file format (.hgt) is widely supported. The major part of the topographic phase has been removed by using the 90-m pixel size SRTM DEM.

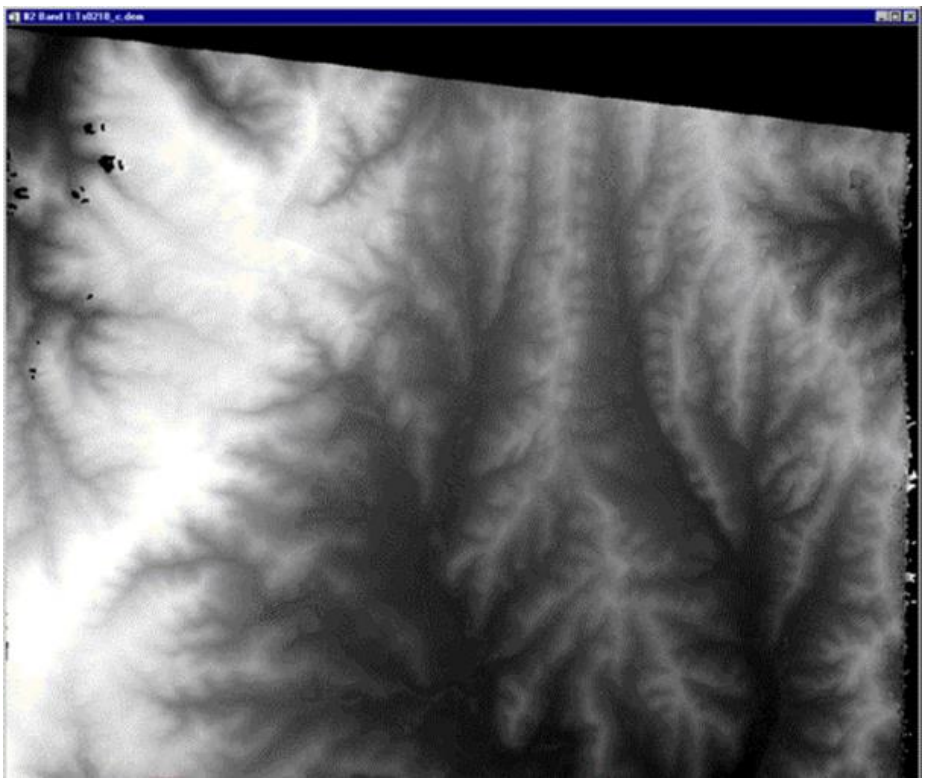

Figure 44 DEM Digital Elevation Model derived from SRTM, used in order to remove topographic component during the processing.

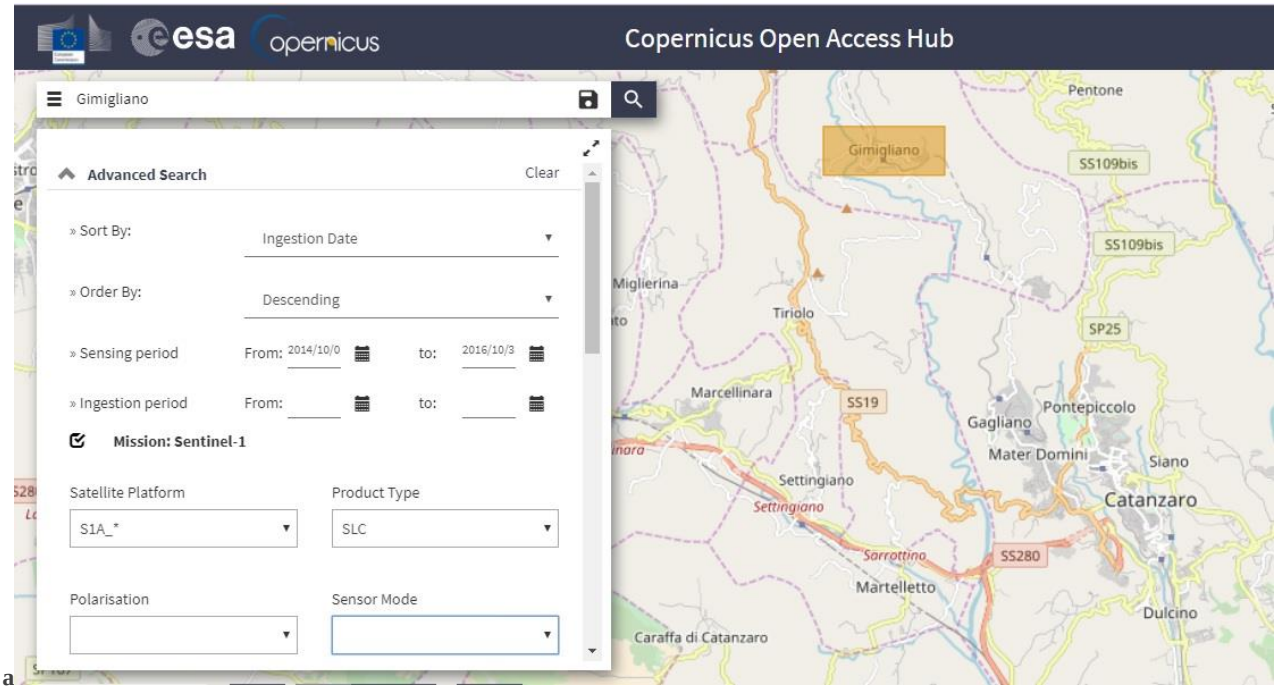

a

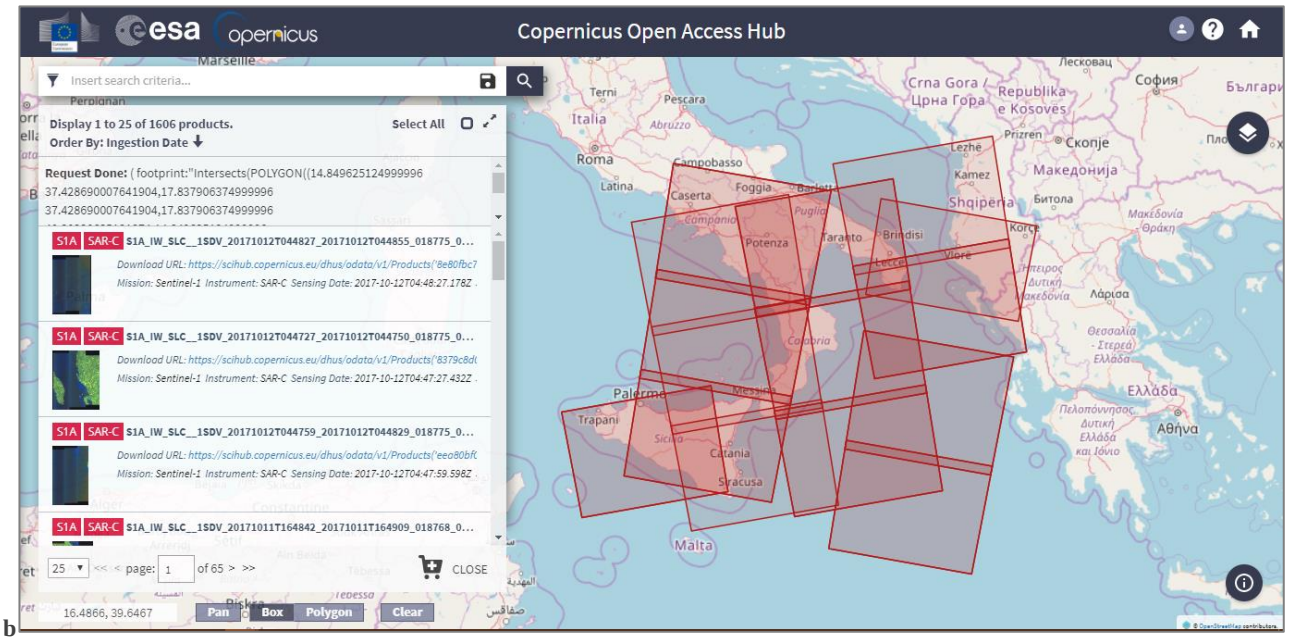

b

Fig.48 a- b. Open Access Hub : access point for all Sentinel missions with access to the interactive graphical user interface.

From the images download to the interferogram generation executing scrips elaborated in Linux Coding were applied, explaining all the necessary steps to get a set of interferograms.

By editing this scrips it was defined all variables and working parameters and directory of following processing steps.

The starting point is a set of N single look complex SAR images from which a set of M interferograms is calculated (M ≫N).

Three main steps following are described:

1. Point selection is based on DA criterion. DA represents a statistical parameter that estimates the temporal variability of the scattered response for each point and it is used to calculate the phase noise criterion is based on the. (Ferretti et al.2001). The procedure consists in an iterative search propagation criterion that starts with the selection of one or more seed PSs located on the ground, with no motion or thermal expansion and characterized by small noise. The PS analysis was applied to points with DA lower than 0.3.
2. Atmospheric phase and orbital error components estimation and removal from the original interferograms: a sequence of spatial and temporal filters were applied in order to estimate and remove Atmospheric Phase Screen contribution to the phase based on the assumption that the atmospheric component is characterized by smooth spatial phase gradients and a random behaviour in time.
3. Linear deformation velocity and RTE estimation over the atmosphere free interferograms: This step provides for each selected point three parameters:
    a. the deformation velocity using a linear model of the deformation during the measured period and with respect to a reference point,
    b. the height of each measured PS with respect to the DEM used to calculate the network of differential interferograms (residual topographic error or RTE)
    c. an associated statistical parameter named temporal coherence ranging between 0 and 1 that evaluates the agreement between the observed interferometric phases (interferograms) and the linear deformation model (Tab 1 a-b.)

Table

Table Options

FID	Shape *	ID	Row	Col	Fi	Lambda	E	N	H	Etopo_m	Velocity_m
0	Point ZM	0	241	1895	38.966573	16.532931	632805.008	4314184.493	383.18	3.8	3.7
1	Point ZM	1	242	1895	38.966702	16.532944	632805.867	4314198.885	385.72	2.5	3.9
2	Point ZM	2	269	1896	38.970286	16.533902	632882.188	4314598.067	493.54	3.3	14
3	Point ZM	3	270	1895	38.970416	16.533915	632883.07	4314612.459	499.08	6.7	11.4
4	Point ZM	4	276	1844	38.9708	16.531235	632650.163	4314651.146	488.08	0.6	-3.9
5	Point ZM	5	277	1981	38.972213	16.540255	633428.884	4314821.138	663.79	55.6	1.3
6	Point ZM	6	278	1892	38.971407	16.533703	632862.831	4314722.184	508.76	3.3	13.5
7	Point ZM	7	279	2008	38.972563	16.540914	633485.352	4314860.963	630.4	13.9	0.8
8	Point ZM	8	280	2008	38.972684	16.540867	633481.085	4314874.334	629.33	10.8	0.6
9	Point ZM	9	281	1682	38.970465	16.524426	632060.909	4314604.086	534.94	33.9	3.2
10	Point ZM	10	281	1998	38.972746	16.540405	633440.965	4314880.515	631.24	13	2.6
...	...	...	...	...	...	...	...	...	...	...	...
601	Point ZM	601	558	1896	39.006577	16.529541	632436.668	4318619.265	751.07	36.2	3.7
602	Point ZM	602	559	1779	39.005783	16.523075	631878.28	4318521.742	683.29	12.7	4.2
603	Point ZM	603	574	1632	39.006661	16.515802	631246.878	4318608.629	676.7	-11.8	1.7
604	Point ZM	604	575	1631	39.006781	16.515751	631242.24	4318621.922	678.21	-10.2	1.8
605	Point ZM	605	575	1632	39.006783	16.515766	631243.486	4318622.175	676.25	-11.7	3
606	Point ZM	606	576	1631	39.006901	16.515694	631237.067	4318635.114	676.48	-12	2.6
607	Point ZM	607	576	1632	39.006905	16.515725	631239.701	4318635.643	675.53	-12	3.6

1 (0 out of 608 Selected)

Ascending PS

Table

Geocod_Desc

FID	Shape *	ID	Row	Col	Fi	Lambda	E	N	H	Etopo_m	Velocity_m
0	Point ZM	0	1067	2326	38.980974	16.524122	632015.012	4315769.963	682.38	6.4	-3.3
1	Point ZM	1	1074	2321	38.979859	16.525821	632164.299	4315648.647	684.66	0.9	-5.8
2	Point ZM	2	1075	2323	38.979795	16.525351	632123.682	4315640.832	653.76	-2.4	-0.1
3	Point ZM	3	1087	2324	38.97823	16.525655	632152.932	4315467.614	582.98	-5.4	-5.6
4	Point ZM	4	1091	2319	38.977546	16.526968	632267.902	4315393.683	627.94	0.5	1.6
5	Point ZM	5	1091	2319	38.977556	16.526898	632261.87	4315394.6	630.23	6.1	0
6	Point ZM	6	1091	2319	38.977559	16.526874	632259.784	4315394.921	628.98	6	2.4
7	Point ZM	7	1092	2319	38.977418	16.52698	632269.204	4315379.411	627.98	1.6	-0.2
8	Point ZM	8	1092	2319	38.97742	16.526966	632268.014	4315379.596	625.93	0.2	2.6
9	Point ZM	9	1092	2319	38.977426	16.526914	632263.492	4315380.285	626.87	3.6	1.5
10	Point ZM	10	1092	2319	38.977432	16.526872	632259.795	4315380.855	623.96	2.7	0
...	...	...	...	...	...	...	...	...	...	...	...
829	Point ZM	829	1295	2324	38.952431	16.520803	631780.42	4312597.462	519.31	-11.7	4.5
830	Point ZM	830	1295	2324	38.952404	16.521007	631798.173	4312594.782	499.37	-23.4	2.2
831	Point ZM	831	1295	2327	38.952636	16.519253	631645.746	4312617.997	547.4	-40.4	-11.6
832	Point ZM	832	1295	2327	38.952655	16.519111	631633.38	4312619.873	555.74	-37.9	-12.1
833	Point ZM	833	1296	2311	38.951242	16.528831	632478.291	4312477.104	301.28	-17.8	6.7
834	Point ZM	834	1296	2311	38.95126	16.528692	632466.193	4312478.939	308.96	-14.6	7.1
835	Point ZM	835	1296	2322	38.952031	16.522868	631960.128	4312556.056	441.13	-25.1	8
836	Point ZM	836	1297	2311	38.951162	16.528471	632447.233	4312467.737	325.01	-10.7	9.1
837	Point ZM	837	1297	2321	38.951887	16.522997	631971.511	4312540.259	431.66	-30.3	15.2

1 (0 out of 838 Selected)

Geocod_Desc

Tab 1. Geocoding Table in GIS softwareis :a: ascending geocoding; -b:descending geocoding.

In this work, only the points with temporal coherence higher than 0.65 have been used. High threshold value maybe induces a critical loose of measurements in areas affected by strong non-linear deformations but in this case it is more interesting to evaluate linear deformation pattern.

The deformation phases were reached directly from the interferometric phases of the total consecutive temporally connected interferograms (551 interferograms obtained from ascending images and 182 from descending ones) over a set of points selected using a temporal consistency criterion. The interferograms used have a temporal baseline of 12 days and perpendicular baselines.

Processed area is relative small, finally including one burst (number six) of Swath 1 in ascending orbit and descending one burst (number 5) in Swath 2, accounting for approximately 3500 km2.

The topographic error, thermal dilation and the linear velocity of deformation are assessed from a stack of differential interferometric wrapped phases.

So as to visualize the outputs in Envi, vectorial files are converted to raster files. It is also possible visualize them in Google Earth or in a GIS Software.

Geocoding assigns to each line-column position of a vector the corresponding WGS84 and UTM-WGS84 coordinates. The geocoding utilize the orbit information and the DEM.

Each measurement is referred temporally to a unique reference image, chosen to minimize the effects of spatial and temporal baselines and to maximize the total coherence of the interferometric stack and to keep as low as possible the dispersion of the normal baseline values.

Velocity deformation map of the burst under study derived from 51 Sentinel-1 images and a total of 731 interferograms. Positive values (blue) indicate displacements towards the SAR, while the negative ones (red) denote displacements away from the SAR sensor. Note that these values refer to the SAR Line-of-Sight (LOS). The map shows a large area affected by subsidence (red) with displacement values of up to 27 mm/yr during the two years of observations.

As reported in Table 2 Sentinel 1 datasets in ascending geometry, the number of natural benchmarks detected is smaller than in the descending orbits. Moreover, also the absolute values of registered velocities are lower in the ascending geometry (Fig.42).This is mainly related to the SAR looking geometry with respect to the topographic aspect and to the direction of slope movement.

	Time period	Number of PS	Mean (mm/yr)	Minimum (mm/yr)	Maximum (mm/yr)
ASCENDING	01/10/2014 28/10/2016	607	- 0.66	-26.7	24.5
DESCENDING	01/10/2014 29/09/2014	837	-1.21	-23	16.7

Table 2. Within study area, mean and maximum velocity for each datasets.

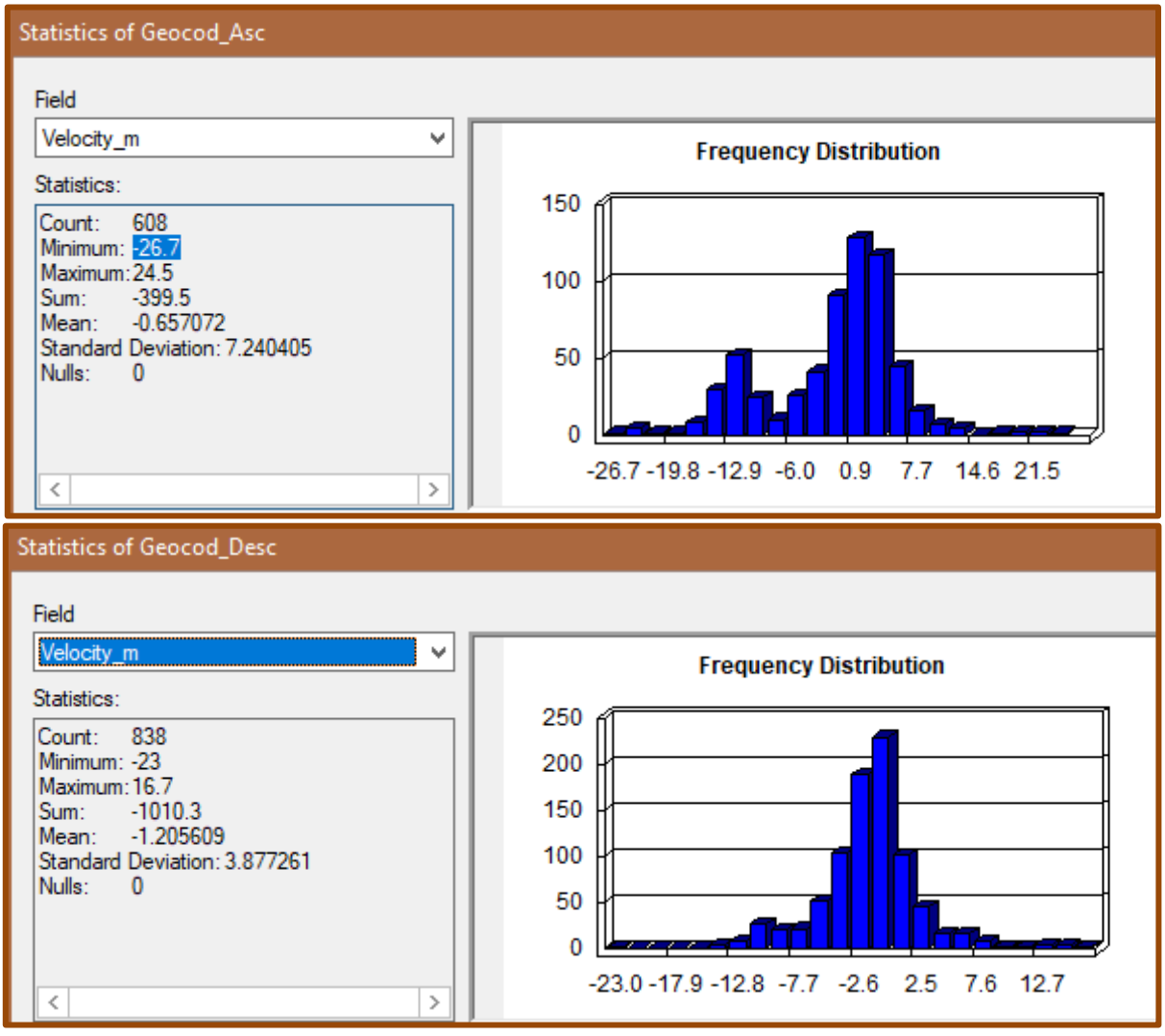

Fig.49 Statistics of PS results from both ascending and descending acquisition geometry.

SENTINEL-1 satellite is potentially able to map the global landmasses in the Interferometric Wide swath mode once every 12 days, in a single pass (ascending or descending). Each SENTINEL-1 satellite will be in a near-polar, sun-synchronous orbit, with a 12-day repeat cycle and 175 orbits per cycle.

The PS analysis makes known an significant subsidence area, which is mainly associated with the occurrences of a deep-seated gravitational slope deformations (DSGSDs), highlighting geomorphological component of ground deformations.

PSI has proved to be effective in detecting surface deformation of specific site involved in ground deformation due to geomorphological instability and tectonics, too.

The areas subjected to the maximum velocities of subsidence approximately coincide with the main scarp of one of the bigger landslide that occurred in Gimigliano involving weathered rocks and sediments.

A detailed inventory map, including information on landslide activity, in Corace River Basin, using tectonics impact factor as a triggering factor to landslide susceptibility. In particular we focus on Gimigliano Municipality (Fig. 44-46)

A set of Sentinel-1 SLC images, acquired during a temporal span of 24 months, over the Calabria region (Southern Italy), in an area where geological structure deeply controls geomorphological context, most of all structural discontinuities and variation in erodibility of different lithotypes.

The tectonic context is dominated by strike-slip tectonics, lasting from Late Miocene to Quaternary (and, presumably, still active) in which late emplacement mechanisms of the deep-seated Mesozoic carbonate rocks, and their geometric relationships with the overlying units of the Calabrian Arc are led by the development of the area.

A higher frequency of landslides is related to areas with higher indexes of active tectonics in the northeaster slopes of Corace basin and mostly in Gimigliano village. These correlations between density of landslides and active tectonics intensity, expressed by geomorphic indexes, suggest the usefulness of the integration of the active tectonics between the main determinant factors in landslide susceptibility assessment of mountain alpine areas which may be applied to similar areas around the world.

Analysing a only two bursts of a Sentinel-1 frame (approximately 3500 km2), a couple number of landslides have been detected, thus allowing to improve the pre-existing inventory maps both in terms of landslide boundaries and state of activity.

Ground deformations within Gimigliano area were evaluated using PS data and their interpretation. Results obtained by processing acquired by the European Space Agency (ESA) Sentinel 1 SAR sensors over Southern Calabria show that the PS approach pushes measurement accuracy very close

to its theoretical limit allowing the description of millimetric deformation phenomena occurring in a complex area characterized by ground deformation due to tectonics and gravity phenomena. A comparison with corresponding displacement time series relative to permanent GPS stations available from past measurements is carried out. Also a comparison with geological, morphological and geotechnical conditions (e.g., areal extent, rate of movement, surface topography) at different periods is performed.

In order to limit the effects of geometrical distortions induced by the side-looking view of SAR sensors and to couple the analysis of both acquisition geometries, data were acquired from both ascending and descending orbits. A total of 55 Sentinel-1 satellites SAR scenes was collected from the ESA archive and interferometrically processed by means of the PSinSAR technique.

Moreover, vertical deformation in the upper part of the landslide body is thought to reflect a complex movement, evolving downhill into an earth flow.

Results of the multi-interferogram PS approach are the map of the Ps identified in the image and their coordinates: latitude, longitude and precise elevation. As in all differential interferometry applications, results are not absolute both in time and space. Deformation data are referred to the master images (in time) and results are computed with respect to a reference point of know elevation and motion (in space).

The results of this analysis consisted of the yearly average velocity of 1445 PS with coherence higher than 0.65 (608 in descending orbit and 837 in ascending orbit) covering the whole territory of Gimigliano Municipality.

SAR sensors are side-looking radar and operate with a LOS direction tilted with respect to the vertical direction. Because of the rather small incidence angle (usually between 23° and 45°), the sensor is much more sensitive to vertical deformation than to horizontal deformation. Hence, the resulting datasets can estimate only a small component of the 3D real motion of the landslide, i.e., the projection along the satellite LOS. N-S deformation components are underestimate because of satellite geometry acquisition.

Combining ascending and descending information permits one to extract the vertical and horizontal (in the east-west direction) components of the movement and, consequently, the real vector of displacement. In this case is not necessary to extract ascending and descending component because of landslide is a 3D phenomenon.

Given the sensitivity of the sensor and the standard deviation analysis of the velocity values for the stable areas, the values of velocity between −1.5 and 1.5 mm/ yr have been substantially considered as stable (green colour).

The red zones (negative values) have moved away from the satellite and the blue parts of the map (positive values) indicate zone that moved toward the satellite. In particular, red zones are indicative of subsidence phenomenon, while the blue zones indicate a relative ground uplift.

In facts, velocity map (Fig. 43 a-b) shows that mainly motions are due to vertical deformation, given that the LOS is inclined at an angle close to the vertical and the horizontal displacements are significantly underestimated. And because of every deformation , above all landslides are defined as three dimensional phenomena.

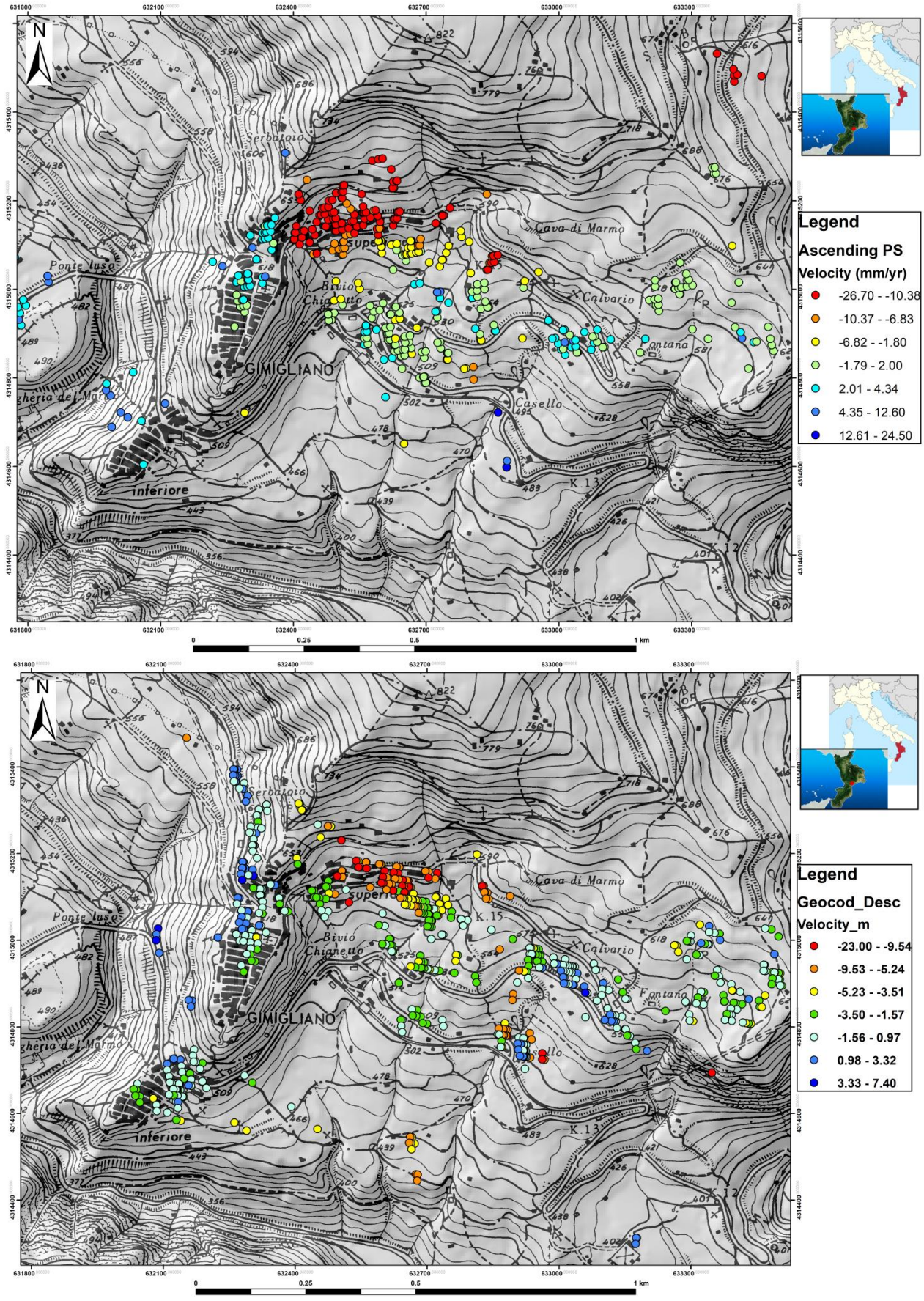

Figure 50 a-b Map view of October 2014- October 2016 range-change rate measurement of PS ascending orbit and descending orbit. The underlying image is a relief from a 5m pixel DTM of the area and topographic map at scale 1:10.000.

The 0.65 coherence threshold has been selected to obtain a dataset with errors less than 3 to 5 mm/year. The precision on single PS LOS measurements depends on both the number of available SAR images and the PS multiinterferogram coherence.

The Line of Sight (LOS) displacement rates vary from 24 to −26 mm/year in ascending dataset and ranges from --23 to 7 in descending geometry and are relative to reference points assumed motionless.

Most of the PSs are in the urban area, where the density of man-made structures is high. Smaller amount of PS were detected in the mountain sectors because of the morphological (steep slopes) features. The results have been compared also with deformation values detected during GPS and geotechnical campaigns ordered by the Gimigliano Municipality.

Figure 51 Overview of the Gimigliano landslides system. The landslide on the right affects the entire town and has a translational kinematics with low rotational component. The landslide on the left shows a more pronounced rotational component.

Figure 15 General view of the main Gimigliano landslide.

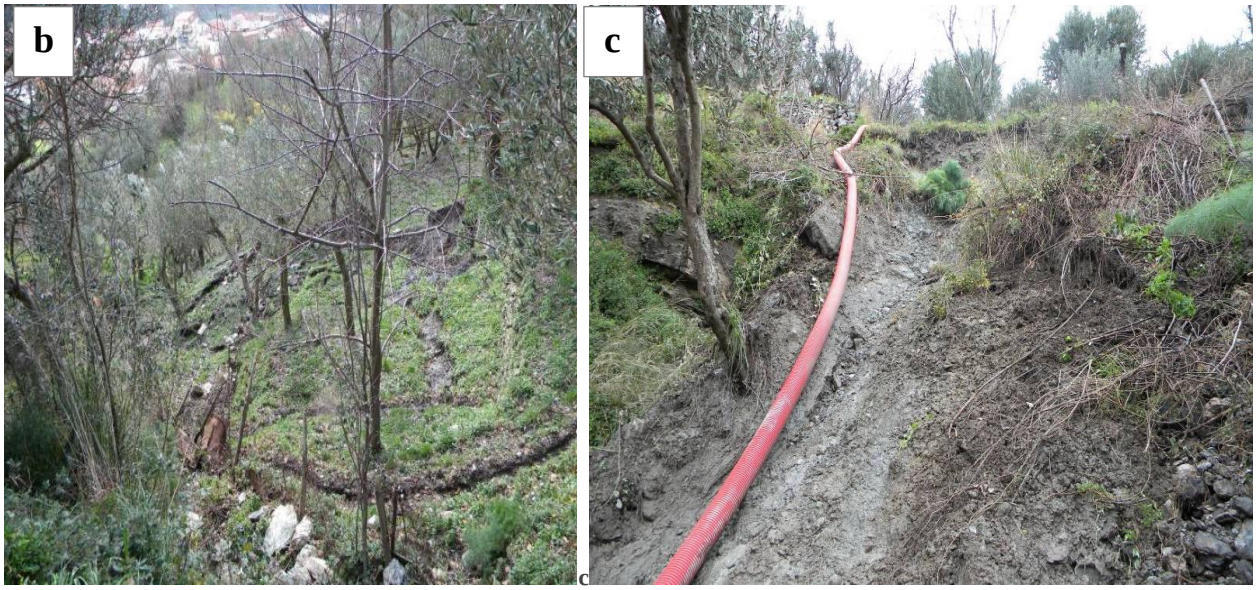

Figure 52 a-b-c. Wide world displacements, diffused over thw whole area.

Within Gimigliano town the PS analysis highlights that the modern downhill built-up area was affected by surface ground deformation before time.

Moreover, PS ERS analysis also reveals the instability of the eastern part of old Gimigliano Superiore, confirming the presence of several active landslide already mapped with a LOS deformation velocity of about −9 mm/yr, while the old urbanized centre of Gimigliano Superiore and Inferiore turn out to be stable.

The PS velocity map overlapped on orthophotos referred to 2008. Active landslides affecting the eastern part of Gimigliano Superiore is confirmed to be moving, with average LOS velocities of about −12 mm/yr. The head of the landslide is characterized by mean rates of displacement ranging between −2.5 and −8 mm/yr; the main body involving the town appears to be almost stable with minor predisposition to move.

A group of some moving PS can be noticed in the north-eastern part of the built-up area, located on a steeper slope and characterized by higher velocity values of about −8 mm/yr. The old village of Gimigliano Inferiore exhibits green point targets with average velocities ranging more or less ±1.50 mm/yr, from now it looks to be steady.

Unfortunately, no PS were detected in any of the mapped landslides in lower portion of the slope, because of the west-facing aspect of the slopes that are not properly visible by an ascending orbit sensor.

The PS data distribution suggests that the maximum deformation velocities are recorded in the southwestern Mt. Gimigliano mountainside towards Corace river and in the southern side on old eastern built-up area of Gimigliano Superiore. Mt. Gimigliano southern slope and the new modern

downhill town of Gimigliano Superiore, is extensively affected by high rates of ground motion; this area was already subjected to displacement in the past, according to historical data sets and is still showed increasing in deformation rate.

Active deformations along Mt. Gimigliano southern slope were identified: the wide landslide phenomena affecting this area and including the whole new modern part of Gimigliano showed an average PS velocity value of -12 mm/yr and was still active from 20012 nowadays.

The majority of PS radar targets that fall in the old central part of Gimigliano Superiore village results to be almost stable, especially eastwards.

It can be detected that Gimigliano Inferiore village includes moving PS and appears to be slightly affected by ground movements that were increase compared to the velocity rates in the previous time periods.

The hill slope towards Corace River shows high yearly average LOS velocities of about −26 mm/yr; the negative sign corresponds for a an increasing distance from the sensor and, given the descending LOS geometry and the general southwest facing hill orientation, it evidences high downward movements along the slope and reveals the state of activity of the landslide which is still active. New complex failure on the slope on the western side of Corace Rive are recognized, confirmed by comparing regional topographic map CTR (Scale 1.500) , dated 2008 and current detection.

Previously mapped t slides were extended, tracing new lateral limits and/or reclassify in type or activity state, especially where weathered green-schists, fillades and clays were outcropped.

The modern built-up village located in a gentle gradient, shows moving PS but with velocity lower than −18 mm/year, that corresponding to the main body of largest landslide (Fig.48 A-B).

The boundaries of the velocity colour classes were fixed not to be excessively large compared to the distribution of velocity values, in order to prevent most radar targets to fall into the stable class and defined calculating frequency values distribution to underline variability of collected data.

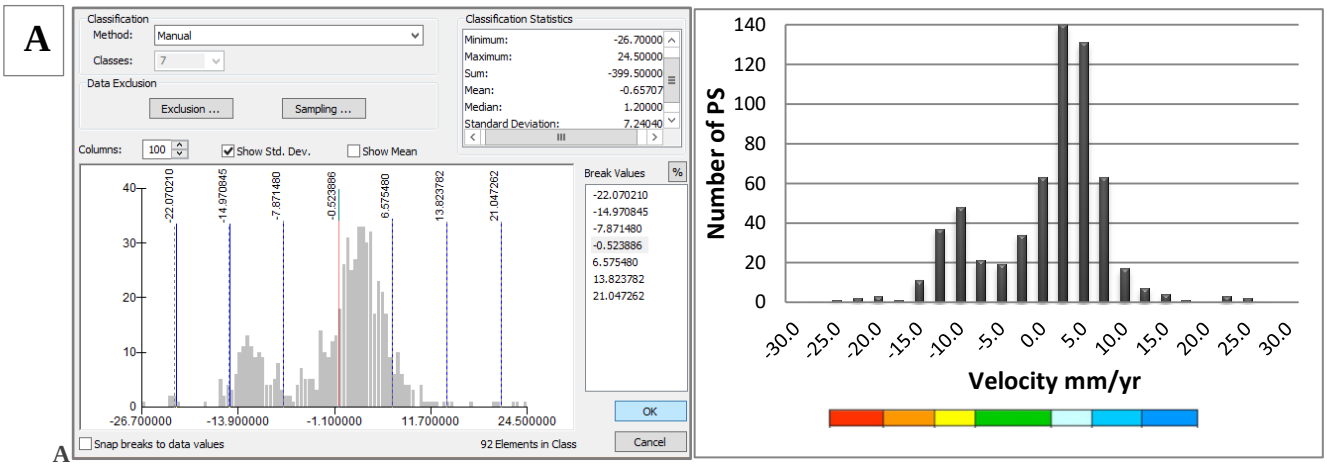

A

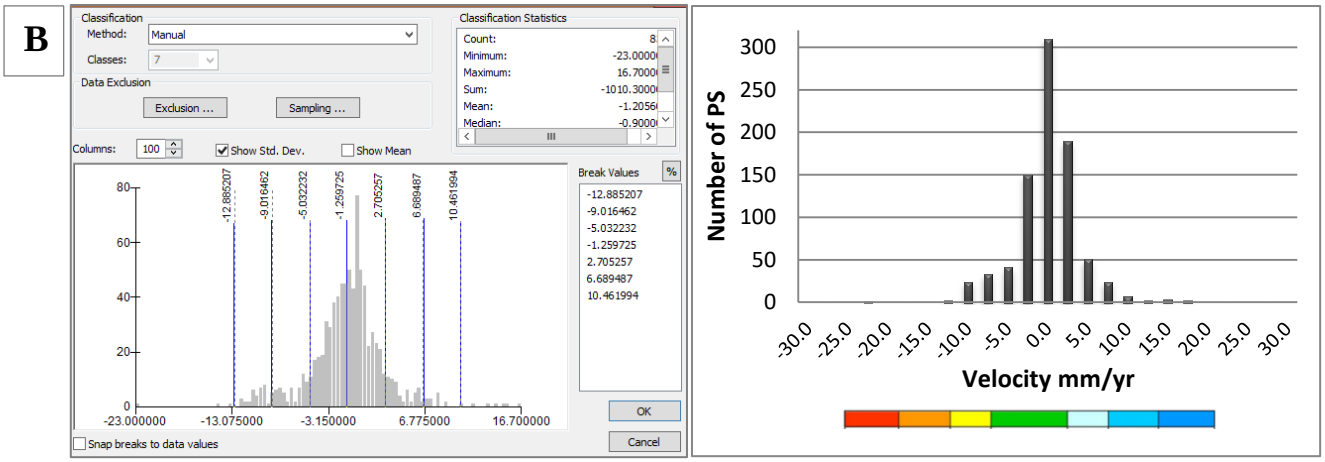

Figure 5345 A-B The boundaries of the velocity colour classes were fixed not to be excessively large compared to the distribution of velocity values.

The range intervals must be chosen to be not too thin because the width of velocity classes can be reduced to facilitate the identification of more detailed spatial variations of the landslide phenomena, but it cannot fall below the resolution of the technique.

Discussion and conclusion

Spaceborne differential synthetic aperture radar interferometry (DInSAR) has already proven its potential for mapping ground deformation phenomena.

Deformation phenomena associated with mass movements, river erosion, and frantic phenomena affect the entire territory of Gimigliano. Overall, it is quite obvious how the territory falls within a complex and constantly evolving geomorphological context.

This could suggest a greater stability of the area closest to the centre, instead, the greater instability recorded in recent years. In this regard, however, it should be considered:

the influence of the topographic factor (higher altitudes compared to the slope of accumulation of the sectors closest to the Gimigliano Municipality and the influence of geological, structural and hydrogeological factors, weathered and fractured rocks which are involved in the phenomenon of landslides, together with the underground water circulation.

By mean this research in the Gimigliano area it is possible to highlight that PS data are enable to detail and study spatial and temporal evolution of ground movements underling the capability for detecting, mapping and monitoring ground deformations,

Rock weathering of the outcropping sedimentary and metamorphic litotypes across time could be caused an increasing in ground displacement phenomenon.

A large numbers of Sentinel 1 PS were identified in the Gimigliano area, corresponding to a very high spatial density of measurements observing the number and the density of detected PS datasets, in both ascending and descending orbits.

Considering that slope visibility depends on the availability of the satellite orbit, slope orientation and inclination with respect to the LOS direction control the of PSI analysis performance.

PS technique has highlighted intrinsically limitations in ground motion detection: spatial facet related to the combination of the local slope characteristics with the satellite acquisition parameters, and a temporal constraint related to the signal decorrelation. Also spatial feature, vegetation and topography introduce a constraint in the number and reliability of detected scattering points.

Moreover, due to the phase ambiguity of SAR data processing and satellite acquisition parameters in C band, the PSI analysis of landslides is limited to phenomena ranging from "extremely slow" (velocity < 16 mm/yr) to "very slow" (16 mm/yr < velocity < 1.6 m/yr).

A Map of the PS identified in the image and their coordinates: latitude, longitude and precise elevation (accuracy on elevation better than 1 m) was obtained and the Average LOS deformation rate of every PS (accuracy usually between 0.1 and 1 mm/year, depending on the number of available interferograms and on the phase stability of each single PS) was estimated.

Within the PS velocity, a stable threshold range of ±1.5 mm/yr (away or toward the satellite direction) was fixed for classifying PS rates and for distinguishing moving from not moving areas. Therefore, the movement threshold of ±1.5 mm/yr is assumed as a good conservative rate of the average deformation.

Landslide phenomena are widespread across time up to nowadays, all over Gimigliano area. The mass movements are mainly triggered by geological and geomorphological complex assessment. The choice of the study area was driven by previous works on landslide hotspots mapping in Calabria Region that demonstrated the priority landslide-prone areas characterized by the higher hydrogeological hazard.

Previous SAR observations conducted with PS Differential Interferometry within and near the Gimigliano town of the period 1993-2010 indicated that "the maximum dynamics had been recorded before 2000, when most of the municipal territory - and in particular the recent settlements and artefacts located in the lower / east part of it - showed medium-speed subsidence movements of over -2 cm / year. The disruption dynamics significantly attenuates and apparently migrates, organizing around two predominant but medium / low deformation zones:

- subsidence rate of the order of 0.3-0.4 cm / yr and mainly associated with the ancient portion of Gimigliano, directional development around N-S;

- subsidence rate between 0.4 and 1.2 cm / yr associated with the eastern / low part of the town of Gimigliano.

Over the years, measured measurements with topographic techniques have shown that lowered measurements reach higher value declines. Subsequently, subsidence phenomena showed a slowdown. Variable speeds ranging from 0.1 to 4.6 cm per year were observed, until 2013.

It can be observed that velocity value considered worldwide Gimigliano Municipality highlights in an increase in subsidence value. Average velocity reaches a few cm / year during the two years of observation.

The approach of this paper has permitted to exploit PSI analysis of C-band SAR data for ground displacement and monitoring over a small area across time.

The outcomes of this work represent a valuable example of deformation multi-temporal detection and characterization by PSI analysis at local scale.

PS interpretation allowed us monitoring ground-induced phenomena and providing an updated scenario. In particular, using and integrating different interferometric and geomorphological data referred to different time intervals, it was possible to reconstruct the dynamic of the area of interest and to provide estimates of the mean yearly velocities during two year, from October 2014 to October 2016.

This procedure resulted in a successful deformation map. As it is shown in the the deformation map of Gimigliano Municipality seems to be affected by subsidence (red PSs colour) with displacement values of up to -27 mm/yr occurred during the two years of observations. The results of research show that Sentinel-1 can give a significant improvement in terms of exploitation of SAR data for landslide mapping and monitoring.

Two years of observation are not absolutely capable to underline a tectonic influence on deformations that are collected in whole Gimigliano area. Indeed a strong vertical component are highlighted and a subsidence phenomenon are underlined . By analysing longer periods, it is predictable a better understanding of landslide behaviour and its relationship with tectonic activity considered like triggering factors.

Bibliografia

AdB Calabria PAI, “Piano Stralcio di Bacino per l’As- setto Idrogeologico,” 2001.

Antronico L, Borrelli L., Peduto D., Fornaro G., Gullà G., Paglia L., Zeni G., 2013, Conventional and innovative techniques for the monitoring of displacements in landslide affected area. In: C. Margottini et al. (eds.), *Landslide Science and Practice*, Vol. 2, Springer-Verlag Berlin Heidelberg.

Antronico L., Borrelli L., Coscarelli R., Pasqua A.A, Petrucci O., Gullà G., 2013, Slope movements induced by rainfalls damaging an urban area: the Catanzaro case study (Calabria, southern Italy). *Landslides*, 10 (6), 801-814.

Antronico L., Sorriso-Valvo M., Tansi C., Gullà G., 2001, Carta litologico-strutturale e dei movimenti in massa della Stretta di Catanzaro (Scala 1:50000). Consiglio Nazionale delle Ricerche - Gruppo Nazionale per la Difesa dalle Catastrofi Idrogeologiche, LINEA 2 - Previsione e Prevenzione di Eventi Franosi a Grande Rischio, Unità Operativa 2.56 (Pubblicazione n. 2119), S.EL.CA. - Firenze.

Azor, A., Keller, E.A. and Yeats, R.S., 2002, Geomorphic indicators of active fold growth: South Mountain-Oak Ridge anticline, Ventura basin, southern California. *Geological Society of America Bulletin,* 114(6), 745-753.

Bianchini S., Cigna F., Del Ventisette C., Moretti S., Casagli N., 2013, Monitoring Landslide-Induced Displacements with TerraSAR-X Persistent Scatterer Interferometry (PSI): Gimigliano Case Study in Calabria Region (Italy), *International Journal of Geosciences*, 4, 1467-1482.

Bianchini S., Cigna F., Righini G., Proietti C. and Casagli N., 2012, Landslide Hot Spot Mapping by Means of Persistent Scatterer Interferometry,” *Environmental Earth Sciences*, 67(4) 1155-1172.

Biescas E.; Crosetto M.; Agudo M.; Monserrat O. and Crippa B., 2007,Two Radar Interferometric Approaches to Monitor Slow and Fast Land Deformation, *Journal of Surveying Engineering*, 2, 66-71.

Brutto, F., Muto, F., Loreto, M. F., De Paola, N., Tripodi, V., Critelli, S., & Facchin, L., 2016. The Neogene-Quaternary geodynamic evolution of the central Calabrian Arc: A case study from the western Catanzaro. Trough basin. *Journal of Geodynamics*, 102, 95–114.

Bull, W.B. and McFadden, L.D., 1977, Tectonic geomorphology north and south of the Garlock fault, California. In *Geomorphology in Arid Regions, Proceedings 8th Annual Geomorphology Symposium*. Doehring, D.C. (Ed.), 115-137.

Burbank, D.W. and Anderson, R.S., 2001, *Tectonic geomorphology*. Blackwell Science, Malden, MA.

Buttafuoco G, Caloiero T, Coscarelli R. 2011a. Spatial and temporal patterns of the mean annual precipitation at decadal time scale in southern Italy (Calabria region). Theor Appl Climatol 105(3–4): 431–444.

Buttafuoco G, Caloiero T, Coscarelli R. 2011b. Spatial patterns of variability for rain fields at different timescales: An application in southern Italy. European Water 36: 3–13.

Cannon, P.J., 1976. Generation of explicit parameters for a quantitative geomorphic study of Mill Creek drainage basin. *Oklahoma Geology Notes* 36, 3–16.

Chiarella, D., Moretti, M., Longhitano, S. G., & Muto, F., 2016, Deformed cross-stratified deposits in the early Pleistocene tidally-dominated Catanzaro strait-fill succession, Calabrian Arc (Southern Italy): Triggering mechanisms and environmental significance. *Sedimentary Geology*, 344, 277–289.

Cigna F., Del Ventisette C., Liguori V. and Casagli N., 2011 Advanced Radar-Interpretation of InSAR Time Series for Mapping and Characterization of Geological Processes, *Natural Hazards and Earth System Science*, 11(3), 865-881.

Colesanti C., Ferretti A., Prati C., Rocca F., 2002, Monitoring landslides and tectonic motions with the Permanent Scatters Technique. *Engineeriong Geology*, 68, 3-14.

Crosetto M., Crippa B., Biescas E., Monserrat O., Agudo M., and Fernández P., 2005b. "Land deformation monitoring using SAR interferometry: State-of-the-art." *Photogrammetrie Fernerkundung und Geoinformation*, 6, 497–510.

Crosetto M., Monserrat O., Cuevas-González M., Devanthéry N., 2016, . Persistent Scatterer Interferometry: a review. *ISPRS J. of Photogrammetry and Remote Sensing*, 115, 78-89.

Crosetto M., Monserrat O., Devanthéry N., Cuevas-González M., Barra A., Crippa B., Persistent Scatterer Interferometry using Sentinel-1 data, 2016, *The International Archives of the Photogrammetry, Remote Sensing and Spatial Information Sciences*, XLI-B7.

Crosetto M., Monserrat O., Iglesias R., Crippa B., 2010, Persistent Scatterer Interferometry: potential, limits and initial C- and X-band comparison". *Photogrammetric Engineering and Remote Sensing*, 76(9), 1061-1069.

Crosetto, M., Biescas, E., Duro, J., Closa, J., Arnaud, A., 2008, Generation of Advanced ERS and Envisat Interferometric SAR Products Using the Stable Point Network Technique, *Photogrammetric Engineering and Remote Sensing*, 74(4), 443–450.

Crosetto, M., Crippa, B., and Biescas, E., 2005a, "Early detection and in-depth analysis of deformation phenomena by radar interferometry." *Eng. Geol. (Amsterdam)*, 79,1–2, 81–91.

Cruden D. M. and. Varnes D. J, 1996, Landslide Types and Processes, In: A. K. Turner and R. L. Schuster, Eds., *Landslides*: *Investigation and Mitigation*, Sp. Rep. 247, Transportation Research Board, National Research Coun-cil, National Academy Press, Washington DC, 36-75.

D. Notti, J. C. Davalillo, G. Herrera and O. Mora, 2010, Assessment of the Performance of X-Band Satellite Radar Data for Landslide Mapping and Monitoring: Upper Tena Valley Case Study, *Natural Hazards and Earth System Sciences*,10, 1865-1875.

De Bartolo S.G., Gaudio R., Primavera L., Gabriele S., Veltri M. 2004. A new method for assessment of river network fractal dimensions: introduction, computation and comparison. *River flow proceeding of the second International Conference on fluvial hydraulics*,Vol.1, 75-81.

Dehbozorgi, M., Dehbozorgi A., Pourkermani M., Arian M., Matkan A.A., Motamedi H. Hosseiniasl A. 2010. Quantitative analysis of relative tectonic activity in the Sarvestan area, central Zagros, Iran, *Geomorphology* 121(3).

Della Seta, M., Del Monte, M., Fredi, P., Miccadei, E., Nesci, O., Pambianchi, G., Piacentini, T. and Troiani, F., 2008, Morphotectonic evolution of the Adriatic piedmont of the Apennines: advancement in the knowledge of the Marche-Abruzzo border area. *Geomorphology*, 102, 119-129.

Devanthéry, N., Crosetto, M., Monserrat, O., Cuevas-González, M., and Crippa, B., 2014, An approach to Persistent Scatterer Interferometry, *Remote Sensing*, 6(7), 6662-6679.

El Hamdouni R., Irigaray C., Fernández T., Chacón J., Keller E.A. 2008. Assessment of relative active tectonics, southwest border of the Sierra Nevada (Southern Spain). *Geomorphology*, 96, 150-173.

Ferretti, A., Prati, C., Rocca, F. (2001). Permanent scatterers in SAR interferometry, *IEEE Trans. Geosci. Remote Sens*., 39(1), 8–20.

Ferretti, A., Prati, C., Rocca, F., 2000, Nonlinear subsidence rate estimation using permanent scatterers in differential SAR interferometry. *IEEE Trans. Geosci. Remote Sens.*, 47(5), 2202–2212.

Ge D., Wang Y., Zhang L., Guo X. and Ye Xia Y., 2010, Mapping Urban Subsidence with TerraSAR-X Data by PSI Analysis, *IEEE International Geoscience and Remote Sensing Symposium*, Honolulu, 3323-3326.

Goldrick G., Bishop P. 2007. Regional analysis of bedrock stream long profile: evaluation of Hack's SL form, and formulation and assessment of an alternative (the DS form). *Earth Surface Processes and Landform* 32, 649-671.

Gulla' G., Antronico L., Iaquinta P., Terranova O. , 2008, Susceptibility and triggering scenarios at a regional scale for shallow landslides. *Geomorphology* 99, 39-58.

Iovine G. & Tansi C., 1998, Gravity-accomodate "structural-wedges" along thrust ramps: a kinematic scheme of gravitational evolution. *Natural Hazard*, 17, 195-224.

ISPRA-Istituto Superiore per la Protezione e Ricerca Ambientale, "Progetto IFFI-Inventario dei Fenomeni Franosi in Italia," 2007.

Keller, E.A., Pinter, N., 2002. Active Tectonics: Earthquakes, Uplift, and Landscape. *Prentice Hall*, New Jersey.

Kirby, E. and Whipple, K., 2001, Quantifying differential rock-uplift rates via stream profile analysis. *Geology*, 29(5), 415-418.

Kobor, J. S., Roering J.J., 2004, Systematic variation of bedrock channel gradients in the central Oregon Coast Range: Implications for rock uplift and shallow landsliding, *Geomorphology*, 62, 239-256.

Li, W., Li, Y., Gao, F.B., 2005, Abelson, enabled, and p120 catenin exert distinct effects on dendritic morphogenesis, *Drosophila*, 234(3), 512-522.

Lifton N. A., Chase C. G. 1992. Tectonic, climatic and lithologic influence on landscape fractal dimension and hypsometry: implication for landscape avolution in San Gabriel Mountains, California. *Geomorphology*, 5, 77-114.

Longhitano, S. G., Chiarella, D., & Muto, F., 2014, Three dimensional to two-dimensional cross-strata transition in the lower Pleistocene Catanzaro tidal strait transgressive succession (southern Italy), *Sedimentology*, 61, 2136–2171.

Luo, Z., W.B. Rossow, T. Inoue, and C.J. Stubenrauch, 2002, Did the eruption of the Mt. Pinatubo volcano affect cirrus properties? *J. Climate*, 15, 2806-2820.

Mahmood S. A., Gloaguen R., 2012 Appraisal of active tectonics in Hindu Kush: Insights from DEM derived geomorphic indices and drainage analysis, *Geoscience Frontiers* 3(4), 407–428

Massonnet, D., Rossi, M., Carmona, C., Adragna, F., Peltzer, G., Felgl, K., and Rabaute, T., 1993,"The displacement field of the Landers earthquake mapped by radar interferometry." *Nature (London)*, 364, 138–142.

Molin, P., Pazzaglia, F.J., Dramis, F., 2004. Geomorphic expression of active tectonics in a rapidly-deforming forearc, sila massif, Calabria, southern Italy. *American Journal of Science* 304, 559–589.

Monaco C., Tortorici L., 2000, Active Faulting In The Calabrian Arc And Eastern Sicily. *J. Of Geodynamics*, 29, 407-424.

Ohmori, H., 1993. Changes in the Hypsometric Curve through Mountain Building Resulting from Concurrent Tectonics and Denudation. *Geomorphology*, 8, 263-277.

Pérez-Peña J.V., Azor A., Azañón J.M., Keller E.A. 2010. Active tectonics in the Sierra Nevada (Betic Cordillera, SE Spain): Insights from geomorphic indexes and drainage pattern analysis. *Geomorphology* 119, 74-87.

R. Soeters and C. J. Van Westen, "Slope Instability Rec- ognition, Analysis and Zonation," In: A. K. Turner and R. L. Schuster, Eds., *Landslides*: *Investigation and Mitiga- tion*: Sp. Rep. 247, Transportation Research Board, Na-tional research Council, National Academy Press, Wash- ington DC, 1996, pp. 129-177.

Ramírez-Herrera M.T. 1998 Geomorphic assessment of active tectonics in the Acambay Graben, Mexican Volcanic Belt. *Earth Surface Processes and Landforms* 23 (4), 317–332.

Righini, G. Pancioli V. and Casagli N., 2012, Updating Landslide Inventory Maps Using Persistent Scatterer Interferometry (PSI), *International Journal of Remote Sensing*, 33(7), 2068-2096.

Rockwell, T.K., Keller, E.A. and Johnson, D.L. 1985: Tectonic geomorphology of alluvial fans and mountain fronts near Ventura, California. In Morisawa, M. and Hack, J.T., 183-207.

Schumm, S.A. ,1956, Evolution of drainage systems and slopes in Badlands at Perth Amboy, New Jersey. *Bull. Geol. Soc. Amer*., 67, 597-646.

Seeber L., Gornitz V. 1983. River profiles along the Himalaya Arc as Indicators of active tectonics. *Tectonophysics* 92(4), 355-367.

Silva, P.G., Goy, J.L., Zazo, C., Bardajm, T., 2003. Fault generated mountain fronts in Southeast Spain: geomorphologic assessment of tectonic and earthquake activity. *Gemorphology* 250, 203–226.

Strahler, A.N., 1952. Hypsometric (area-altitude) analysis of erosional topography. *Geological Society of America Bulletin* 63, 1117–1142.

Strahler, A.N.,1964, Quantitative geomorphology of drainage basins and channel networks, Handbook of Applied Hydrology, 4.39-4.76

Tansi C., Muto F. and Critelli S., 2007, "Neogene-Quaternary Strike-Slip Tectonics in the Central Calabrian Arc (South- ern Italy)," *Journal of Geodynamics*, 43(3), 393-414.

Tofani V., Raspini F., Catani F. and Casagli N. Persistent Scatterer Interferometry (PSI) Technique for Landslide Characterization and Monitoring, **2013,** *Remote Sensing , 5*, 1045-1065.

Tripodi V., F. Muto, and S. Critelli (2013). Structural style and tectono - stratigraphic evolution of the Neogene - Quaternary Siderno Basin, southern Calabrian Arc, Italy, *International Geology Review*, 55, 468 – 481.

Van Dijk, J.P., Bello, M., Brancaleoni, G.P., Cantarella, G., Costa, V., Frixa, A., Golfetto, F., Merlini, S., Riva, M., Torricelli, S., Toscano, C., Zerilli, A., 2000. A regional structural model for the northern sector of the Calabrian Arc (southern Italy*). Tectonophysics* 324, 267–320.

Varnes D. J., 1978, Slope Movement Types and Processes," In: R. L. Schuster and R. J. Krizek, Eds., *Special Report* 176: *Landslides*: *Analysis and Control*, Transportation and Road Research Board, National Academy of Science, Washington DC, 11-33.

Vilardo G., Ventura G., Terranova C., Matano F., Nardò S, 2008, Ground deformation due to tectonic, hydrothermal, gravity, hydrogeological, and anthropic processes in the Campania Region (Southern Italy) from Permanent Scatterers Synthetic Aperture Radar Interferometry, *Remote Sensing of Environment*, 113 (2009) 197–21.

Whipple K. X., Tucker G. E., 1999, Dynamics of the stream-power river incision model: Implications for height limits of mountain ranges, landscape response timescales, and research needs, Geodesy and Gravity Tectonophysics, 104, B8, 17661–17674. AdB Calabria PAI, "Piano Stralcio di Bacino per l'As- setto Idrogeologico," 2001.